University of Alberta

Adsorptive Removal of CO_2 by Amine Functionalized Sorbents: Experimental and Kinetics Study

by

An Zhao

A thesis submitted to the Faculty of Graduate Studies and Research
in partial fulfillment of the requirements for the degree of

Master of Science
in
Chemical Engineering

Department of Chemical and Materials Engineering

Fall 2012
Edmonton, Alberta

Abstract

Adsorption processes using functionalized ordered mesoprous silica sorbents have shown a great potential for post-combustion CO_2 capture from flue gas. In this work an experimental and theoretical investigation was conducted on the adsorptive removal of CO_2 onto amine functionalized mesoporous SBA-15. The adsorption of CO_2 on the functionalized sorbent has been measured by thermogravimetric method over the CO_2 partial pressure range of 10–100 kPa and temperature range of 303–373 K under atmospheric pressure. The functionalization of SBA-15 silica with tetraethylenepentamine (TEPA) has been achieved using conventional wet impregnation technique. The structural properties of the sorbents have been characterized by nitrogen adsorption/ desorption, SAXS, SEM, TEM and FTIR techniques. Temperature swing adsorption/desorption cycles in a simulated flue gas were also explored. Different chemisorption kinetic models have been investigated to analyze the experimental data. The model was validated with the experimental results of isothermal adsorption measurements of CO_2 on SBA-15/TEPA.

Acknowledgements

I would like to express my sincere gratitude to my research advisor, Professor Rajender Gupta, for providing me such a valuable research opportunity in my life, and for his countless guidance, understanding and encouragement during the course of my research.

I also would like to extend many thanks to Dr. Arunkumar Samanta for his unselfish assistance and continuous support in helping complete the work. This work could not have occurred without his extensive help, for which I am really grateful.

Many thanks to Mr. Tong Qiu who kindly offered great help in material characterization. I am also grateful for my close colleagues, Xiaotian Zhang, Nikhil Mittal, Mingwen Gao and Su Tian for their valuable assistance and cooperation, and all the group members for creating such a pleasant working environment.

Lastly, I would like to dedicate this work to my loved parents who have always unconditionally supported and guided me in my life.

Table of Contents

List of Tables

List of Figures

Nomenclature

a_0	Unit cell parameter
C_0	the concentration of CO_2 in the feed stream
C_t	the effluent concentration of CO_2 at time *t*
d_{100}	*d*-value 100 reflections
d_p	Mean pore diameter (nm)
D_{BJH}	BJH mean pore diameter (nm)
F	Total molar flow rate (mol/min)
k_1, k_2	Rate constant for pseudo-first order and pseudo-second order model, respectively
k_n	Model constant for fractional-order model
M	Mass of adsorbent loaded in the column
m	Fractional-order model constant
N	Total number of experimental points
n	Fractional-order model constant
q	CO_2 adsorption capacity (mmol /g)
q_e	CO_2 adsorption capacity at equilibrium (mmol /g)
q_t	CO_2 adsorption capacity at time *t* (mmol /g)
q_{cal}	Calculated adsorption capacity (mmol /g)
q_{exp}	Experimental adsorption capacity (mmol /g)
S_{BET}	BET surface area (m^2/g)
V_{tot}, V_{micro}	Total pore volume and micropore volume, respectively (cm^3/g)
t	Adsorption time (s)
t_q	Breakthrough stoichiometric time
w_d	Wall thickness (nm)

Abbreviations

AAD	Average absolute deviation
AC	Activated carbon
CMS	Carbon molecular sieves
CNT	Carbon nanotube
FTIR	Fourier transform infrared spectroscopy
MFC	Mass flow controller
MOF	Metal-organic framework
MS	Mass spectrometry
PEI	Polyethylenimine
PSA	Pressure swing adsorption
PSD	Pore size distribution
SAXS	Small-angle X-ray scattering
SEM	Scanning electron microscopy
HRTEM	High-resolution transmission electron microscopy
TEPA	Tetraethylenepentamine
TGA	Thermogravimetric analysis
TSA	Temperature swing adsorption

CHAPTER 1

Overview

1.1 Introduction

Tendency of global energy use in the 21st century projects a continuously increasing dependence on the utilization of fossil energy, which is considered to be the major contributor to the anthropogenic carbon dioxide (CO_2) emission. According to the Intergovernmental Panel on Climate Change (IPCC) report, the worldwide greenhouse gas emissions gained to 49 Gt equivalent-CO_2 in 2004,

56.6% of which is attributed to CO_2 emissions from fossil fuel use[1]. Starting from the year of 1958 when the continuous observation on atmospheric CO_2 concentration was initiated, its growth rate has accelerated from less than 1 part per million per year (ppm yr^{-1}) prior to 1970 to the level beyond 2 ppm yr^{-1} in recent times[2]. The fact has inevitably aroused numerous public concerns on excessive and uncontrolled CO_2 emission with respect to its impact on climate and environment change. However, the endeavor to offset its increasing trend is becoming even more challenging. Unless taking effective and proper measures, the energy-related CO_2 emission by 2050 is estimated to double the level of 29 Gt CO_2 in 2007. It possibly obstructs the expected long term scenario, proposed by International Energy Agency, to reduce the global energy-related CO_2 emission in 2050 to 14 Gt, equivalent to the half of the CO_2 level in 2005[3]. Therefore, the agenda on globe wide cooperation in carbon dioxide emission reduction and mitigation has been explicitly put forward from a standpoint of long term sustainable development.

1.2 Carbon Capture & Storage (CCS)

Carbon capture and sequestration (CCS) is widely acknowledged and identified to be the major and crucial approach to limit the CO_2 level in the realm of carbon reduction and its derived technologies. It is expected that by the time of 2020, the number of operational CCS projects is estimated to be 100 globally, which will grow to over 3000 by 2050[4]. CCS encompasses the removal and sequestration of CO_2 from industrial low CO_2 level containing streams, the generation of high concentrated CO_2 stream, and the transport and storage of compressed CO_2. In

this context, it should be noted that CCS is more suitable and economically feasible for large point sources – fossil fuel or biomass energy facilities, natural and synthesis gas production, refineries, steel or cement plants – than for small, dispersed emission sources.

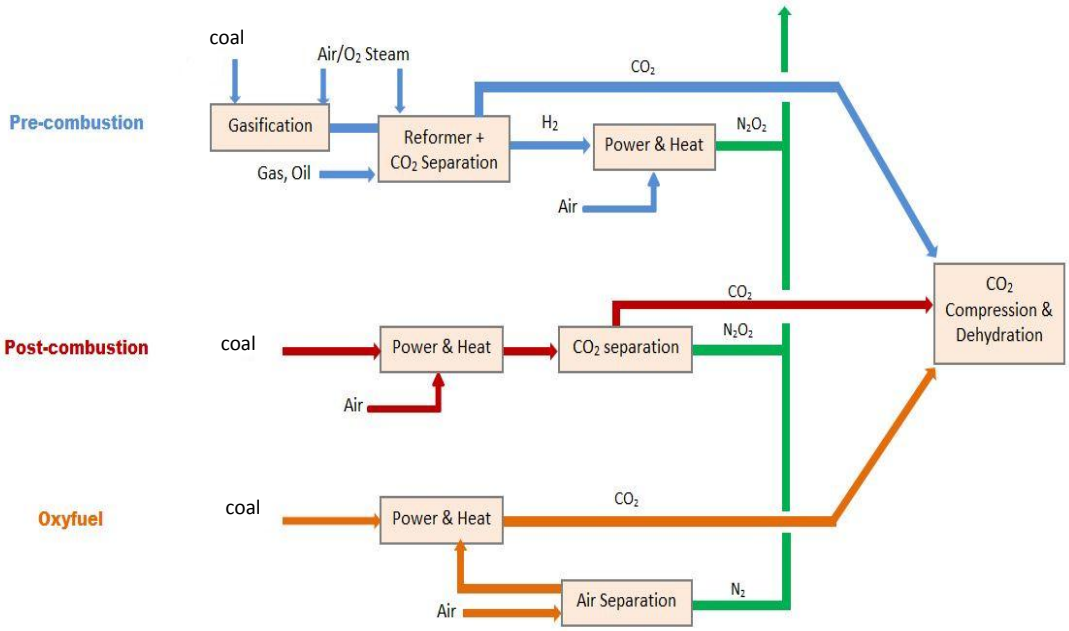

Figure 1-1. Schematic of CO_2 capture processes and systems[5]

Currently, three types of CCS processes are mainly being developed that could be applied to industries with large CO_2 emissions. A schematic representation of every capture system is illustrated in Figure 1-1. The primary fuel (coal, natural gas, oil or biomass) in *pre-combustion* systems undergoes a process of partial oxidation to form syngas and finally produces separate streams of CO_2 for storage and hydrogen (H_2) which is used as a fuel. *Oxyfuel combustion* is still in the demonstration phase that needs more investigations. High purity oxygen is used to combust with fuels instead of air. This results in producing the flue gas with H_2O and high CO_2 content that is readily captured, however, at the cost of increased

energy requirement in the separation of oxygen from air. *Post-combustion* is basically used to sequester CO_2 from flue gases produced by the combustion of a primary fuel. Compared to other options, post-combustion capture of CO_2 is more economically favored for existing power plants because retrofitting existing plants with post-combustion CO_2 capture is expected to be easily conducted and have a relative less cost, while integrated power plant system would suggest more profound adjustment.[5]

Understanding each capture system or process is of great significance in selecting the appropriate approach for different situations, because the practical application of each capture option largely depends on some key factors such as the concentration of CO_2 in the gas stream, the pressure of the gas stream even the fuel type (solid or gas). As shown in Table 1-1, the fraction of CO_2 in the gas stream varies greatly from around 3% to more than 30% according to the respective industrial facilities. As a rule of thumb, the lower the partial pressure of CO_2 in a gas stream, the more stringent the conditions for CO_2 capture systems [5]. Besides, the presence of impurities (e.g. SO_x, NO_x, trace elements and particulates) also induces extra technical problems when implementing CO_2 capture system into energy intensive plants. Future treatment of flue gases may be suggested to remove pollutants and impurities to minimize their negative effects on CO_2 capture processes.

Table 1-1. Typical gas compositions in various CO_2 capture situations

Process	CO_2 (dry) (vol%)	Impurities
Natural gas turbine exhaust	3-4	Low SO_x and NO_x levels, O_2: 12-15%
Coal/Oil Fired Boiler	11-14	High SO_x and NO_x levels, O_2: 2-5%
IGCC syngas turbine exhaust	4.5-6	Low SO_x and NO_x
Blast furnace gas (after combustion)	27	SO_x and NO_x present
Cement kiln off-gas	14-33	SO_2 and NO_x trace elements, particulates

1.3 Technologies for Post-combustion CO_2 Capture

Current anthropogenic CO_2 emission from stationary sources comes from the combustion systems such as power plants, cement kilns, steel and iron production plants. For these large-scale processes, the direct combustion of fuel with air in a combustion chamber has been the most economic strategy to make use of energy contained in the fuel. Therefore, the practical importance of the post-combustion capture systems becomes evident when confronted with the reality of today's CO_2 emission sources.

There are several technologies, such as absorption, sorbents, membranes or cryogenics, available which can be in principle applied for CO_2 capture from flue gases. This section describes the separation of CO_2 from the flue gases generated in large-scale combustion processes fired with fossil fuels (e.g. coal fired power generation plants) via chemical solvent based regenerative absorption and solid sorbent based adsorption. Membrane separation process, although received wide

attention, is not suitable for the applications at low partial pressure of CO_2 which lead to a lower driving force for gas separation and larger volumetric flow rate.

1.3.1 Absorption Process

Absorption process based on chemical solvents is one of the widely used technologies in chemical process industries for CO_2 removal from process gas streams and is one of the preferred options for post-combustion CO_2 capture. Compared to other existing post-combustion capture process, it offers high capture selectivity and efficiency[5]. A schematic representation of absorption processes in post-combustion CO_2 capture is presented in Figure 1-2. Basically, absorption in post-combustion capture makes use of the reversible reaction mechanism of chemical solvents, normally aqueous alkaline or amine solvents, with acid or sour gases. The state-of-the-art absorption processes utilize 20–30 wt% aqueous monoethanolamine (MEA)/ diethanolamine (DEA) for regenerative operation of CO_2 that are being practiced quite well over last few decades.

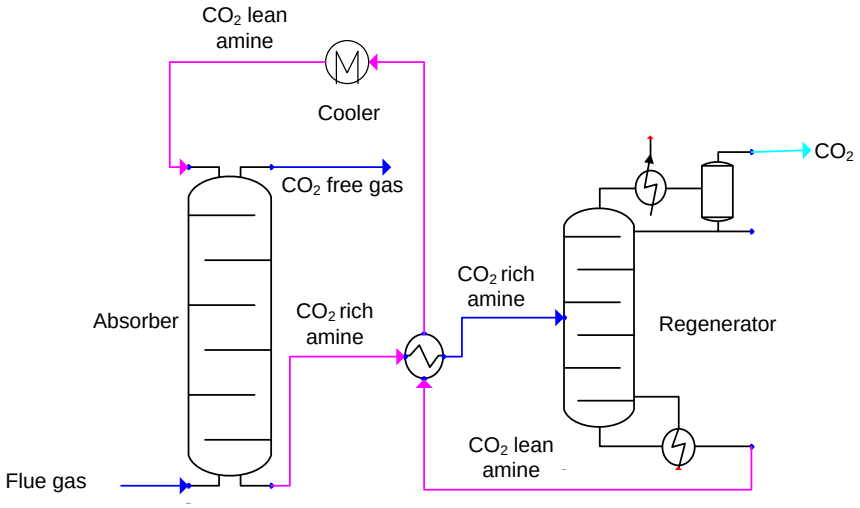

Figure 1-2. Flow diagram of CO_2 recovery process by chemical absorption

However, careful attention has to be paid to the limitations of absorption processes in post-combustion CO_2 capture. A key feature determining the techno-economical viability of CO_2 recovery using absorption processes from flue gas is the high energy requirement and the resulting energy penalty on power cycles. Considerable energy input (approximately 2.7–3.3 GJ/tCO_2) is necessarily required with regards to the solvent regeneration and steam use for stripping[5]. Moreover, the performance of the chemical solvent is also affected by oxidative degradation/decomposition and other loss during the operations due to the presence of SO_x and NO_x in flue gas from coal combustion. As a result, energy requirement and consequently cost of post-combustion CO_2 capture using absorption process is still high. It is thus desirable to develop alternative improved, cost effective processes for CO_2 capture from flue gas streams of coal based power plants.

1.3.2 Adsorption Process

As an emerging alternative to substitute the energy intensive amine scrubbing process, adsorption process has prompted a growing interest in post-combustion CO_2 capture[6]. In general, adsorbents used for CO_2 capture from flue gas can be physisorbent and chemisorbent. The physisorbents for CO_2 capture mainly include carbon-based materials, alumino-silicas such as zeolites and more recently metal organic frameworks (MOFs). For chemisorbents, also discussed in this work, mainly refer to a few solid adsorbents obtained through the incorporation of specific functional groups resulting in enhancing chemical reaction effect between CO_2 molecules and adsorbents.

Unlike the absorption process, adsorption using solid sorbents has the promising advantages such as the reduced energy requirement, greater capacity and selectivity, the ease of handling, etc. CO_2 adsorption and desorption are normally done using appropriate solid sorbents that are capable of CO_2 removal and regeneration reversibly by pressure swing adsorption (PSA) or temperature swing adsorption (TSA) process. Suitable sorbents for CO_2 capture from flue gas are supposed to provide competitive performance and cost benefits over solvent-based processes. Efforts on the screening and evaluation of solid sorbents have been undergoing so far as the recent times[6-8]. The criteria for selecting a promising CO_2 adsorbent, however, still need explicitly addressing and putting forward ahead in the next section.

1.3.2.1 Criteria for Screening Sorbents

A good solid sorbent material for CO_2 removal from flue gas should combine several attributes including[7-8]:

- *High CO_2 adsorption capacity:* equilibrium CO_2 adsorption capacity is one of main parameters to look into a new sorbent for CO_2 capture. It is of paramount importance in determining and screening whether a sorbent is capable of capturing CO_2 to its greatest extent. Considering the relative low CO_2 concentration and partial pressure in the flue gas, a favorable CO_2 adsorption isotherm should exhibit a steep slope corresponding to a high CO_2 uptake at its low partial pressure [7]. However, working adsorption capacity, determined for a short adsorption time, is more preferred to use in place of equilibrium capacity in real practice. Gray et al. suggested an

optimal CO_2 adsorption capacity of 3–6 mmol-CO_2/g-sorbent (hereafter shortened to mmol g^{-1}) in order to be competitive with conventional aqueous amine scrubbers [9].

- *Fast adsorption/desorption kinetics:* Adsorption/desorption kinetics affects the overall performance of an adsorbent represented in working capacity. For large volume processing vessels, e.g. fixed-bed columns, fast kinetics may not only shorten the cyclic operation time, but also to some extent reduce the amount of solid sorbents needed to capture a given volume of flue gas. However, it should be pointed out that determination of adsorption properties such as intraparticle diffusion is one of the most challenging topics in the realm of adsorption science, as it encompasses the sorbent particle size or the gas-solid mixing that are not always readily acquired.
- *High CO_2 selectivity:* Since combustion flue gas generally contains oxygen, nitrogen, moisture and other impurities (as seen in Table 1), an ideal sorbent should selectively sequester CO_2 over bulk gas components in the flue gas. In addition, careful attention must be also paid to its tolerance of contaminates such as NO_x and SO_x resulting in irreversible deterioration of sorbent porous structure. It is thus desirable to carry out flue gas pretreatment to lower other sour gases down to the appropriate level.
- *Mild regeneration condition:* The ease of regeneration of the adsorbent is also a key property in the selection of an ideal adsorbent for post-

combustion CO_2 capture. The interaction between CO_2 molecules and porous sorbent media should be in the optimal range, which could be also represented and measured by the heat of adsorption. Heats of adsorption, a measure of the energy required for regeneration, are normally in the range of –25 to –50 kJ/mol for physisorption and –60 to –90 kJ/mol for chemisorption [8]. Too strong bonding results in the higher adsorption capacity at low partial pressure but requires more energy necessarily that makes the regeneration difficult and costly.

- *Sufficient cyclic stability and mechanical strength:* An ideal sorbent is expected to be carried out under real flue gas environment for a long period of operation cycles without significant performance deterioration. On one hand, CO_2 capture sorbents should retain the appropriate working capacity and selectivity during their whole lifetime in order to reduce the frequency of material replacement. On the other hand, the sorbents should demonstrate enough structural and morphological strength to overcome thermal decomposition and mechanical abrasion, in particular, happening in fluidized reactors.

It should be further noted that rarely is a single adsorbent equipped with all abovementioned attributes. However, reliable and viable adsorbents will be those that can adsorb CO_2 from flue gas streams effectively and economically in a given condition. A comprehensive literature review related to various adsorbents used for CO_2 capture is discussed in the following chapter.

References

1. IPCC *Climate Change 2007: Mitigation of Climate Change*; Cambridge, United Kingdom and New York, NY, USA, 2007.

2. Hofmann, D. J.; Butler, J. H.; Tans, P. P., A new look at atmospheric carbon dioxide. *Atmospheric Environment* **2009,** *43* (12), 2084-2086.

3. IEA, *Energy Technology Perspectives 2010- Scenarios & Strategies to 2050*. 2010; p 650.

4. IEA *Technology Roadmap: Carbon capture and storage*; 2009.

5. IPCC, *Carbon Dioxide Capture and Storage*. Cambridge University Press: 2005; p 431.

6. Sjostrom, S.; Krutka, H., Evaluation of solid sorbents as a retrofit technology for CO_2 capture. *Fuel* **2010,** *89* (6), 1298-1306.

7. Sayari, A.; Belmabkhout, Y.; Serna-Guerrero, R., Flue gas treatment via CO_2 adsorption. *Chemical Engineering Journal* **2011,** *171* (3), 760-774.

8. Samanta, A.; Zhao, A.; Shimizu, G. K. H.; Sarkar, P.; Gupta, R., Post-Combustion CO_2 Capture Using Solid Sorbents: A Review. *Industrial & Engineering Chemistry Research* **2012,** *51* (4), 1438-1463.

9. Gray, M. L.; Champagne, K. J.; Fauth, D.; Baltrus, J. P.; Pennline, H., Performance of immobilized tertiary amine solid sorbents for the capture of carbon dioxide. *International Journal of Greenhouse Gas Control* **2008,** *2* (1), 3-8.

CHAPTER 2

Literature Review

2.1 Introduction

The interest and endeavor in understanding the mechanism of adsorption physically and chemically will never end in order to better describe the adsorption phenomena. Possible mechanisms of adsorption separation are based on: 1) kinetic effect, due to differences in the diffusion rates of various gaseous components in the mixture; 2) the thermodynamic equilibrium effect, because of

the preferential adsorbate-surface or adsorbate packing interactions; and 3) the molecular sieving effect, due to the diversity in molecular size or shape of different component in a gas mixture[1]. Therefore, the intrinsic structural properties of mesoporous (pore size between 2 and 50 nm) and microporous (pore size < 2 nm) adsorbents are of paramount significance in terms of pore volume, pore size and surface area.

In this chapter, a comprehensive literature review is made on two distinguished classes: physical adsorbents and amine functionalized adsorbents. Physical adsorbents discussed here include conventional carbon materials, alumina-silicas such as zeolites and more recently metal-organic frameworks (MOFs). The amine functionalized adsorbents refer to those sorbents modified through amine incorporation onto or into solid supports such as mesoporous silica.

2.2 Physical adsorbents

This section summarizes most physisorbent available in the literature, namely carbon-based solid sorbents, zeolites and zeolite-like sorbents. As a new class of physical adsorbent, metal organic frameworks (MOFs) will be also introduced later on. This section also looks into their recent progress and application in post-combustion CO_2 capture, specifically highlighting the availability for CO_2 removal from flue gas in coal burned power plants.

2.2.1 Carbon-based Solid Sorbents

2.2.1.1 Activated Carbons

Amongst carbon-based solid sorbents reported in the literature, activated carbons (ACs) are primarily investigated and reviewed because of the low cost of raw material and the wide availability of sources. Activated carbons can be produced by means of either physical or chemical activation with various carbonaceous precursors that are easily acquired, such as coals[2] (e.g. bituminous coal), fly ashes[3], anthracites[4], and wood or other biomass sources[5] (e.g. bamboo chips, coconut shells, etc.). The activation and treatment process together with the intrinsic nature of different precursors strongly determines the structural characteristics of the resulting activated carbons in terms of pore size distribution, porosity, surface area as well as pore volume. Maroto-Valer et al.[4] studied the effects of activation time and temperature on the formation of anthracite-based activated carbons. They found that the structural properties of anthracites treated at different conditions varied considerably but are mainly kept in the range of micropores. It has been reported by them the maximum surface area and pore volume were 1071 m^2/g and 0.599 mL/g for the anthracite at 890 ℃ for 2 hours.

Table 2-1. CO_2 Adsorption Capacity of Carbonaceous Solid Sorbents

carbonaceous sorbents	BET surface area (m^2 g^{-1})	pore volume (cm^3 g^{-1})	adsorption temperature (K)	adsorption pressure p_{CO_2}(atm)	CO_2 capacity (mmol g^{-1})	Ref.
Activated anthracite	540	–	303	1	1.49	4
Norit R1 Extra	1450	0.47	298	0.15	0.54	6-7
BPL	1150	0.43	298	1	2.07	7-8
AC	1567	–	275	2	3.00	5
AC	1943	0.91	275	2	~5.60	9
AC (granular)	954	0.48	298	0.10	0.57	10
SWNT	1587	1.55	308	1	2.07	11
CNT	407	0.45	293	0.15	0.64	12
CMS	1152	-	298	1	~2.27	13

The consequences of activation on different carbonaceous raw materials lead to highly porous adsorbents with high surface area, large pore volume and pore size. Table 2-1 incorporates the structural characteristics and CO_2 adsorption capacity of various commercial and synthesized activated carbons in the literature. It should be noted, however, that in terms of CO_2 adsorption capacity, it does not exhibit a linear relationship with structural characteristics. Maroto-Valer et al.[4] observed the highest CO_2 adsorption capacity of 1.49 mmol g^{-1} for activated anthracite treated at 800 ℃ for 2 h, which presents specific surface area of only 540 m^2/g. This result does not correspond to the samples with the maximum structural properties in terms of surface area and pore volume. It is primarily due

to the fact that not all of inner pores but certain pores with a range of sizes were effective for CO_2 capture.

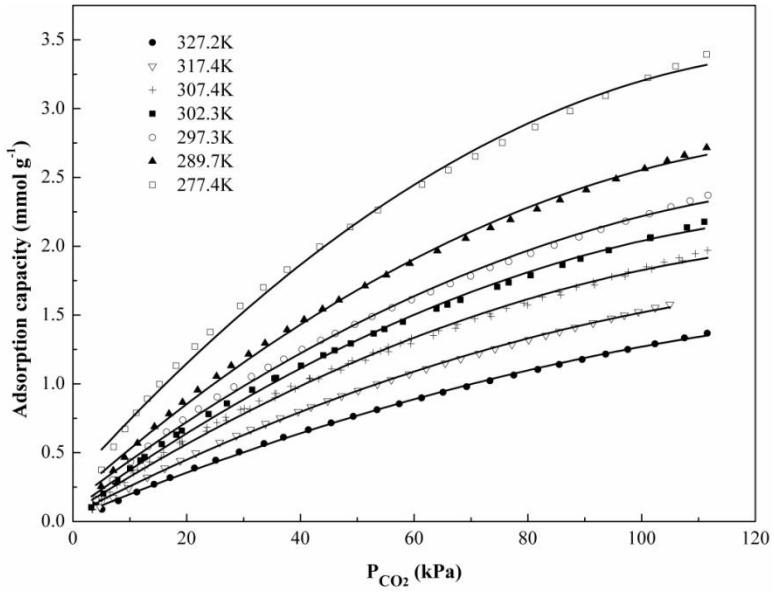

Figure 2-1. Isotherms for adsorption of CO_2 on activated carbons[14]

Typical CO_2 adsorption isotherms on activated carbons are shown in Figure 2-1. It can be clearly seen that the equilibrium CO_2 adsorption capacity of activated carbon increases as the pressure rises up and the temperature drops, which are found to be extremely reproducible, indicating the excellent reversibility of adsorption[15]. Dreisbach et al.[6] conducted adsorption equilibria of CO_2 on Norit type activated carbons at high pressure up to 6 MPa at 298 K where they found a fairy high pure CO_2 loading up to 11.27 mmol g^{-1}. However, at low CO_2 pressure, activated carbons exhibits lower adsorption capacity and selectivity than zeolites due to their less favorable adsorption isotherms[16].

Due to the large variation in CO_2 adsorption capacity at high and low CO_2 partial pressures, relative less costly pressure swing adsorption (PSA) process outstands to be a potential method for adsorption and desorption[8,16-18]. In addition,

considering the real gas environments to be separated in various applications, CO_2 selectivity studies were also conducted using CO_2 contained gas mixtures (e.g. including CH_4, O_2 and N_2)[5,17]. Sayari et al.[19] summarized the CO_2 versus N_2 selectivity at 298 K is in the range of 1.2 and 2 by comparing adsorption capacity molar ratio of CO_2 and N_2. Despite the hydrophobic attribute of carbon-based adsorbent, the CO_2 adsorption capacities of activated carbons are negatively affected by the presence of moisture because of the water's ability to adsorb competitively.

In summary, activated carbons are low cost with fast adsorption kinetics and easy handling of regeneration. They have shown great promise in CO_2 removal at high pressure and low temperature (e. g. room temperature). However, at low partial pressure of CO_2, activate carbons cannot be capable of providing high adsorption capacity and selectivity. These limitations make them not suitable for their application in low pressure CO_2 capture from flue gas treatment.

2.2.1.2 Carbon Nanotubes

Great interest in carbon nanotubes derives from their outstanding thermal, optical, electrical, and mechanical properties, which allow extensive and broad applications.[20] As a new class of emerging materials, single-walled or multi-walled carbon nanotubes are an appealing option for CO_2 separation by tailoring the pore dimension and choosing the optimal conditions. The mechanism of CO_2 adsorption on carbon nanotubes is primarily due to the physical force and the exothermic nature of adsorption process well explained the experimental fact that the capacities of CO_2 via carbon nanotubes decreases with elevated temperature.[12]

Carbon nanotubes exhibit an excellent CO_2 separation from other gas components. Using molecular simulations, Huang et al.[21] observed that regardless of the effects of pore size, temperature and pressure, the CO_2 selectivity of carbon nanotubes over methane is generally above 8, which is larger than ever reported in activated carbon and metal organic frameworks. A similar observation were found by Razavi et al.[22] through studying the competitive adsorptive behavior of binary CO_2 and N_2 mixture on carbon nanotubes.

However, the dispute with regards to the CO_2 adsorption capacity of carbon nanotubes still needs discussions. Cinke et al.[11] reported the improved adsorption capacity (2.07 mmol g^{-1} at 308K, 1 atm), which is approximated twice the volume of CO_2 adsorbed in activated carbon tested (see Figure 2-2). On the contrary, the multi-walled carbon nanotubes are found by Su et al.[12] to show reduced physical adsorption capacity than other carbon-based adsorbents.

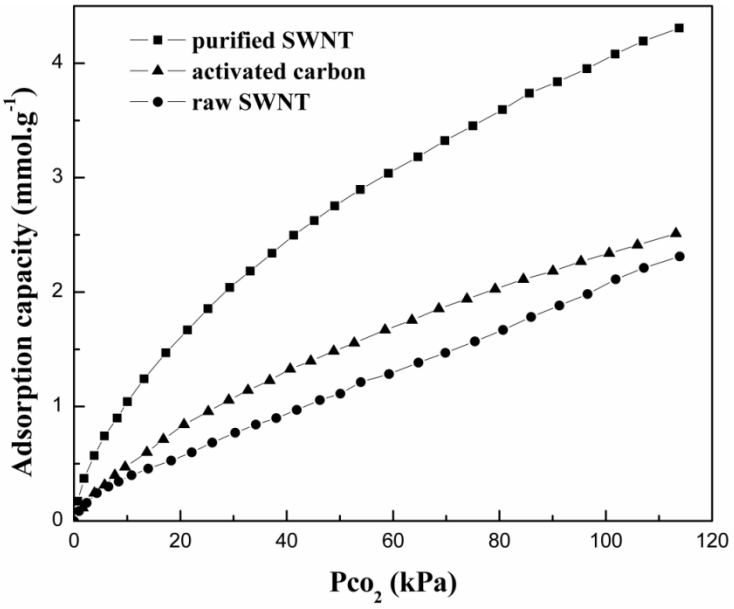

Figure 2-2. Comparison of CO_2 adsorption capacities of high-pressure CO conversion (HiPco) single-walled nanotubes (SWNTs) and activated carbons (AC) at 35 ℃[11]

It is worth pointing out that the unit cost of carbon nanotube (US $5/g) is much higher than typical cost for granular activated carbon (US $1/g).[12] Therefore, the future endeavor in extending the repeated availability, as well as improving the CO_2 adsorption performance on carbon nanotube, still carries on to seek more reliable and effective pathway in CO_2 capture.

2.2.1.3 Carbon Molecular Sieves

The structural variability of porous solids, particularly microporous adsorbents, enables the possibility of controlling the equilibrium and kinetic properties over a wide range.[23] As a subclass of activated carbons, carbon molecular sieves (CMS) are microporous carbon materials who share with zeolites the ability to separate molecules on the basis of size and shape.[24] Additionally, its unique textural nature, e.g. narrow pore size distribution (PSD), also allows kinetic separation of gas mixture, for instance, separation due to differences in the diffusion rates of the gaseous species. However, analysis of the equilibrium and kinetics of batch adsorption of CO_2 on a Takeda 5A CMS revealed no molecular sieving action; instead, micropore diffusion became a rate-limiting step in the adsorption dynamics.[25] More recently, microporous carbon monoliths prepared from nitrated coal tar pitch were reported to possess faster CO_2 kinetics than commercially available Takeda 3A CMS.[26]

For a CMS to be better applicable in CO_2 separation, it should be tailored to have appropriate pore mouths of molecule sizes and possess a relatively high micropore volume, which largely affect the selectivity and capacity, respectively.[24] However, little work has been done in the realm of post-combustion CO_2 capture from flue

gas. The isotherms of a monolithic carbon fiber composite molecular sieve prepared by Burchell et al.[13] showed a CO_2 uptake approximately 2.27 mmol g^{-1} at one atmosphere and 298K but this value reduced at elevated temperature.

2.2.2 Zeolites

A zeolite material is a crystalline aluminosilicate with a three dimensional framework structure that forms uniformly sized pores on a molecular scale. As they generally exhibit a narrow pore size distribution that can be tuned to preferentially adsorb molecules that fit inside the pores and exclude larger molecules, they act as molecular sieves for the use of gas separation.[27] In addition to molecular sieving effect, separation of gases in zeolites can also realized through selective adsorption of those molecules that possess large energetic dipole or quadruple. The presence of Al^{3+} in the crystallized framework replaces Si^{4+} at some places in these silicate-based molecular sieves. As a result, it introduces negative charges that are compensated with exchangeable cations within the pores. Some of those cations, normally alkali cations such as sodium or lithium, are amenable to generating strong electrostatic interactions with CO_2, which has high quadrupole moment (-14.29×10^{-40} C m^2).[28] Therefore, the number and nature of extraframework cations largely affect the CO_2 adsorption performance of zeolites. Some studies[29-31] revealed that a low Si/Al ratio, corresponding to high content of extraframework cations, may favor the adsorption of CO_2 over zeolites. Maurin et al.[31] investigated experimentally and theoretically, the adsorption mechanism of CO_2 in various faujusite-based zeolites, namely dealuminated Y zeolite (Si/Al=∞), NaY (Si/Al=2.4) and low silica NaX (Si/Al=1). They emphasized that the CO_2

affinities for these adsorbents increase in the order of Si/Al ratio. A more pronounced affinity for low silica NaX, which has the lowerst Si/Al ration, attributed to the presence of more accessible extraframework exchanged cations. In addition to above, an extensive screening study of more synthetic zeolites with various Si/Al ratio, including 5A, 13X, NaY, ZSM-5, HiSiv-3000 was carried out by Harlick et al.[32] Pure component isotherm data (see Figure 2-3) revealed an increasing trend of adsorption capacity with the Si/Al ratio in the following order:

13X (Si/Al = 2.2) > NaY (Si/Al = 5.1) >

H-ZSM-5-30 (Si/Al = 30) > HiSiv-3000 (Si/Al >1000)

Zeolites have a great potential in separation of CO_2 from gas streams. There is exhaustive published literature and work focusing on the use of different types of zeolites for adsorption and separation of CO_2.[10,16-17,27,30,32-51]Table 2-2 summarizes the various natural and synthesised zeolites that have been studied so far for application of CO_2 separation from gas mixtures.

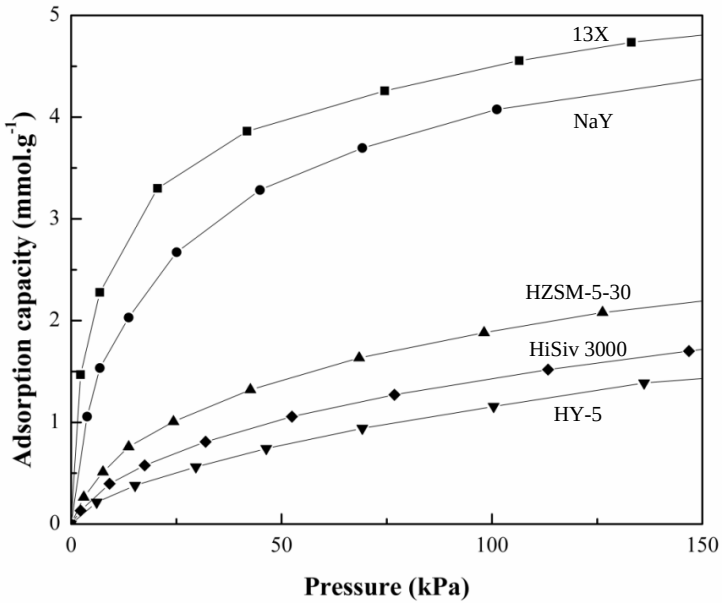

Figure 2-3. Comparison of CO_2 adsorption isotherms for fresh zeolites at 295K.[32]

Table 2-2. CO_2 Adsorptin Capacity of Zeolites.

sorbents	adsorption temperature (K)	adsorption pressure p_{CO_2}(atm)	CO_2 adsorption capacity (mmol g^{-1})	reference
Zeolite 13X	298	1	4.66	34
Zeolite 13X	293	0.15	2.18	52
Zeolite 4A	293	0.15	1.65	52
NaX	305	1	5.71	53
NaY	305	1	5.5	53
NaY	295	1	4.06	32
silicalite	303	0.15	0.48	54
erionite (ZAPS)	290	1	2.8	39
mordenite (ZNT)	290	1	1.8	39
clinoptilolite (Zn-19)	290	1	1.7	39
ZSM-5	313	0.1	0.32	55

Recent studies also focused on the modification of zeolites via the introduction of large and electropositive, polyvalent cations to enhance the adsorption of CO_2.[30,35-36,41-42,48,56] The selection of proper cations may effectively improve the adsorption capacity. Walton et al.[30] carried out the substation of sodium on NaX and NaY zeolites with other alkali metal cations, such as Li^+, K^+, Rb^+, and Cs^+ and compared their corresponding CO_2 adsorption capacities. For Y-type zeolite, CO_2 capacity increased as Cs < Rb ≈ K < Li ≈ Na; For X-type zeolite, the capacity for CO_2 in the order of decreasing ionic radii, Cs < Rb < K < Na < Li. Adsorption equilibrium on each ion-exchanged material indicated cation size and acid-base surface nature can have an important effect on tailoring adsorptive properties of zeolites by ion exchange.

In terms of CO_2 adsorption kinetics, although rarely reported, zeolites are considered to be one of the fastest adsorbents, reaching equilibrium capacity within minutes.[57] Moreover, most of efforts in adsorption using zeolites have been put on pressure swing adsorption (PSA) or vacuum swing adsorption (VSA) for separating CO_2 from flue gas in power stations.[17,38,40,43,47,58] Besides, the temperature swing adsorption (TSA) process has also been suggested by various researchers.[44] A detrimental effect of water on CO_2 adsorption over zeolites still constrains their applications in highly humid environment. The presence of water can significantly decrease the CO_2 adsorption capacity, because it gets preferentially adsorbed on the zeolites and thus competitively inhibits CO_2 adsorption.[33,45]

In conclusion, zeolites have been studied extensively to determine the effect of type of ions incorporated into the structure on the adsorption equilibrium and energetics. In general, adsorption kinetics of CO_2 on zeolites is comparatively fast and achieved equilibrium capacity within a few minutes. However, CO_2 adsorption on zeolites is strongly influenced by the temperature and pressure. The presence of water vapor may limit the application of zeolite sorbents by decreasing its capacity. It is therefore obvious, that by carefully considering and optimizing different important factors, such as basicity, pore size of zeolites, electric field strength caused by the presence of exchangeable cations in their cavities may significantly influence the CO_2 adsorption capacities of zeolites.

2.2.3 Metal-organic Frameworks

A relatively new class of solid sorbent materials is metal-organic frameworks (MOFs).[59] MOFs are network solids composed of metal ion or metal cluster vertices linked by organic spacers. The ability to readily incorporate and vary organic linkers in these materials translates to abundant options to control pore size, pore shape, and the chemical potential of the adsorbing surfaces and, consequently, their selectivity, kinetics, and capacity.

Yazaydin et al.[60] reported that, HKUST-1, which is a MOF, exhibited enhanced CO_2 uptake in the presence of 4% water. It was recognized that this did not translate to better uptake of CO_2 in the presence of higher degrees of hydration. Work by Liu et al.[61] examined the Ni-analogue of MOF74 and HKUST-1 for CO_2 sorption in humid atmospheres. For the Ni-MOF74 material, high CO_2 capacities (3.28 mmol g^{-1}) were found at a point of interest for flue gas application (25 ℃, 0.1 atm CO_2 partial pressure). Ni-MOF74 has a higher CO_2 capacity than benchmark zeolites (5A and NaX) under these conditions. Adsorbed water vapor impacted CO_2 adsorption in the MOFs, but not nearly as greatly on 5A and NaX zeolites. Most importantly, Ni-MOF74 was found to retain substantial CO_2 capacity with moderate H_2O loadings.

Given that the field of MOFs is still emerging, a general statement on the prospects for MOF materials is still largely based on their potential. MOFs have very high capacity at high pressures, however, at atmospheric pressures their capacity is lower as compared to other physical sorbents. Further research is

needed to develop MOFs targeting key material properties such as stability, multicycle applicability and competitive sorption.

2.3 Amine Functionalized Solid Sorbents

Most of the conventional physisorbents, such as zeolites, ACs, CMS and CNTs described above suffer from low CO_2 adsorption capacities at relatively low CO_2 partial pressure and lower selectivity towards CO_2. Recently, modifications in the surface chemistry of the porous materials by incorporating basic sites capable of interacting strongly with acidic CO_2 in order to increase CO_2 adsorption capacity and to keep high selectivity for CO_2 are considered very promising.

A variety of microporous or mesoporous materials loaded with basic nitrogen functionality, more specifically, organic amine functionality has been synthesized and characterized to chemisorb CO_2 from flue gas streams. Amine functionalized sorbents have been classified into three classes.

- Class 1: This class of supported sorbents is prepared by physically loading monomeric or polymeric amine species into or onto the porous support, typically porous silica by impregnation technique.
- Class 2: This class of supported adsorbents is that in which the amine, mainly amine-containing silane is covalently tethered to a solid support, such as porous silica. This is accomplished by binding amines to oxides via the use of silane chemistry or via preparation of polymeric supports with amine-containing side chains. This provides covalently tethered amine sorbents the potential to be completely regenerable through multi-cycle adsorption/desorption uses.

- Class 3: These supported adsorbents are based on porous supports upon which amino-polymers are polymerized in situ. This category of supported sorbents can be considered a hybrid of the other two classes.[62]

The structure of widely used amines for sorbent functionalization is given in Table 2-3.

Table 2-3. Structure of Amines for Sorbents Functionalization[63]

Name	Structure	Name	Structure
Amines		Silanes	
Monoethanolamine (MEA)	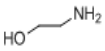	3-aminopropyltrimethoxysilane (APTS)	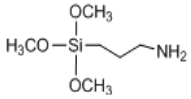
Diethanolamine (DEA)	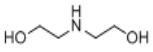	3-aminopropyltriethoxysilane (APTES)	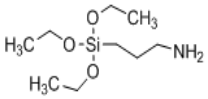
Triethanolamine (TEA)	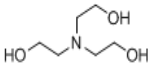	N-[3-(trimethoxysilyl)propyl]-ethylenediamine (AEAPTS)	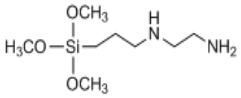
Polyethyleneimine (PEI)	 (R=H for linear, R=H or CHx for branched)	N-[3-(trimethoxysilyl)propyl]-diethylenetriamine (DAEAPTS)	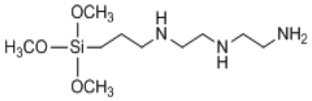
Diethylenetriamine (DETA)	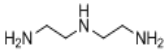	Ethylhydroxyl-aminopropyl-trimethoxyslane (EHAPTS)	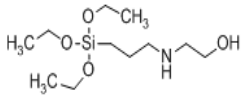
Tetraethylenepentamine (TEPA)	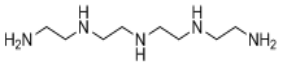	Diethylhydroxyl-aminopropyl-trimethoxyslane (DEHAPTS)	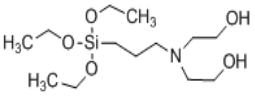
		Cyclic	
Tetraethylenepentamine-acrylonitrile (TEPAN)	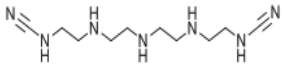	Aziridine	
Pentaethylenehexamine (PEHA)	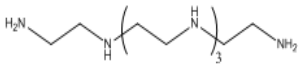	1,8-diazabicyclo[5.4.0]undec-7-ene (DBU)	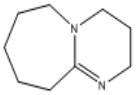
2-Amino-2-methyl-1,3-propanediol (AMPD)	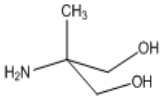	1,5-diazobicyclo [4.3.0]non-5-ene (DBN)	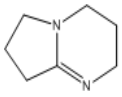
2-(2-Aminoethylamino)ethanol (AEAE)	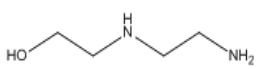	N-methyltetrahydropyrimidine (MTHP)	

2.3.1 Amine Impregnated Sorbents

2.3.1.1 Ordered Mesoporous Supports

The first amine-impregnated silica used to capture CO_2 was reported by Xu et al. in 2002.[64] They used wet impregnation of hydrothermally synthesized MCM-41, a high-surface-area mesoporous silica with cylindrical pores of relatively small diameter (2.8 nm), with PEI to create an adsorbent, termed as "molecular basket".[64-68] In 2003, Xu et al.[65] reported the highest CO_2 adsorption capacity of 3.02 mmol g^{-1} with MCM-41-PEI at a PEI loading of 75 wt% under a pure CO_2 atmosphere at 75 ℃. Increased PEI loadings resulted in higher adsorption of CO_2, as expected. The physical adsorption on the unmodified pore wall of MCM-41 (and the capillary condensation in the mesopores) is negligible, in comparison with the chemical adsorption for higher loadings. In addition, it has been hypothesized that there is a synergetic effect of MCM-41on the PEI for the adsorption of CO_2.[65] The highest synergetic adsorption gain was obtained when the mesoporous pores were loaded with ~50 wt % PEI.

Compared with conventional adsorbents (ACs and zeolites), PEI-impregnated MCM-41 showed an increase in adsorption capacity with increasing temperature. Xu et al.[65] assumed that the low adsorption capacity at low temperature could be a result of low adsorption rate caused by kinetic limitations, and the overall process is kinetically controlled. They also verified that the adsorption capacity at low temperature will be even larger than that high temperature if the adsorption time is sufficiently long to overcome the diffusion limitation.

A series of performance and stability studies using a MCM-41-PEI sorbent was also carried out by Song and his groups[66-68] to separate CO_2 from simulated flue gas, flue gas from a natural gas-fired boiler, and simulated humid flue gas using a packed-bed adsorption column. The adsorbent was tested with simulated flue gas (14.9% CO_2/4.25% O_2/80.85% N_2) at the temperature range of 25 ℃–100 ℃ by Xu et al.[68] The adsorbent showed a separation selectivity of >1000 for CO_2/N_2 and ~180 for CO_2/O_2. The cyclic adsorption/desorption operation indicated that the adsorbent was stable at 75 ℃ after 10 cycles of operation. However, it was not stable when the operation temperature was >100 ℃. NO_x was observed to be adsorbed simultaneously with CO_2, indicating the need for removal of NO_x from flue gas.[66-67]

More recently, a nanoporous SBA-15-supported sorbent with 50 wt% PEI loading was developed by Ma et al.[69] This sorbent showed a sorption capacity of 3.18 mmol g^{-1} at 75 ℃ under a CO_2 partial pressure of 15 kPa. The reported CO_2 adsorption capacity was ~50% higher than that of their previously developed MCM-41-PEI sorbent, possibly due to the higher pore diameter and pore volume of SBA-15. This allows the PEI modified sample prepared from SBA-15 to have a higher surface area for the same PEI loading (50 wt %).

Ahn and co-workers[70] synthesized and studied a series of PEI-loaded (50 wt %) ordered mesoporous silica supports, namely, MCM-41, MCM-48, SBA-15, SBA-16, and KIT-6 to assess their CO_2 adsorption performance. All impregnated sorbents showed faster adsorption kinetics, as well as substantially higher CO_2

sorption capacities and stability, than that of pure PEI. The CO_2 adsorption capacities were found to be in the following order:

KIT-6 (d_p: 6.5 nm)> SBA-15(d_p: 5.5) ≈ SBA-16(d_p: 4.1) >

MCM-48(d_p: 3.1) > MCM-41(d_p: 2.1)

where dp is the average pore diameter (given in nanometers). The performance was proposed to be influenced by the pore diameter and pore arrangement of mesoporous silica materials. Bulky PEI is assumed to be introduced to the pore easily as the pore size in the support increases. The same research group[71] also developed PEI-impregnated silica monoliths showing a hierarchical pore structure as a support. For 5% diluted CO_2 sorption tests, the amine-impregnated monolith with 65% PEI loading exhibited a maximum adsorption capacity of 3.75 mmol g^{-1} at 75 ℃, outperforming the KIT-6/PEI-50, which has been reported to have an adsorption capacity of 1.95 mmol g^{-1} under the same conditions.[70]

Qi et al.[72] proposed a novel high-efficiency CO_2 capture platform obtained using PEI and TEPA supported on specially designed mesoporous capsules. The novel composite sorbent showed excellent CO_2 capture capacity of 6.6 mmol g^{-1} under 1 atm of moisture-free CO_2 at 75 ℃ and exceptional CO_2 capture capacity of 7.9 mmol g^{-1} under simulated humid flue gas with 10% CO_2 at 75 ℃. The CO_2 capture kinetics was found to be relatively fast and attained 90% of the total capacity within the first few minutes. Besides, sorbents could be regenerated below 100 ℃ and exhibited good cyclic stability over repetitive adsorption/regeneration cycle (~50 cycles).

Further studies took into consideration the mode of regeneration and the lifetime of adsorbents during the evaluations of amine-impregnated adsorbents. Drage et al.[73] demonstrated thermal swing desorption for PEI-functionalized proprietary mesoporous silica, using pure CO_2, and reported good cyclic regeneration capacities (2 mmol g^{-1}). A successive loss of adsorption capacity of the sorbent–and, therefore, lifetime of sorbents–was observed over numerous regeneration cycles. It was probably due to the secondary reaction between CO_2 and PEI above 135 ℃ to form a stable product (e.g., urea), which leads to the irreversible degradation of the adsorbents. The use of steam as a stripping gas instead of CO_2 was suggested in overcoming the problems. In addition to the TSA process, Dasgupta et al.[74] investigated a single column five-step PSA option using PEI-impregnated SBA-15 as an adsorbent. A strong adsorptive rinse cycle was suggested for CO_2 recovery during PSA process. Pirngruber et al.[75] concluded that neither the conventional TSA or VSA modes seem to be a viable option for their amine-immobilized sorbents.

In summary, novel amine-impregnated silica supports, as shown in Table 2-4, are promising and can effectively adsorb CO_2 with relatively higher working capacity; even some cases of >4 mmol g^{-1} stipulated industrial requirements for solid sorbents. The modification of pore size of silica support is shown to enhance the adsorption capacity. Moreover, their adsorption capacities are not impaired by the presence of moisture (in many cases, moisture helps to obtain higher capacity). However, the durability and regeneration kinetics of the amine-impregnated solid sorbents have not been tested adequately under real flue gas conditions. Their

desorption kinetics is still slower. Considerable leaching of the amines may be a major drawback for the use of impregnated amine-functionalized sorbents for CO_2.

Table 2-4. CO_2 Adsorption Capacity of Amine Impregnated Solid Sorbents

Support	Amine	Amine Content (wt%)	Adsorption Capacity (Humid) ($mmol.g^{-1}$)	Experimental Conditions		No. of Cycles	Ref.
				Pco_2 (atm)	T (^oC)		
MCM-41	PEI	75	3.02	1	75		64
MCM-41	PEI	50	2.05	0.1	75		64
PE-MCM-41	DEA	77	2.93	0.05	25		76
PE-MCM-41	DEA	73	2.81 (2.89)	0.05	25		76
MCM-41	PEI	50	(3.08)	0.13	75	10	66
MCM-41	TEPA	50	4.54	0.05	75	6	77
SBA-15	TEPA	50	3.23	0.05	75	6	78
SBA-15	PEI	50	3.18	0.15	75		69
SBA-15	PEI	50	1.36	0.12	75		74
SBA-15	APTES		(2.01)	0.10	25		79
KIT-6	PEI	50	1.95	0.05	75		70
Monolith	PEI	65	3.75	0.05	75	5	71
Mesoporous Silica	PEI	40	2.4	1	75		73
MC400/10	TEPA	83	5.57 (7.93)	0.1	75	50	72
R-IAS[b]	E-100[c]		(4.19)	0.10	25		79
PMMA	TEPA	41	(14.03)	0.15	70		80
PMMA	DBU	29	(3.0)	0.10	25	1	81
PMMA	PEI	40	2.40(3.53)	0.10	45		82
SiO_2 (CARiACT)	PEI	40	2.55(3.65)	0.10	45		82
Zeolite 13X	MEA	10	1.0	0.15	30		83
Zeolite Y60	TEPA	50	(4.27)	0.15	60	20	84
β-zeolite	TEPA	38	2.08	0.10	30		85

a. Low molecular weight PEI (MW ~ca. 800)
b. Reformulated immobilized amine sorbent[16]
c. E-100: ethyleneamine

2.3.1.2 Ordered Microporous Supports

In addition to mesoporous materials, mainly including silica-bases solid supports, activated carbons and zeolites have also been used as supports.

Several amine-impregnated solid sorbents were developed by chemical treatment of carbon-enriched fly ash concentrates with various amine groups by Gray et al.,[86] Maroto-Valer and others,[87] and Arenillas et al.[88] A typical comparison of CO_2 adsorption capacities of activated fly ash carbon and its alkanolamine-modified counterparts at various temperatures is shown in Figure 2-4, based on the maximum possible adsorption capacity data reported by Maroto-Valer and others.[87] the nitrogen enrichment of carbonaceous materials is found to be effective in enhancing the specific CO_2–adsorbate interactions. However, the impregnation of amines resulted in a significant decrease of the surface areas, as well as mesopore or micropore volume.[87,89] This is probably due to the pore filling or blockage, because the amine incorporation is assumed to be affected by the molecular size and shape of alkanolamines used, although the mechanismof pore filling is still not well-understood.

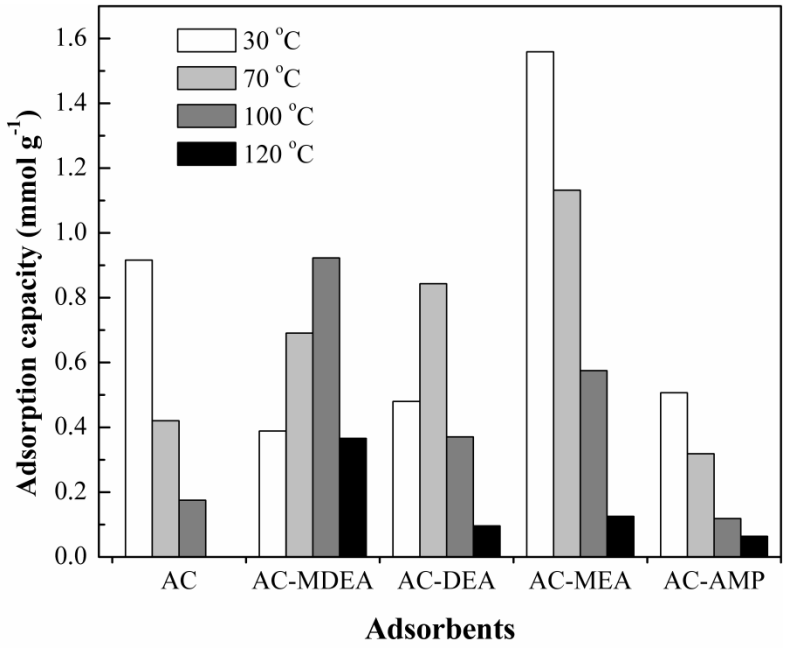

Figure 2-4. CO_2 adsorption capacity of activated fly ash carbon and impregnated fly ash at different temperatures.

Zeolite 13X was modified with MEA by Jadhav et al.[83] via the impregnation method. The aminated zeolites showed improvement in CO_2 adsorption capacity by a factor of ca. 1.6 at 30 ℃. A higher capacity at the temperature of 120 ℃ was obtained with MEA loading of 50 wt %, compared with unmodified zeolite or modified zeolite with low loading level. Unlike at room temperature, where physisorption is dominant, the chemical interaction between CO_2 and amine may be playing a significant role in sorption of CO_2 at 120 ℃, despite reduced pore volume and lower surface area resulted from impregnation. The similar conclusion was also reached by Su et al.[84] They dispersed TEPA into commercially available Y-type zeolite (Si/Al = 60). The CO_2 adsorption capacity reported was 4.27 mmol g^{-1} at 60 ℃ in the presence of 15% CO_2 and 7% water vapor in gas stream. Besides, Fisher et al.[85] employed β-zeolite as a solid support for TEPA impregnation and compared it with TEPA-impregnated silica and

alumina. The TEPA-modified β-zeolite exhibited the CO_2 adsorption capacity up to 2.08 mmol g^{-1} at 30 ℃ under the 10% CO_2/90% argon flow, outperforming TEPA/SiO_2 and TEPA/Al_2O_3 sorbents. It was suggested that the higher capacity of TEPA/β-zeolite could be related to zeolite's high surface area. TEPA/β-zeolite maintained its CO_2 capture capacity for more than 10 adsorption/regeneration cycles.

2.3.2 Amine Grafted Sorbents

Many groups have reported the synthesis and characterization of amine-grafted ordered mesoporous silica sorbents (Class 2 category) for CO_2 capture. Here amine—mainly, amino-silane—is covalently tethered to the silica support.[57]

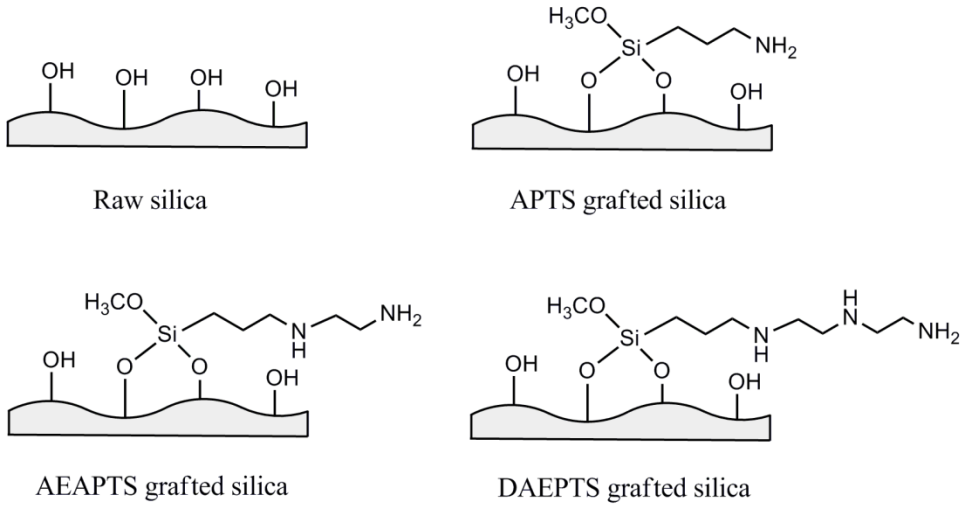

Figure 2-5. Modified hexagonal mesoporous silica (HMS) materials

Leal et al.[90] first described the chemisorption of CO_2 on a APTES grafted surface of silica gel. They confirmed that each molecule of CO_2 uses two surface amino groups to form an ammonium carbamate species in the absence of H_2O and ammonium bicarbonate surface species in the presence of H_2O. However, their sorbent capacity was far below the requirement for industrial application of the

sorbents. Afterward, a series of aminopropyl-functionalized (grafted) hexagonal mesoporous silica (HMS) compounds, as shown in Figure 2-5, was prepared and characterized by Chaffee's group[91-94] to enhance CO_2 adsorption, because of their high porosity. These grafted HMS materials have shown very high surface area with varied concentrations of surface bound amine and hydroxyl functional groups. The modified HMS sorbents have also been shown to reversibly adsorb substantially more CO_2 than modified silica gel.

Based on a systematic investigation on CO_2 adsorption on different mesoporous silica substrates and their amine-functionalized hybrid product, Knowles et al.[91-92,94] also pointed out that the extent of surface functionalization is found to be dependent on substrate morphology (e.g., available surface area, pore geometry, and pore volume), diffusion of reagents to the surface, as well as the silanol concentration on the substrate surface. Their results showed that the higher nitrogen content of the tether leads to a higher CO_2 capacity on the adsorbent surface. The CO_2 adsorption performance of hybrid materials exhibited good adsorption kinetics, reaching equilibrium within 4 min for each sample, and highest CO_2 capacity of ~1.66 mmol g^{-1} at 20 ℃ in dry 90% CO_2/10% argon mixture.[91]

Hiyoshi et al.[95-96] demonstrated the potential application of aminosilane-modified mesoporous silica for the separation of CO_2 from gas streams containing moisture (see Table 2-5). The characterization of the adsorbents showed the significant decrease in the surface area or pore volume after grafting, which was close to the predicted values for each adsorbent. Subsequently, they found that the

DAEAPTS-SBA-15 showed improved CO_2 adsorption capacity after SBA-15 was boiled in water for 2 h, followed by the grafting of aminosilanes. The amount of CO_2 adsorbed reached 1.58 and 1.80 mmol g^{-1} in the absence and presence of water vapor, respectively, under the same experimental conditions. The efficiencies of the aminosilanes at identical amine surface density, were found to be in the following order:

APTES > AEAPTS > DAEAPTS

Gray and co-workers[79,97-99] prepared a series of amine grafted SBA-15 sorbents for CO_2 adsorption. They reported that APTES-grafted SBA-15 could adsorb up to 0.4 mmol g^{-1}, whereas SBA-15 grafted with AEAPTS could adsorb 0.79 mmol g^{-1} at 25 ℃.[97] CO_2 was found to adsorb on the amine sites in the form of bicarbonate and carbonates. Therefore, enhanced CO_2 adsorption capacity was reported in the presence of H_2O, because it helps to form carbonate and bicarbonate, which was confirmed by Khatri et al.[99] Zheng et al.[100] investigated the thermal stability of several grafted SBA-15 and found these to be stable up to 250 ℃. In addition, the SO_2 adsorption on APTES-SBA-15 resulted in a negligible CO_2 adsorption capacity, indicating the necessity of SO_2 removal before amine-based CO_2 adsorption.

Table 2-5. CO_2 Adsorption Capacity of Amine Grafted Solid Sorbents

Support	Amine	Amine Content (mmol. g^{-1})	Adsorption Capacity (Humid[a]) (mmol. g^{-1})	Experimental Conditions		Ref.
				Pco_2 (atm)	T (^oC)	
SBA-15	APTES	2.7	0.52 (0.5)	0.15	60	95
SBA-15	DAEAPTS	5.1	1.1 (1.21)	0.15	60	95
SBA-15	AEAPTS		1.95	1	22	100
SBA-15	APTES		0.4	0.04	25	97
SBA-15	APTES	2.72	1.53	0.1	25	101
SBA-15	Aziridine polymer	9.78	(5.55)	0.1	25	102
SBA-15	Aziridine polymer	7	(3.11)	0.1	25	103
SBA-16	AEAPTS	0.76	1.4	1	27	104
SBA-12	APTES	2.76	1.04	0.1	25	101
MCM-41	APTES	3	0.57	0.1	25	101
PE-MCM-41	DAEAPTS	7.95	2.65	0.05	25	105
PE-MCM-41	DAEAPTS	7.8	2.28	0.05	70	106
MCM-48	APTES	2.3	2.05	1	25	107
MCM-48	APTES	2.3	1.14	0.05	25	107
HMS[b]	APTS	2.29	1.59	0.9	20	92
HMS[b]	DAEAPTS	4.57	1.34	0.9	20	94
MSP[c]	AEAPTS		0.73	0.1	60	108
Silica gel	APTES	1.26	0.89	1	50	90
CNTs	APTES		1.32	0.15	20	109
CNTs	AEAPTS		2.59	0.5	20	12

a. CO_2 adsorption capacity within parentheses indicates humid condition result.
b. Hexagonal mesoporous silica.
c. Mesoporous spherical-silica particles.

As a continuous effort to develop high-capacity, water-tolerant amine-grafted silica-based sorbents with large amine loadings, as well as with large pore volume and pore size, Sayari and coworkers[105-106,110-118] developed pore-expanded MCM-41 mesoporous silica (PE-MCM-41) grafted with amine, such as DAEAPTS. The sorbent was prepared through a post-synthesis hydrothermal treatment of the as-synthesized MCM-41.[110] The DAEAPTS grafted PE-MCM-41 support showed an adsorption capacity of 2.05 mmol g^{-1} at 25 ℃ and 1.0 atm for a dry 5% CO_2 in N_2 feed mixture with amino-silane loading of 5.98 mmol (N) g^{-1}.[111] They showed

that the effect of amine surface density of the sorbent has a strong impact on the adsorption efficiency. However, the presence of moisture did not significantly enhance the performance of the amine-impregnated PE-MCM-41 sorbents as expected toward the bicarbonate formation pathway.

Subsequently, Harlick and Sayari[105] also focused on optimizing the grafting conditions and concluded that, in comparison to the dry grafting procedure, wet grafting via the co-addition of water at 85 ℃ showed an increase in the total amine content, resulting in a 90% overall improvement. They found that, through regeneration under a vacuum at 70 ℃, the sorbent showed good stability over 100 cycles with an average working adsorption capacity of 2.28 mmol g^{-1} for pure CO_2,[106] while the temperature swing regeneration process was suitable only above 120 ℃.[116] In addition to thermal stability, it also showed infinitely high selectivity for CO_2 over N_2 and O_2.[114,116-117]

A novel covalently tethered hyperbranched aminosilica (HAS) sorbent (Figure 2-6) with high amine content capable of capturing CO_2 reversibly from flue gas was developed and compared with other covalently supported solid sorbents by Jones and his research group.[102-103] HAS was synthesized via a one-step surface polymerization reaction of aziridine monomer inside SBA-15 pores. The HAS sorbent had an amine loading of 7.0 mmol (N) g^{-1} and CO_2 adsorption capacity of 3.08 mmol g^{-1} when tested in a packed-bed reactor under a flow of 10% CO_2/90% argon saturated with water at 25 ℃. It was stable over 12 cycles with regeneration at 130 ℃. Following their early research work, Drese et al.[102] proposed modification of the HAS synthesis conditions, such as the aziridine-to-silica ratio

and the solvent to further tune the sorbent's composition, adsorbent capacity, and kinetics. They found that higher amine loadings—and, therefore, higher potential active adsorption sites—contributed to a better adsorption capacity.

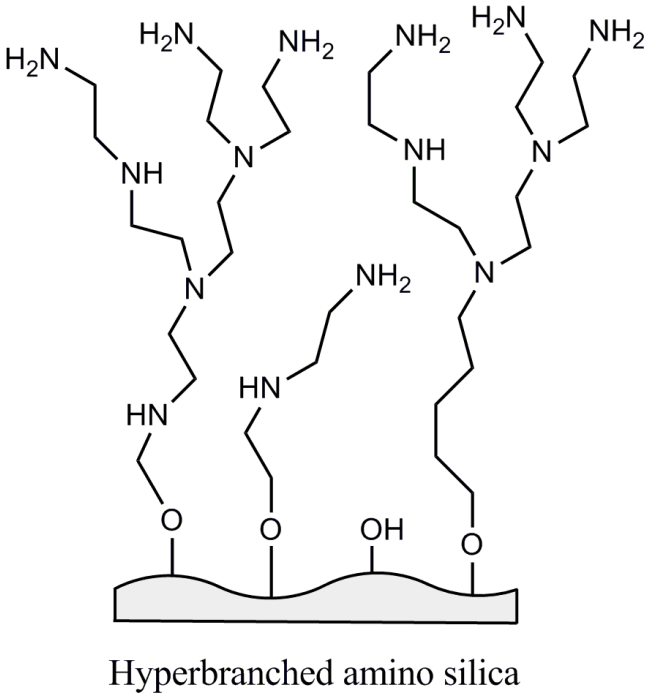

Figure 2-6. Hyperbranched amino silica.

Activated carbon and zeolite-based sorbents without any nitrogen functionality are low cost with fast adsorption kinetics and require low regeneration energy. However, this review identifies that CO_2 adsorption on these sorbents is strongly influenced by the temperature, pressure, and presence of moisture. Metal-organic frameworks (MOFs) as sorbents for post-combustion CO_2 capture are expected to have very high adsorption capacity but require substantial research efforts to be suitable under flue gas conditions. Use of these sorbents for CO_2 adsorption is further limited by the CO_2/N_2 selectivity. In contrast to sorbents based on physisorption, amine functionalized adsorbents have shown promise in working

capacity in simulated flue gas conditions and are stable over multiple cycles. Several of the sorbents tested have theoretical regeneration energies that are significantly lower than that of the industry benchmark. However, additional work is needed to address several important key characteristics for amine functionalized adsorbents, such as kinetic data for CO_2 adsorption and desorption, effect of flue gas components, long-term stability and consistent performance of these sorbents under flue gas conditions through bench-scale and pilot-scale studies before commercialization.

2.4 Objectives

In view of these above, more efforts in this study were focused on the development of amine functionalized SBA-15 sorbent and its CO_2 adsorption performance for post-combustion CO_2 capture. The aim of this work is to conduct research in developing effective and viable solid adsorbents with high CO_2 capacity and fast adsorption kinetics, etc. for post-combustion carbon capture from flue gases. The specific objectives of this study include the following:

1. Screening the CO_2 adsorption performance of various potential adsorbents;
2. Synthesizing and characterizing the mesoporous SBA-15 sorbent and amine functionalized adsorbent for CO_2 capture;
3. Determining the optimal conditions of adsorbent development and adsorption performance of the sorbents for CO_2 capture using amine functionalized SBA-15 adsorbent;

4. Investigating the scale-up of CO_2 adsorption in a fixed-bed reactor under simulated flue gas environment;
5. Developing kinetic model to describe the CO_2 adsorption phenomena on amine functionalized SBA-15 adsorbent.

References

1. D'Alessandro, D. M.; Smit, B.; Long, J. R., Carbon Dioxide Capture: Prospects for New Materials. *Angewandte Chemie International Edition* **2010,** *49* (35), 6058-6082.

2. Lozano-Castelló, D.; Cazorla-Amorós, D.; Linares-Solano, A., Powdered Activated Carbons and Activated Carbon Fibers for Methane Storage: A Comparative Study. *Energy & Fuels* **2002,** *16* (5), 1321-1328.

3. Davini, P., Flue gas treatment by activated carbon obtained from oil-fired fly ash. *Carbon* **2002,** *40* (11), 1973-1979.

4. Maroto-Valer, M. M.; Tang, Z.; Zhang, Y., CO_2 capture by activated and impregnated anthracites. *Fuel Processing Technology* **2005,** *86* (14–15), 1487-1502.

5. Wang, Y.; Zhou, Y.; Liu, C.; Zhou, L., Comparative studies of CO_2 and CH_4 sorption on activated carbon in presence of water. *Colloids and Surfaces A: Physicochemical and Engineering Aspects* **2008,** *322* (1–3), 14-18.

6. Dreisbach, F.; Staudt, R.; Keller, J. U., High Pressure Adsorption Data of Methane, Nitrogen, Carbon Dioxide and their Binary and Ternary Mixtures on Activated Carbon. *Adsorption* **1999,** *5* (3), 215-227.

7. Himeno, S.; Komatsu, T.; Fujita, S., High-Pressure Adsorption Equilibria of Methane and Carbon Dioxide on Several Activated Carbons. *Journal of Chemical & Engineering Data* **2005,** *50* (2), 369-376.

8. Kikkinides, E. S.; Yang, R. T.; Cho, S. H., Concentration and recovery of carbon dioxide from flue gas by pressure swing adsorption. *Industrial & Engineering Chemistry Research* **1993,** *32* (11), 2714-2720.

9. Sun, Y.; Wang, Y.; Zhang, Y.; Zhou, Y.; Zhou, L., CO_2 sorption in activated carbon in the presence of water. *Chemical Physics Letters* **2007,** *437* (1–3), 14-16.

10. Lu, C.; Bai, H.; Wu, B.; Su, F.; Hwang, J. F., Comparative Study of CO_2 Capture by Carbon Nanotubes, Activated Carbons, and Zeolites. *Energy & Fuels* **2008,** *22* (5), 3050-3056.

11. Cinke, M.; Li, J.; Bauschlicher Jr, C. W.; Ricca, A.; Meyyappan, M., CO_2 adsorption in single-walled carbon nanotubes. *Chemical Physics Letters* **2003,** *376* (5–6), 761-766.

12. Su, F.; Lu, C.; Cnen, W.; Bai, H.; Hwang, J. F., Capture of CO_2 from flue gas via multiwalled carbon nanotubes. *Science of The Total Environment* **2009,** *407* (8), 3017-3023.

13. Burchell, T. D.; Judkins, R. R.; Rogers, M. R.; Williams, A. M., A novel process and material for the separation of carbon dioxide and hydrogen sulfide gas mixtures. *Carbon* **1997,** *35* (9), 1279-1294.

14. Berlier, K.; Frère, M., Adsorption of CO_2 on Activated Carbon: Simultaneous Determination of Integral Heat and Isotherm of Adsorption. *Journal of Chemical & Engineering Data* **1996,** *41* (5), 1144-1148.

15. Siriwardane, R. V.; Shen, M.-S.; Fisher, E. P.; Poston, J. A., Adsorption of CO_2 on Molecular Sieves and Activated Carbon. *Energy & Fuels* **2001,** *15* (2), 279-284.

16. Chue, K. T.; Kim, J. N.; Yoo, Y. J.; Cho, S. H.; Yang, R. T., Comparison of Activated Carbon and Zeolite 13X for CO_2 Recovery from Flue Gas by Pressure Swing Adsorption. *Industrial & Engineering Chemistry Research* **1995,** *34* (2), 591-598.

17. Dong, F.; Lou, H.; Kodama, A.; Goto, M.; Hirose, T., The Petlyuk PSA process for the separation of ternary gas mixtures: exemplification by separating a mixture of CO_2–CH_4–N_2. *Separation and Purification Technology* **1999,** *16* (2), 159-166.

18. Na, B.-K.; Koo, K.-K.; Eum, H.-M.; Lee, H.; Song, H., CO_2 recovery from flue gas by PSA process using activated carbon. *Korean Journal of Chemical Engineering* **2001,** *18* (2), 220-227.

19. Sayari, A.; Belmabkhout, Y.; Serna-Guerrero, R., Flue gas treatment via CO_2 adsorption. *Chemical Engineering Journal* **2011,** *171* (3), 760-774.

20. Zhou, W.; Bai, X.; Wang, E.; Xie, S., Synthesis, Structure, and Properties of Single-Walled Carbon Nanotubes. *Advanced Materials* **2009,** *21* (45), 4565-4583.

21. Huang, L.; Zhang, L.; Shao, Q.; Lu, L.; Lu, X.; Jiang, S.; Shen, W., Simulations of Binary Mixture Adsorption of Carbon Dioxide and Methane in Carbon Nanotubes: Temperature, Pressure, and Pore Size Effects. *The Journal of Physical Chemistry C* **2007,** *111* (32), 11912-11920.

22. Razavi, S.; Hashemianzadeh, S.; Karimi, H., Modeling the adsorptive selectivity of carbon nanotubes for effective separation of CO_2/N_2 mixtures. *Journal of Molecular Modeling* **2011,** *17* (5), 1163-1172.

23. Coe, C., Structural Effects on the Adsorptive Properties of Molecular Sieves for Air Separation

Access in Nanoporous Materials. Pinnavaia, T.; Thorpe, M., Eds. Springer US: 2002; pp 213-229.

24. Foley, H. C., Carbogenic molecular sieves: synthesis, properties and applications. *Microporous Materials* **1995,** *4* (6), 407-433.

25. Rutherford, S. W.; Do, D. D., Adsorption dynamics of carbon dioxide on a carbon molecular sieve 5A. *Carbon* **2000,** *38* (9), 1339-1350.

26. Alcañiz-Monge, J.; Marco-Lozar, J. P.; Lillo-Ródenas, M. Á., CO_2 separation by carbon molecular sieve monoliths prepared from nitrated coal tar pitch. *Fuel Processing Technology* **2011,** *92* (5), 915-919.

27. Maesen, T., Chapter 1 The zeolite scene — an overview. In *Studies in Surface Science and Catalysis*, Jiří Čejka, H. v. B. A. C.; Ferdi, S., Eds. Elsevier: 2007; Vol. Volume 168, pp 1-12.

28. Coriani, S.; Halkier, A.; Rizzo, A.; Ruud, K., On the molecular electric quadrupole moment and the electric-field-gradient-induced birefringence of CO_2 and CS_2. *Chemical Physics Letters* **2000,** *326* (3–4), 269-276.

29. Barrer, R. M.; Gibbons, R. M., Zeolitic carbon dioxide: energetics and equilibria in relation to exchangeable cations in faujasite. *Transactions of the Faraday Society* **1965,** *61*, 948-961.

30. Walton, K. S.; Abney, M. B.; Douglas LeVan, M., CO_2 adsorption in Y and X zeolites modified by alkali metal cation exchange. *Microporous and Mesoporous Materials* **2006,** *91* (1–3), 78-84.

31. Maurin, G.; Llewellyn, P. L.; Bell, R. G., Adsorption Mechanism of Carbon Dioxide in Faujasites: Grand Canonical Monte Carlo Simulations and Microcalorimetry Measurements. *The Journal of Physical Chemistry B* **2005,** *109* (33), 16084-16091.

32. Harlick, P. J. E.; Tezel, F. H., An experimental adsorbent screening study for CO_2 removal from N_2. *Microporous and Mesoporous Materials* **2004,** *76* (1–3), 71-79.

33. Brandani, F.; Ruthven, D. M., The Effect of Water on the Adsorption of CO_2 and C_3H_8 on Type X Zeolites. *Industrial & Engineering Chemistry Research* **2004,** *43* (26), 8339-8344.

34. Cavenati, S.; Grande, C. A.; Rodrigues, A. E., Adsorption Equilibrium of Methane, Carbon Dioxide, and Nitrogen on Zeolite 13X at High Pressures. *Journal of Chemical & Engineering Data* **2004,** *49* (4), 1095-1101.

35. Diaz, E.; Munoz, E.; Vega, A.; Ordonez, S., Enhancement of the CO_2 Retention Capacity of Y Zeolites by Na and Cs Treatments: Effect of Adsorption Temperature and Water Treatment. *Industrial & Engineering Chemistry Research* **2008,** *47* (2), 412-418.

36. Díaz, E.; Muñoz, E.; Vega, A.; Ordóñez, S., Enhancement of the CO_2 retention capacity of X zeolites by Na^+ and Cs^+ treatments. *Chemosphere* **2008,** *70* (8), 1375-1382.

37. Goj, A.; Sholl, D. S.; Akten, E. D.; Kohen, D., Atomistic Simulations of CO_2 and N_2 Adsorption in Silica Zeolites: The Impact of Pore Size and Shape†. *The Journal of Physical Chemistry B* **2002,** *106* (33), 8367-8375.

38. Gomes, V. G.; Yee, K. W. K., Pressure swing adsorption for carbon dioxide sequestration from exhaust gases. *Separation and Purification Technology* **2002,** *28* (2), 161-171.

39. Hernández-Huesca, R.; Díaz, L.; Aguilar-Armenta, G., Adsorption equilibria and kinetics of CO_2, CH_4 and N_2 in natural zeolites. *Separation and Purification Technology* **1999,** *15* (2), 163-173.

40. Inui, T.; Okugawa, Y.; Yasuda, M., Relationship between properties of various zeolites and their carbon dioxide adsorption behaviors in pressure swing adsorption operation. *Industrial & Engineering Chemistry Research* **1988,** *27* (7), 1103-1109.

41. Katoh, M.; Yoshikawa, T.; Tomonari, T.; Katayama, K.; Tomida, T., Adsorption Characteristics of Ion-Exchanged ZSM-5 Zeolites for CO_2/N_2 Mixtures. *Journal of Colloid and Interface Science* **2000,** *226* (1), 145-150.

42. Khelifa, A.; Benchehida, L.; Derriche, Z., Adsorption of carbon dioxide by X zeolites exchanged with Ni^{2+} and Cr^{3+}: isotherms and isosteric heat. *Journal of Colloid and Interface Science* **2004,** *278* (1), 9-17.

43. Ko, D.; Siriwardane, R.; Biegler, L. T., Optimization of a Pressure-Swing Adsorption Process Using Zeolite 13X for CO_2 Sequestration. *Industrial & Engineering Chemistry Research* **2003,** *42* (2), 339-348.

44. Konduru, N.; Lindner, P.; Assaf-Anid, N. M., Curbing the greenhouse effect by carbon dioxide adsorption with Zeolite 13X. *AIChE Journal* **2007,** *53* (12), 3137-3143.

45. Li, G.; Xiao, P.; Webley, P.; Zhang, J.; Singh, R.; Marshall, M., Capture of CO_2 from high humidity flue gas by vacuum swing adsorption with zeolite 13X. *Adsorption* **2008,** *14* (2), 415-422.

46. Merel, J.; Clausse, M.; Meunier, F., Experimental Investigation on CO_2 Post−Combustion Capture by Indirect Thermal Swing Adsorption Using 13X and 5A Zeolites. *Industrial & Engineering Chemistry Research* **2008,** *47* (1), 209-215.

47. Siriwardane, R. V.; Shen, M.-S.; Fisher, E. P., Adsorption of CO_2, N_2, and O_2 on Natural Zeolites. *Energy & Fuels* **2003,** *17* (3), 571-576.

48. Zhang, J.; Singh, R.; Webley, P. A., Alkali and alkaline-earth cation exchanged chabazite zeolites for adsorption based CO_2 capture. *Microporous and Mesoporous Materials* **2008,** *111* (1–3), 478-487.

49. Zhang, Z.; Zhang, W.; Chen, X.; Xia, Q.; Li, Z., Adsorption of CO_2 on Zeolite 13X and Activated Carbon with Higher Surface Area. *Separation Science and Technology* **2010,** *45* (5), 710-719.

50. Zukal, A.; Mayerová, J.; Kubů, M., Adsorption of Carbon Dioxide on High-Silica Zeolites with Different Framework Topology. *Topics in Catalysis* **2010,** *53* (19), 1361-1366.

51. Zukal, A.; Pawlesa, J.; Čejka, J., Isosteric heats of adsorption of carbon dioxide on zeolite MCM-22 modified by alkali metal cations. *Adsorption* **2009,** *15* (3), 264-270.

52. Kamiuto, K.; Abe, S.; Ermalina, Effect of desorption temperature on CO_2 adsorption equilibria of the honeycomb zeolite beds. *Applied Energy* **2002,** *72* (3–4), 555-564.

53. Choudhary, V. R.; Mayadevi, S.; Singh, A. P., Sorption isotherms of methane, ethane, ethene and carbon dioxide on NaX, NaY and Na-mordenite zeolites. *Journal of the Chemical Society, Faraday Transactions* **1995,** *91* (17), 2935-2944.

54. Dunne, J. A.; Mariwala, R.; Rao, M.; Sircar, S.; Gorte, R. J.; Myers, A. L., Calorimetric Heats of Adsorption and Adsorption Isotherms. 1. O_2, N_2, Ar, CO_2, CH_4, C_2H_6, and SF_6 on Silicalite. *Langmuir* **1996,** *12* (24), 5888-5895.

55. Harlick, P. J. E.; Tezel, F. H., Adsorption of carbon dioxide, methane and nitrogen: pure and binary mixture adsorption for ZSM-5 with SiO_2/Al_2O_3 ratio of 280. *Separation and Purification Technology* **2003,** *33* (2), 199-210.

56. Maurin, G.; Belmabkhout, Y.; Pirngruber, G.; Gaberova, L.; Llewellyn, P., CO_2 adsorption in LiY and NaY at high temperature: molecular simulations compared to experiments. *Adsorption* **2007,** *13* (5), 453-460.

57. Choi, S.; Drese, J. H.; Jones, C. W., Adsorbent Materials for Carbon Dioxide Capture from Large Anthropogenic Point Sources. *ChemSusChem* **2009,** *2* (9), 796-854.

58. Zhang, J.; Webley, P. A., Cycle Development and Design for CO_2 Capture from Flue Gas by Vacuum Swing Adsorption. *Environmental Science & Technology* **2008,** *42* (2), 563-569.

59. Li, J.-R.; Kuppler, R. J.; Zhou, H.-C., Selective gas adsorption and separation in metal-organic frameworks. *Chemical Society Reviews* **2009,** *38* (5), 1477-1504.

60. Yazaydın, A. O. z. r.; Benin, A. I.; Faheem, S. A.; Jakubczak, P.; Low, J. J.; Willis, R. R.; Snurr, R. Q., Enhanced CO_2 Adsorption in Metal-Organic Frameworks via Occupation of Open-Metal Sites by Coordinated Water Molecules. *Chemistry of Materials* **2009,** *21* (8), 1425-1430.

61. Liu, J.; Wang, Y.; Benin, A. I.; Jakubczak, P.; Willis, R. R.; LeVan, M. D., CO_2/H_2O Adsorption Equilibrium and Rates on Metal−Organic Frameworks: HKUST-1 and Ni/DOBDC. *Langmuir* **2010,** *26* (17), 14301-14307.

62. Li, W.; Choi, S.; Drese, J. H.; Hornbostel, M.; Krishnan, G.; Eisenberger, P. M.; Jones, C. W., Steam-Stripping for Regeneration of Supported Amine-Based CO_2 Adsorbents. *ChemSusChem* **2010,** *3* (8), 899-903.

63. Samanta, A.; Zhao, A.; Shimizu, G. K. H.; Sarkar, P.; Gupta, R., Post-Combustion CO_2 Capture Using Solid Sorbents: A Review. *Industrial & Engineering Chemistry Research* **2012,** *51* (4), 1438-1463.

64. Xu, X.; Song, C.; Andresen, J. M.; Miller, B. G.; Scaroni, A. W., Novel Polyethylenimine-Modified Mesoporous Molecular Sieve of MCM-41 Type as High-Capacity Adsorbent for CO_2 Capture. *Energy & Fuels* **2002,** *16* (6), 1463-1469.

65. Xu, X.; Song, C.; Andrésen, J. M.; Miller, B. G.; Scaroni, A. W., Preparation and characterization of novel CO_2 "molecular basket" adsorbents based on polymer-modified mesoporous molecular sieve MCM-41. *Microporous and Mesoporous Materials* **2003,** *62* (1–2), 29-45.

66. Xu, X.; Song, C.; Miller, B. G.; Scaroni, A. W., Influence of Moisture on CO_2 Separation from Gas Mixture by a Nanoporous Adsorbent Based on Polyethylenimine-Modified Molecular Sieve MCM-41. *Industrial & Engineering Chemistry Research* **2005,** *44* (21), 8113-8119.

67. Xu, X.; Song, C.; Miller, B. G.; Scaroni, A. W., Adsorption separation of carbon dioxide from flue gas of natural gas-fired boiler by a novel nanoporous "molecular basket" adsorbent. *Fuel Processing Technology* **2005,** *86* (14–15), 1457-1472.

68. Xu, X.; Song, C.; Andresen, J. M.; Miller, B. G.; Scaroni, A. W., Adsorption separation of CO_2 from simulated flue gas mixtures by novel CO_2 "molecular basket" adsorbents. *International Journal of Environmental Technology and Management* **2004,** *4* (1), 32-52.

69. Ma, X.; Wang, X.; Song, C., "Molecular Basket" Sorbents for Separation of CO_2 and H_2S from Various Gas Streams. *Journal of the American Chemical Society* **2009,** *131* (16), 5777-5783.

70. Son, W.-J.; Choi, J.-S.; Ahn, W.-S., Adsorptive removal of carbon dioxide using polyethyleneimine-loaded mesoporous silica materials. *Microporous and Mesoporous Materials* **2008,** *113* (1–3), 31-40.

71. Chen, C.; Yang, S.-T.; Ahn, W.-S.; Ryoo, R., Amine-impregnated silica monolith with a hierarchical pore structure: enhancement of CO_2 capture capacity. *Chemical Communications* **2009,** (24), 3627-3629.

72. Qi, G.; Wang, Y.; Estevez, L.; Duan, X.; Anako, N.; Park, A.-H. A.; Li, W.; Jones, C. W.; Giannelis, E. P., High efficiency nanocomposite sorbents for CO_2 capture based on amine-functionalized mesoporous capsules. *Energy & Environmental Science* **2011,** *4* (2), 444-452.

73. Drage, T. C.; Arenillas, A.; Smith, K. M.; Snape, C. E., Thermal stability of polyethylenimine based carbon dioxide adsorbents and its influence on selection of regeneration strategies. *Microporous and Mesoporous Materials* **2008,** *116* (1–3), 504-512.

74. Dasgupta, S.; Nanoti, A.; Gupta, P.; Jena, D.; Goswami, A. N.; Garg, M. O., Carbon Di-Oxide Removal with Mesoporous Adsorbents in a Single Column Pressure Swing Adsorber. *Separation Science and Technology* **2009,** *44* (16), 3973-3983.

75. Pirngruber, G. D.; Cassiano-Gaspar, S.; Louret, S.; Chaumonnot, A.; Delfort, B., Amines immobilized on a solid support for postcombustion CO_2 capture–A preliminary analysis of the performance in a VSA or TSA process based on the adsorption isotherms and kinetic data. *Energy Procedia* **2009,** *1* (1), 1335-1342.

76. Franchi, R. S.; Harlick, P. J. E.; Sayari, A., Applications of Pore-Expanded Mesoporous Silica. 2. Development of a High-Capacity, Water-Tolerant Adsorbent for CO_2. *Industrial & Engineering Chemistry Research* **2005,** *44* (21), 8007-8013.

77. Yue, M. B.; Sun, L. B.; Cao, Y.; Wang, Y.; Wang, Z. J.; Zhu, J. H., Efficient CO2 Capturer Derived from As-Synthesized MCM-41 Modified with Amine. *Chemistry – A European Journal* **2008,** *14* (11), 3442-3451.

78. Yue, M. B.; Chun, Y.; Cao, Y.; Dong, X.; Zhu, J. H., CO_2 Capture by As-Prepared SBA-15 with an Occluded Organic Template. *Advanced Functional Materials* **2006,** *16* (13), 1717-1722.

79. Gray, M. L.; Soong, Y.; Champagne, K. J.; Pennline, H.; Baltrus, J. P.; Stevens Jr, R. W.; Khatri, R.; Chuang, S. S. C.; Filburn, T., Improved immobilized carbon dioxide capture sorbents. *Fuel Processing Technology* **2005,** *86* (14–15), 1449-1455.

80. Lee, S.; Filburn, T. P.; Gray, M.; Park, J.-W.; Song, H.-J., Screening Test of Solid Amine Sorbents for CO_2 Capture. *Industrial & Engineering Chemistry Research* **2008,** *47* (19), 7419-7423.

81. Gray, M. L.; Champagne, K. J.; Fauth, D.; Baltrus, J. P.; Pennline, H., Performance of immobilized tertiary amine solid sorbents for the capture of carbon dioxide. *International Journal of Greenhouse Gas Control* **2008,** *2* (1), 3-8.

82. Gray, M. L.; Hoffman, J. S.; Hreha, D. C.; Fauth, D. J.; Hedges, S. W.; Champagne, K. J.; Pennline, H. W., Parametric Study of Solid Amine Sorbents for the Capture of Carbon Dioxide†. *Energy & Fuels* **2009,** *23* (10), 4840-4844.

83. Jadhav, P. D.; Chatti, R. V.; Biniwale, R. B.; Labhsetwar, N. K.; Devotta, S.; Rayalu, S. S., Monoethanol Amine Modified Zeolite 13X for CO_2 Adsorption at Different Temperatures. *Energy & Fuels* **2007,** *21* (6), 3555-3559.

84. Su, F.; Lu, C.; Kuo, S.-C.; Zeng, W., Adsorption of CO_2 on Amine-Functionalized Y-Type Zeolites. *Energy & Fuels* **2010,** *24* (2), 1441-1448.

85. Fisher, J. C.; Tanthana, J.; Chuang, S. S. C., Oxide-supported tetraethylenepentamine for CO_2 capture. *Environmental Progress & Sustainable Energy* **2009,** *28* (4), 589-598.

86. Gray, M. L.; Soong, Y.; Champagne, K. J.; Baltrus, J.; Stevens Jr, R. W.; Toochinda, P.; Chuang, S. S. C., CO_2 capture by amine-enriched fly ash carbon sorbents. *Separation and Purification Technology* **2004,** *35* (1), 31-36.

87. Maroto-Valer, M.; Lu, Z.; Zhang, Y.; Tang, Z., Sorbents for CO_2 capture from high carbon fly ashes. *Waste Management* **2008,** *28* (11), 2320-2328.

88. Arenillas, A.; Smith, K. M.; Drage, T. C.; Snape, C. E., CO_2 capture using some fly ash-derived carbon materials. *Fuel* **2005,** *84* (17), 2204-2210.

89. Plaza, M. G.; Pevida, C.; Arenillas, A.; Rubiera, F.; Pis, J. J., CO_2 capture by adsorption with nitrogen enriched carbons. *Fuel* **2007,** *86* (14), 2204-2212.

90. Leal, O.; Bolívar, C.; Ovalles, C.; García, J. J.; Espidel, Y., Reversible adsorption of carbon dioxide on amine surface-bonded silica gel. *Inorganica Chimica Acta* **1995,** *240* (1–2), 183-189.

91. Knowles, G. P.; Delaney, S. W.; Chaffee, A. L., Amine-functionalised mesoporous silicas as CO_2 adsorbents. In *Studies in Surface Science and Catalysis*, Abdelhamid, S.; Mietek, J., Eds. Elsevier: 2005; Vol. Volume 156, pp 887-896.

92. Knowles, G. P.; Graham, J. V.; Delaney, S. W.; Chaffee, A. L., Aminopropyl-functionalized mesoporous silicas as CO_2 adsorbents. *Fuel Processing Technology* **2005,** *86* (14–15), 1435-1448.

93. Chaffee, A. L., Molecular modeling of HMS hybrid materials for CO_2 adsorption. *Fuel Processing Technology* **2005,** *86* (14–15), 1473-1486.

94. Knowles, G. P.; Delaney, S. W.; Chaffee, A. L., Diethylenetriamine[propyl(silyl)]-Functionalized (DT) Mesoporous Silicas as CO_2 Adsorbents. *Industrial & Engineering Chemistry Research* **2006,** *45* (8), 2626-2633.

95. Hiyoshi, N.; Yogo, K.; Yashima, T., Adsorption of Carbon Dioxide on Amine Modified SBA-15 in the Presence of Water Vapor. *Chemistry Letters* **2004,** *33* (5), 510-511.

96. Hiyoshi, N.; Yogo, K.; Yashima, T., Adsorption characteristics of carbon dioxide on organically functionalized SBA-15. *Microporous and Mesoporous Materials* **2005,** *84* (1–3), 357-365.

97. Chang, A. C. C.; Chuang, S. S. C.; Gray, M.; Soong, Y., In-Situ Infrared Study of CO_2 Adsorption on SBA-15 Grafted with γ-(Aminopropyl)triethoxysilane. *Energy & Fuels* **2003,** *17* (2), 468-473.

98. Khatri, R. A.; Chuang, S. S. C.; Soong, Y.; Gray, M., Carbon Dioxide Capture by Diamine-Grafted SBA-15: A Combined Fourier Transform Infrared and Mass Spectrometry Study. *Industrial & Engineering Chemistry Research* **2005,** *44* (10), 3702-3708.

99. Khatri, R. A.; Chuang, S. S. C.; Soong, Y.; Gray, M., Thermal and Chemical Stability of Regenerable Solid Amine Sorbent for CO_2 Capture. *Energy & Fuels* **2006,** *20* (4), 1514-1520.

100. Zheng, F.; Tran, D. N.; Busche, B. J.; Fryxell, G. E.; Addleman, R. S.; Zemanian, T. S.; Aardahl, C. L., Ethylenediamine-Modified SBA-15 as Regenerable CO_2 Sorbent. *Industrial & Engineering Chemistry Research* **2005,** *44* (9), 3099-3105.

101. Zeleňák, V.; Badaničová, M.; Halamová, D.; Čejka, J.; Zukal, A.; Murafa, N.; Goerigk, G., Amine-modified ordered mesoporous silica: Effect of pore size on carbon dioxide capture. *Chemical Engineering Journal* **2008,** *144* (2), 336-342.

102. Drese, J. H.; Choi, S.; Lively, R. P.; Koros, W. J.; Fauth, D. J.; Gray, M. L.; Jones, C. W., Synthesis–Structure–Property Relationships for Hyperbranched Aminosilica CO_2 Adsorbents. *Advanced Functional Materials* **2009,** *19* (23), 3821-3832.

103. Hicks, J. C.; Drese, J. H.; Fauth, D. J.; Gray, M. L.; Qi, G.; Jones, C. W., Designing Adsorbents for CO_2 Capture from Flue Gas-Hyperbranched Aminosilicas Capable of Capturing CO_2 Reversibly. *Journal of the American Chemical Society* **2008,** *130* (10), 2902-2903.

104. Knöfel, C.; Descarpentries, J.; Benzaouia, A.; Zeleňák, V.; Mornet, S.; Llewellyn, P. L.; Hornebecq, V., Functionalised micro-/mesoporous silica for the adsorption of carbon dioxide. *Microporous and Mesoporous Materials* **2007,** *99* (1–2), 79-85.

105. Harlick, P. J. E.; Sayari, A., Applications of Pore-Expanded Mesoporous Silica. 5. Triamine Grafted Material with Exceptional CO_2 Dynamic and Equilibrium Adsorption Performance. *Industrial & Engineering Chemistry Research* **2006,** *46* (2), 446-458.

106. Serna-Guerrero, R.; Belmabkhout, Y.; Sayari, A., Influence of regeneration conditions on the cyclic performance of amine-grafted mesoporous silica for CO_2 capture: An experimental and statistical study. *Chemical Engineering Science* **2010,** *65* (14), 4166-4172.

107. Huang, H. Y.; Yang, R. T.; Chinn, D.; Munson, C. L., Amine-Grafted MCM-48 and Silica Xerogel as Superior Sorbents for Acidic Gas Removal from Natural Gas. *Industrial & Engineering Chemistry Research* **2002,** *42* (12), 2427-2433.

108. Lu, C.; Su, F.; Hsu, S.-C.; Chen, W.; Bai, H.; Hwang, J. F.; Lee, H.-H., Thermodynamics and regeneration of CO2 adsorption on mesoporous spherical-silica particles. *Fuel Processing Technology* **2009,** *90* (12), 1543-1549.

109. Hsu, S.-C.; Lu, C.; Su, F.; Zeng, W.; Chen, W., Thermodynamics and regeneration studies of CO2 adsorption on multiwalled carbon nanotubes. *Chemical Engineering Science* **2010,** *65* (4), 1354-1361.

110. Sayari, A.; Hamoudi, S.; Yang, Y., Applications of Pore-Expanded Mesoporous Silica. 1. Removal of Heavy Metal Cations and Organic Pollutants from Wastewater. *Chemistry of Materials* **2004,** *17* (1), 212-216.

111. Harlick, P. J. E.; Sayari, A., Applications of Pore-Expanded Mesoporous Silicas. 3. Triamine Silane Grafting for Enhanced CO_2 Adsorption. *Industrial & Engineering Chemistry Research* **2006,** *45* (9), 3248-3255.

112. Serna-Guerrero, R.; Da'na, E.; Sayari, A., New Insights into the Interactions of CO_2 with Amine-Functionalized Silica. *Industrial & Engineering Chemistry Research* **2008,** *47* (23), 9406-9412.

113. Belmabkhout, Y.; Serna-Guerrero, R.; Sayari, A., Adsorption of from dry gases on MCM-41 silica at ambient temperature and high pressure. 1: Pure adsorption. *Chemical Engineering Science* **2009,** *64* (17), 3721-3728.

114. Belmabkhout, Y.; Serna-Guerrero, R.; Sayari, A., Adsorption of CO_2-Containing Gas Mixtures over Amine-Bearing Pore-Expanded MCM-41 Silica: Application for Gas Purification. *Industrial & Engineering Chemistry Research* **2009,** *49* (1), 359-365.

115. Serna-Guerrero, R.; Belmabkhout, Y.; Sayari, A., Triamine-grafted pore-expanded mesoporous silica for CO_2 capture: Effect of moisture and adsorbent regeneration strategies. *Adsorption* **2010,** *16* (6), 567-575.

116. Serna-Guerrero, R.; Belmabkhout, Y.; Sayari, A., Further investigations of CO_2 capture using triamine-grafted pore-expanded mesoporous silica. *Chemical Engineering Journal* **2010,** *158* (3), 513-519.

117. Belmabkhout, Y.; Sayari, A., Isothermal versus Non-isothermal Adsorption−Desorption Cycling of Triamine-Grafted Pore-Expanded MCM-41 Mesoporous Silica for CO_2 Capture from Flue Gas. *Energy & Fuels* **2010,** *24* (9), 5273-5280.

118. Sayari, A.; Belmabkhout, Y., Stabilization of Amine-Containing CO_2 Adsorbents: Dramatic Effect of Water Vapor. *Journal of the American Chemical Society* **2010,** *132* (18), 6312-6314.

CHAPTER 3

Experiment Materials and Methods

3.1 Material Synthesis

A list of all chemicals used in this study is shown in Table 3-1.

Table 3-1. Summary of chemicals used in this work

Chemical	Manufacturer	Properties, Purity (%) and/or Grade
Pluronic P123	Sigma-Aldrich Corp.	average MW ~5800
Tetraethyl orthosilicate (TEOS)	Sigma-Aldrich Corp.	reagent grade, 98%
Methanol	Sigma-Aldrich Corp.	≥ 99.9%
Hydrochloric acid (HCl)	Capital Scientific, Inc.	36.8 – 38.0%
Amines		
Tetraethylenepentamine (TEPA)	Sigma-Aldrich Corp.	technical grade
Polyethylenimine (PEI)	Sigma-Aldrich Corp.	average MW ~800
Gas cylinders		
Carbon dioxide (CO_2)	Praxair	Grade 4.8
Nitrogen (N_2)	Praxair	Grade 5.0

3.1.1 Synthesis of SBA-15 silica substrate

The mesoporous SBA-15 material used in this work was synthesized according to the method reported elsewhere[1-2] using amphiphilic triblock copolymer Pluronic P123 (poly(ethylene glycol)-block-poly(propylene glycol)-block-poly (ethylene glycol), $EO_{20}PO_{70}EO_{20}$, MW_{avg} = 5800, Aldrich) as the organic structure directing agent, tetraethyl orthosilicate (TEOS, Aldrich) as silica source and HCl as pH controlling agent. In a typical synthesis procedure,

1. 4 g of Pluronic P123 was dissolved in 30 ml of deionized water and 120 ml 2M HCl solution while stirring for 2 h at room temperature.

2. The resultant solution was transferred into a Teflon autoclave and solution temperature was raised to 40, 50 or 60 ℃, respectively.
3. 8.5 g of TEOS was added dropwise to the homogenous solution under vigorous stirring for 30 min and a precipitated product appeared.
4. The resulting gel was stirred isothermally for 20 h at low stirring rate and then aged at 105 ℃ for 48 h without stirring.
5. The white precipitated solid was filtered then, washed with deionized water and dried in air at room temperature for 12 h and subsequently in an oven at 80 ℃ for 2 h.
6. Final SBA-15 product was obtained by calcinations in flowing air at 550 ℃ for 5 h.

The calcined and as-synthesised product was thus denoted as S-*n* and unS-*n*, respectively, where *n* dictates the synthesis temperature applied in the corresponding sorbent.

3.1.2 Functionalization of SBA-15

Amine functionalized SBA-15 adsorbents were prepared by wet impregnation method using tetraethylenepentamine (TEPA, Aldrich). The desired amount of amine was dissolved in 8 g of methanol under stirring for 15 min. 2 g of calcined SBA-15 was then added to the amine-methanol solution. The resulting slurry mixture was stirred at room temperature for 30 minutes and finally dehydrated at 80 ℃ under vacuum (~ 0.1 atm) for 2 h.

The amine modified SBA-15 sorbents are denoted as S-*n*/T*x* for those prepared using TEPA. Here, the alphabet *x* refers to the weight percentage of amine in the

sorbent. A detailed scheme of SBA-15 formation and amine modification is presented in Figure 3-1.

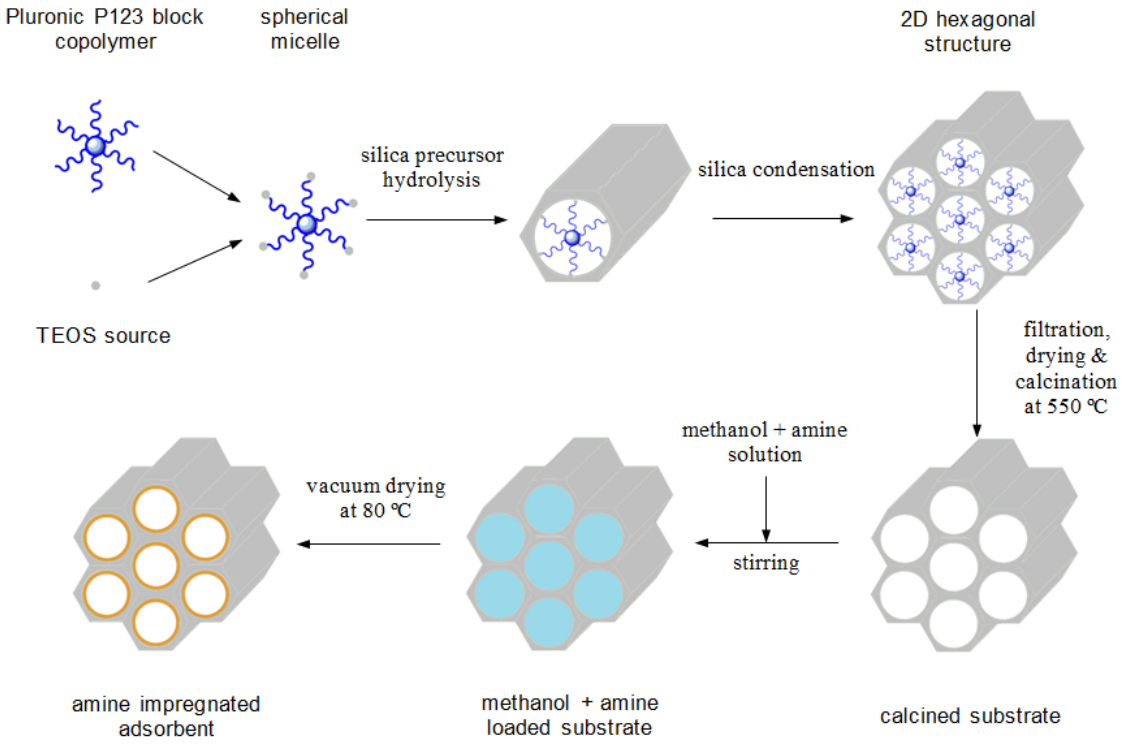

Figure 3-1. Scheme of amine impregnated adsorbent preparation

3.2 Material Characterization

The resulting SBA-15 materials, after drying and calcination and subsequent impregnation, were characterized by nitrogen adsorption, small-angle X-ray scattering (SAXS), scanning electron microscopy (SEM), transmission electron microscopy (TEM), Fourier transform infrared spectroscopy (FTIR).

3.2.1 Nitrogen (N_2) Adsorption/desorption

Nitrogen adsorption isotherms were measured with Autosorb I (Quantachrome, USA) at a relative pressure range of 0–0.997. The samples were degassed in a

vacuum for 2 h at 250 ℃ before nitrogen adsorption measurement. The total pore volume was calculated as the adsorbed volume of liquid nitrogen at a relative pressure of 0.997 and the micropore volume was determined by the t-plot method. The surface area was measured based on multi-point Brunauer-Emmett-Teller (BET) method at a relative pressure of 0.05–0.30. The pore size distribution of samples was collected by the BJH method from the N_2 desorption branch. The sorbents that were sampled for N_2 adsorption/desorption are listed in Table 3-2 with specific descriptions of corresponding preparation conditions.

Table 3-2. Summary of preparation conditions of sorbents for N_2 adsorption/desorption

Sample	Sorbent preparation		N_2 adsorption/desorption	
	Support synthesis temperature (℃)	Support calcination	Degassing temperature (℃)	Degassing time (h)
S–40	40	calcined	250	2
S–50	50	calcined	250	2
S–60	60	calcined	250	2
S-40/T60	40	calcined	80	0.5
unS-40	40	as-synthesized	250	2
Sigma AC	-	-	250	2

3.2.2 Small-angle X-ray Scattering (SAXS)

SAXS patterns of the calcined and impregnated SBA-15 samples were recorded on a NanoStar U small angle X-ray scattering system (Bruker-AXS) and a two-dimensional detector (Bruker HiStar) over the range of $0.15 \leq 2\theta \leq 3.0$ using Cu Kα radiation (λ=0.1541 nm, 45 kV, 110 mA). Powder samples were taken in 2 mm diameter and 25 μm wall thickness X-ray transparent polyethylene capillaries

(MicroRT tubes, MiteGen, Ithaca, NY). The wall thickness (w_d) was calculated by the equation: $w_d = a_0 - d_p$, where d_p represents the mean pore diameter and a_0 the unit cell parameter from the (100) diffraction peak: $a_0 = 2 \times d_{100}/\sqrt{3}$.

3.2.3 Scanning and Transmission Electron Microscopy (SEM/TEM)

The SEM analysis was obtained using a Hitachi S-2700 scanning electron microscope to observe the morphology of the solid sorbents. Samples were deposited on a sample holder with an adhesive carbon foil and sputtered with gold. The high resolution TEM images of the sorbents were recorded on a JEOL 2010 TEM with LaB_6 electron gun. Before TEM characterization samples were dispersed in methanol solution and deposited on the grids made of copper coated with formvar.

3.2.4 Fourier Transform Infrared Spectroscopy (FTIR)

A MB 3000 FTIR spectrometer (ABB, Canada) equipped with MIRacle three reflection diamond attenuated total reflectance (Pike Technologies, USA) device was used to obtain FTIR spectra of samples. Each sample was scanned 100 times at a resolution of 2 cm^{-1} over the frequency range 4000 – 500 cm^{-1}.

3.3 CO_2 Adsorption Measurements

The uptake of CO_2 adsorption as a function of time was measured using thermogravimetric (TG) apparatus (TA Instruments Q500 SDT). Pure CO_2 (99.99%) or CO_2 balanced with N_2 (purity 99.999%) at 1 atm was used for the adsorption measurements runs and N_2 was used as purging gas for CO_2 desorption. After the sorbents were grinded properly to obtain homogenously

sized particles, about 5 mg of the sorbent were placed in a platinum pan with a depth of 2 mm. Once loaded, the sorbent was firstly activated by heating at 10 ℃/min up to 105 ℃ under flowing N_2 stream at 100 cm^3 min^{-1}. After being isothermal for 30 minutes to have all moisture and adsorbed CO_2 removed, the temperature was then cooled to desired adsorption temperature (e. g. 30, 50, 75, 100 ℃). The gas was switched from N_2 to CO_2 containing mixed gases at 100 cm^3 min^{-1} and the temperature was kept constant at desired adsorption temperature for 2–3 hours. Considering the small and uniform sample particles with a small amount (5 mg) of samples in a shallow layer (2 mm), the influence of mass transfer resistance from bulk phase to adsorbent surface layer is reduced to be negligible and thus does not significantly affect the experiment measurement. Furthermore, according to the analysis from Sayari et al,[3] at low adsorbate concentration the operation can be considered isothermal despite the inherent release of heat associated with CO_2 adsorption. Since our experiment procedure meets these conditions, the assumptions of negligible axial dispersion through the adsorbent layer and isothermal operation were considered to adequate for gravimetric measurement in a microbalance. The CO_2 capturing capacity of the solid sorbent was calculated in mmol g^{-1} from the weight gain of the sample (on the dry base) in the adsorption process.

3.4 Fixed-bed Adsorption Breakthrough

The experimental setup used for CO_2 capture studies in a fixed-bed column is presented in Figure 3-2. The stainless steel column consisted of two continuous parts in an up-flow manner, preheating and mixing unit followed by an adsorption

section with a porous frit support in the middle of the column. The preheating and mixing unit was filled with ceramic beads to improve the heat transfer by increasing the contact area between bulk gas and heat flux. The adsorption and desorption took place in the upper reactor that was 3/8'' in diameter, 6'' in height. TEPA impregnated SBA-15 adsorbent was properly grinded and dried in an oven at 105 ℃ to remove most of adsorbed moisture and chemically bonded CO_2 adsorbate. About 0.5 g of adsorbents was uniformly placed in the reactor to form a bed layer with the height of 1.5 cm. Furthermore, in order to reduce the dead volume retained in the reactor and also make the packed bed compact during operation, a layer of inert glass beads (1 mm in diameter) with 1.5 cm thickness was deposed on the top of bed. A K-type thermocouple implanted in the bed was used to continuously monitor the temperature changes by a digital temperature controller (Omron E5CK) with an accuracy of ± 0.6 ℃. Both preheating unit and adsorption section were wrapped with a rope heater (OMEGALUX, 120 volts and 52 watts) on the outer surface of column.

The gas manifold system (see Figure 3-2) was composed of three lines fitted with mass flow controllers from Brooks Instrument 4800 series with a flow accuracy of ± 3.0 % and a flow repeatability of ± 0.15 % in full scale. The CO_2 containing gas mixture was fed through a gas mixer at a CO_2/N_2 ratio of 1:9 akin to the flue gas condition from the bottom of whole column. The *in situ* concentration of CO_2 stream coming from the adsorption column was monitored as a function of time by a VA-3000/VS-3000 multi-component NDIR gas analyzer from Horiba coupled with a mass spectrometer (Extorr Inc. XT300M–6363). To reach a better

sensitivity and response from an analysis standpoint for the gas analyzer, a line featured with a mass flow controller (4 SLPM) was set to compensate the N_2 flowing stream from the rear of adsorption column.

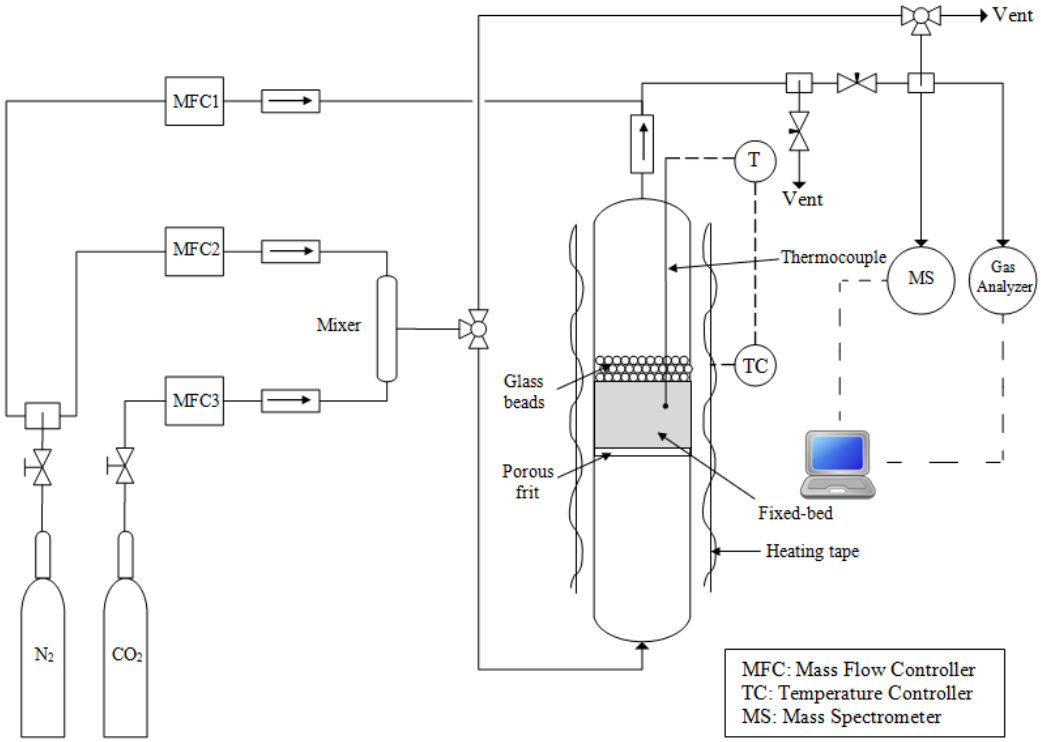

Figure 3-2. Experimental setup of the fixed-bed flowing system for CO_2 adsorption

In a typical adsorption and desorption cycle, the bed was firstly heated up to 105 ℃ and kept for 10 minutes with dry N_2 flow at 200 mL/min. After the drying step, the whole adsorption column was cooled down by compressed air flow to the desired temperature for adsorption. Then this was followed by adsorption step in which a CO_2/N_2 gas mixture (10/90 v/v%) was allowed to be introduced through the preheating unit at a flow rate of 400 mL/min. After 5 minutes for adsorption step, the inlet gas stream was switched to N_2 flow only isothermally for 2.5

minutes to remove the CO_2 that occupied in dead volume of column and line. Afterwards, the temperature was raised up at a heating rate of 7–8 ℃/min to 105 ℃ and kept constant for 10 minutes. The CO_2 breakthrough curves could be obtained by normalizing the detected CO_2 concentration as a function of time to the C_t/C_0, where C_t and C_0 refer to the concentrations of the adsorbate in the upstream and downstream through the column, respectively. The dynamic adsorption capacity (q) of adsorbent was calculated using Eq. (1):

$$q = \frac{FC_0t_q}{M} \tag{1}$$

Where F is the total molar flow rate, C_0 is the concentration of the adsorbate in the feed stream, M is the mass of adsorbent loaded in the column, and t_q is the stoichiometric time, which is calculated from the breakthrough curve according to Eq. (2):

$$t_q = \int_0^{\infty} (1 - \frac{C_t}{C_0})dt \tag{2}$$

The amounts of CO_2 captured or recovered due to adsorption and desorption respectively, were determined by cumulative methodology on the basis of breakthrough and desorption profiles.

References

1. Xu, X.; Song, C.; Andresen, J. M.; Miller, B. G.; Scaroni, A. W., Novel Polyethylenimine-Modified Mesoporous Molecular Sieve of MCM-41 Type as High-Capacity Adsorbent for CO_2 Capture. *Energy & Fuels* **2002,** *16* (6), 1463-1469.

2. Xu, X.; Song, C.; Andrésen, J. M.; Miller, B. G.; Scaroni, A. W., Preparation and characterization of novel CO_2 "molecular basket" adsorbents based on polymer-modified mesoporous molecular sieve MCM-41. *Microporous and Mesoporous Materials* **2003,** *62* (1–2), 29-45.

3. Serna-Guerrero, R.; Sayari, A., Modeling adsorption of CO_2 on amine-functionalized mesoporous silica. 2. Kinetics and breakthrough curves. *Chemical Engineering Journal* **2010**.

CHAPTER 4

Results & Discussions

4.1 Material Characterization

Figure 4-1 and 4-2 display the nitrogen adsorption isotherms and pore size distributions of as-synthesized and calcined S-40 substrates, and S-40/T60 adsorbent, respectively. The corresponding textual properties of surface area, pore volume and average pore diameter are listed in Table 4-1. The properties of other prepared samples used for TEPA impregnation are also shown for comparison. As

seen from the Figure 4-1, calcined SBA-15 substrate shows typical Type IV isotherm with a representative H_1-type hysteresis loop due to capillary condensation occurring at $P/P_0 = 0.65 – 0.80$, which is characteristic of the mesoporous materials with uniform narrow pores. The pore size distribution of calcined S-40 exhibits a sharp peak centered at 6.5 nm, indicating the high uniformity of mesopores distribution (Figure 4-2). As seen in Table 1, calcined SBA-15 (S-40) exhibits the highest BET surface area and pore volume of about 1099 $m^2 g^{-1}$ and 1.844 $cm^3 g^{-1}$, respectively. The combined properties of the large pore volume and pore size would enable calcined SBA-15 for better amine accommodation with little hindrance[1]. However, the as-synthesized SBA-15 has a much lower surface area and pore volume of 226 $m^2 g^{-1}$ and 0.597 $m^2 g^{-1}$, respectively. This can be attributed to pore blocking in the mesoporous channels due to the presence of organic template. On introducing amine functionalities, a marked decrease in specific surface area, pore volume and average pore diameter is also found in amine functionalized SBA-15. This clearly confirms that TEPA was successfully impregnated into the pores of the SBA-15 support.

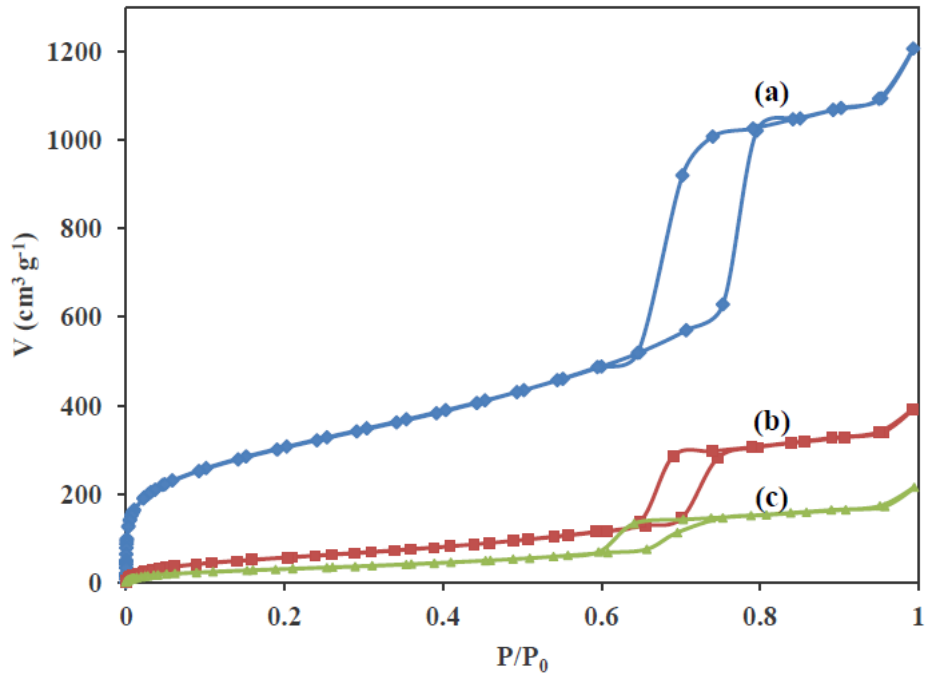

Figure 4-1. N_2 adsorption-desorption isotherms of (a) calcined SBA-15, (b) as-synthesized SBA-15 and (c) TEPA impregnated SBA-15 sorbent (S-40/T60).

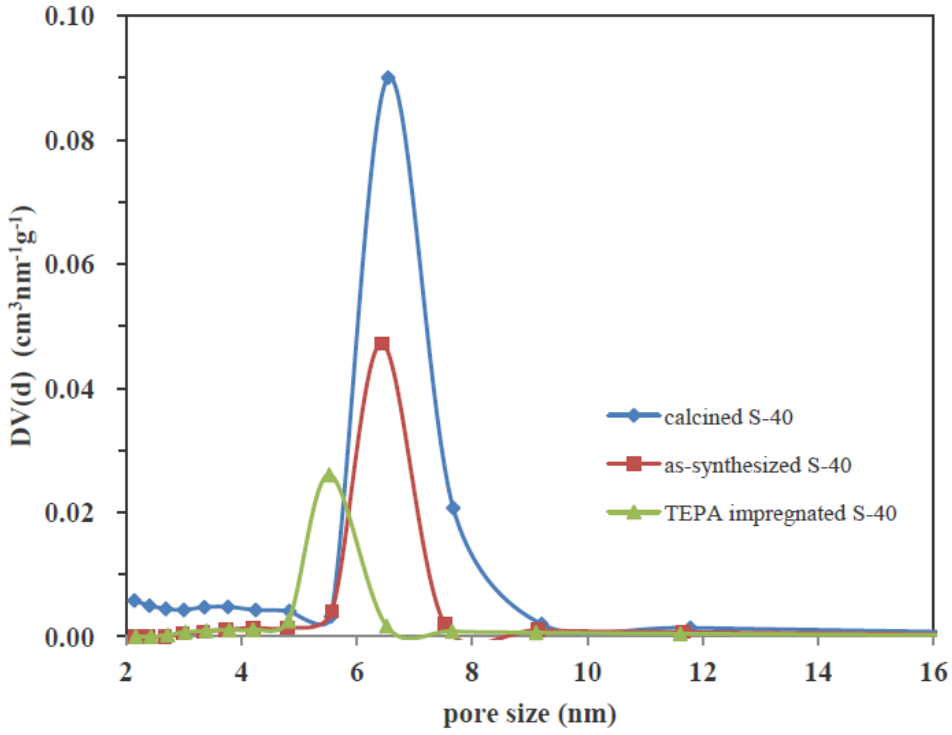

Figure 4-2. The pore size distributions of calcined SBA-15, as-synthesized SBA-15 and TEPA impregnated SBA-15 sorbent (S-40/T60).

Table 4-1. Textual properties of adsorbents

Sample	S_{BET} (m^2/g)	V_{tot} (cm^3/g)	V_{micro}[a] (cm^3/g)	D_{BJH}[b] (nm)
S–40	1099	1.844	0.065	6.5
S–50	620.9	1.124	0.075	5.6
S–60	579.9	1.213	0.056	1.7
S-40/T60[c]	121.1	0.327	~0	5.5
unS-40	222.6	0.597	~0	6.4
Sigma AC	863.1	0.730	0.233	3.4

a. Micropore volume was measured by t-plot method.
b. BJH mean pore diameter.
c. Degassed at 80 ℃ for 30 minutes.

The small angle X-ray diffraction spectra (SAXS) of calcined S-40 and S-40/T60 are shown in Figure 4-3. Three distinct reflective peaks for the (100), (110) and (200) planes are identified in the lower angle range of 2θ = 0.90 to 2.71. This indicates high structural order of the hexagonal mesoporous structures of SBA-15.[2] Comparison of the diffraction pattern for the TEPA impregnated SBA-15 sorbent indicates that the 2D-hexagonal ordering has been retained after the impregnation of TEPA into the mesopore of SBA-15. Xu et al.[3] also observed that the PEI impregnated into the MCM-41 pores did not cause considerable intensity changes of the characteristic peaks. The estimated d-spacing (d_{100}) for calcined SBA-15 is about 9.7 nm.

Complementary to the SAXS data, electron spectrometry images also reveal that calcined S-40 material exhibits a rope-like morphology (Figure 4-4(a)) consisted of ca. 15 μm long and 2.1 μm thick aggregated bundles with 2-D hexagonal arrangement of pore channels (Figure 4-4(c)). The perpendicular HRTEM image of SBA-15 clearly (Figure 4-4(b)) shows the presence of highly ordered parallel

cylindrical pore channels with a mean pore size and wall thickness of approximately 10.4 nm and 4.7 nm, respectively. These results are in accordance with the values obtained from SAXS analysis and N_2 adsorption/desorption isotherms ($a_0 = 2 \times d_{100}/\sqrt{3}$; wall thickness $= a_0 -$ pore size). The averaged wall thickness of SBA-15 is substantially thicker than the walls of MCM-41 (commonly 0.6–1.5 nm) using alkylammonium ion surfactant species as directing agent[2,4]. The nature of SBA-15 in thicker silica walls in turn suggests its outstanding hydrothermal stability at higher temperature under steam, even better than that of MCM-41 materials[5-6].

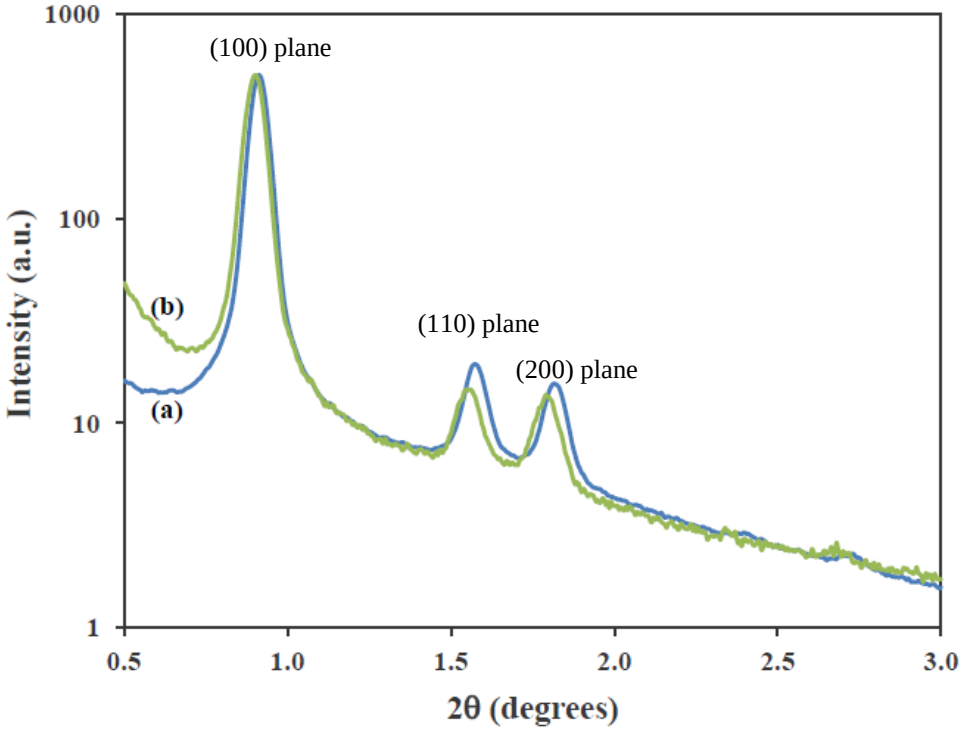

Figure 4-3. SAXS patterns of (a) calcined SBA-15 and (b) TEPA impregnated SBA-15

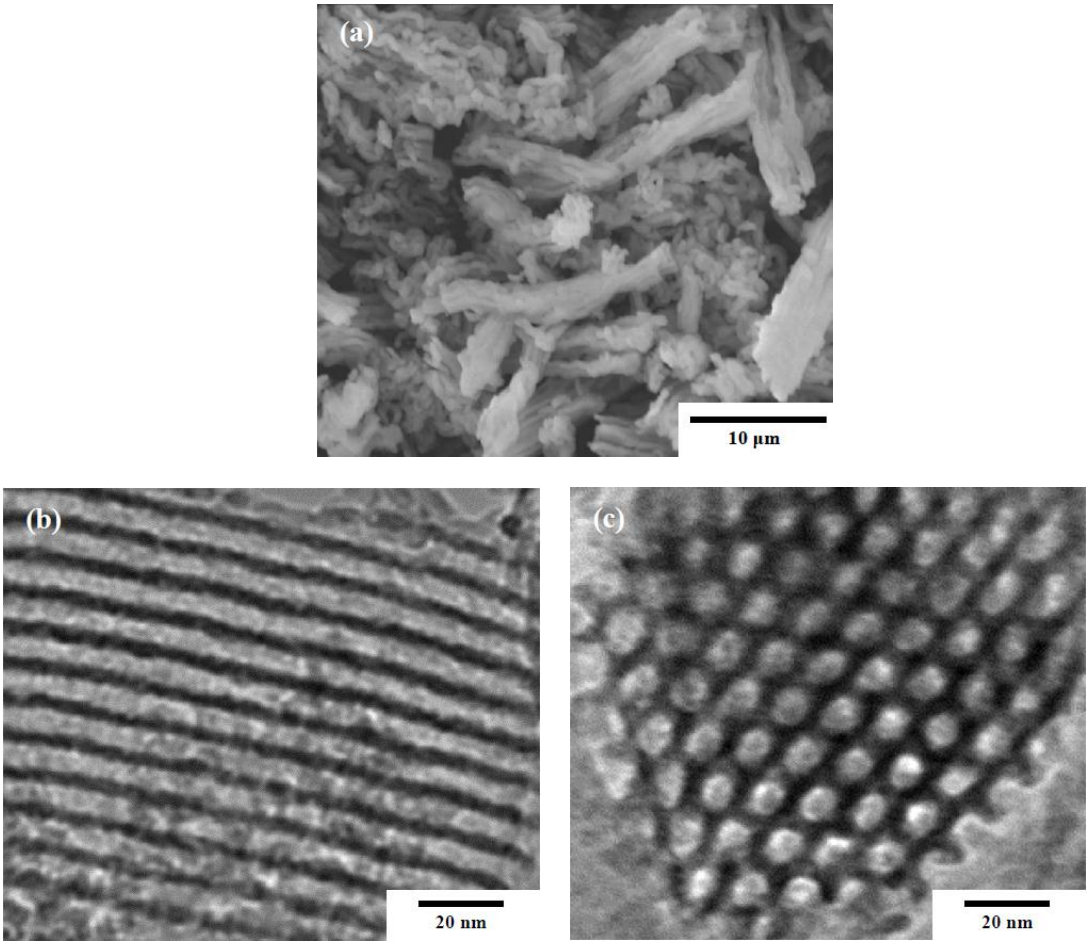

Figure 4-4. (a) SEM analysis of calcined SBA-15. (b) HRTEM image of calcined SBA-15. Micrograph recorded in perpendicular. (c) HRTEM image of calcined SBA-15 along with the hexagonal pore channel direction.

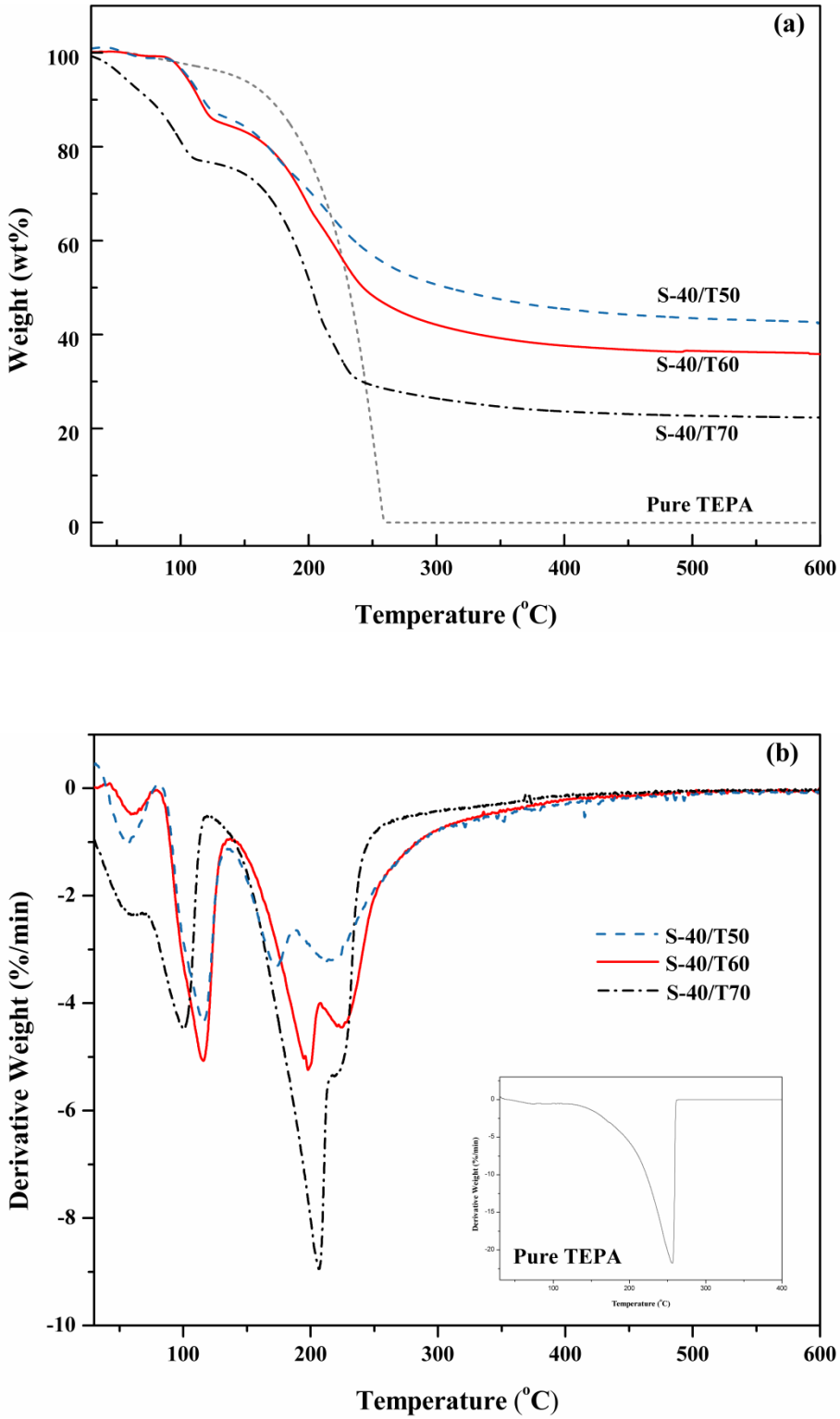

Figure 4-5. TG (a) and DTG (b) profiles of pure TEPA and amine impregnated SBA-15 with different TEPA loadings.

Figure 4-5 shows thermal behaviors of pure TEPA and TEPA impregnated SBA-15 sorbents with different loadings of amine measured by TGA in dry N_2 flow at a heating rate of 10 ℃/min. The pure TEPA started to lose significant mass at around 150 ℃ (5.7 % weight loss), followed by a steep weight loss taking place around 200–250 ℃. When the temperature was above 260 ℃, pure TEPA was completely decomposed. Whereas, for cases of TEPA impregnated SBA-15 sorbents, the thermal behaviors exhibited four major weight-loss steps. For example, in the case of S-40/T60, the first step took place with a weight loss of about 0.93 wt% in the range of ~50 to 80 ℃. This is attributed to the vaporization of methanol solvent used in impregnation procedure. The following weight-loss step around 115 ℃ had a weight decrease of about 14.8 % due to the desorption of adsorbed moisture and CO_2. The other two weight-loss steps occurred continuously from 140 ℃ and became constant at above 350 ℃. It is probably due to the loss of amine which escaped and decomposed from different inner pores of substrate during the continuous increase of temperature. The different weight loss behaviors of pure TEPA and TEPA impregnated SBA-15 also established that TEPA was loaded in pores of the silica support. The final residue accounted for about 35.8% of its original weight of the sorbent. Based on the weight of moisture and CO_2 free sorbent, the actual loading of TEPA (in weight percentage) of S-40/T60 sample is computed to be about 60 wt%. Following the same rational, the TEPA loadings are calculated to be 51.5 wt% and 71.2 wt% for S-40/T50 and S-40/T70, respectively. This confirms that the desired amount of

amine has been successfully immobilized onto the mesoporous silica substrate by impregnation technique without significant loss of amine.

The FTIR spectra of calcined SBA-15 and TEPA impregnated SBA-15 sorbent was performed as part of surface characterization to determine surface functional group and are shown in Figure 4-6. The broad and intense peak at ~1040 cm^{-1} with an associated broad shoulder at ~1200 cm^{-1} are attributed to asymmetric Si-O stretching in siloxane bonds (Si-O-Si) structure and are features of silica framework. A peak located at ~807 cm^{-1} is due to symmetric stretching vibration of Si-O-Si group and also considered as a characteristic of silica skeleton. FITR spectroscopy provides clear evidence for amine impregnation. When silica substrate was modified by TEPA, the amine loaded SBA-15 showed several distinctive peaks at 3358, 3288 and 1576 cm^{-1}, which were assigned to N–H vibration. The presence of C–H was confirmed by appearing peaks at 2935, 2874 and 2820 cm^{-1} due to the C–H stretch and 1457 cm^{-1} as a result of CH_2 deformation. It should be noted that these peaks are absent in calcined SBA-15.

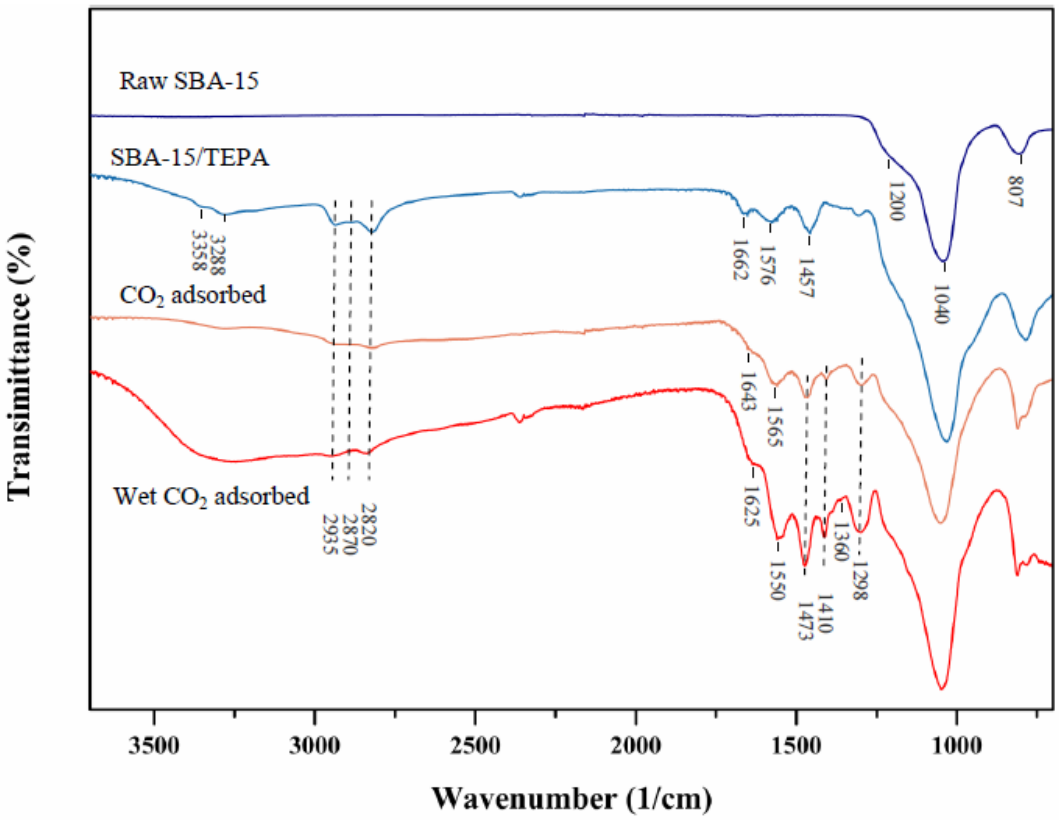

Figure 4-6. FTIR spectra of parent SBA-15 substrate, TEPA impregnated sorbent and its corresponding dry and wet CO_2 adsorbed adsorbents.

4.2 CO_2 Adsorption Performance

The CO_2 adsorption capacities of the amine impregnated sorbents were determined at 30, 50, 75 and 100 ℃ in pure CO_2 and 10 v/v% CO_2 in N_2. Typical CO_2 adsorption capacities results at 75 ℃ in pure CO_2 gas are shown in Figure 4-7. Figure 4-7 also compares the CO_2 adsorption capacities of TEPA and PEI impregnated SBA-15, as-synthesized SBA-15 and activated carbon (Sigma Aldrich). As shown in Figure 4-7, when different solid substrates were modified with the same amount of amines, SBA-15 impregnated with TEPA was found to work better. The maximum CO_2 adsorption capacity achieved was about 4.52 mmol g^{-1} at 75 ℃ using TEPA impregnated SBA-15. In contrast, amine

impregnated as-synthesized SBA-15 exhibited less CO_2 adsorption capacity than amine impregnated calcined SBA-15. This might be due to the fact that during the calcination procedure template was removed from the as-synthesized SBA-15 and thus it optimized the pore structure and enhanced the CO_2 adsorption capacity. Amine modified activated carbon did not show satisfactory performance on adsorption capacity because of the limitations such as relatively lower pore volume and surface area.

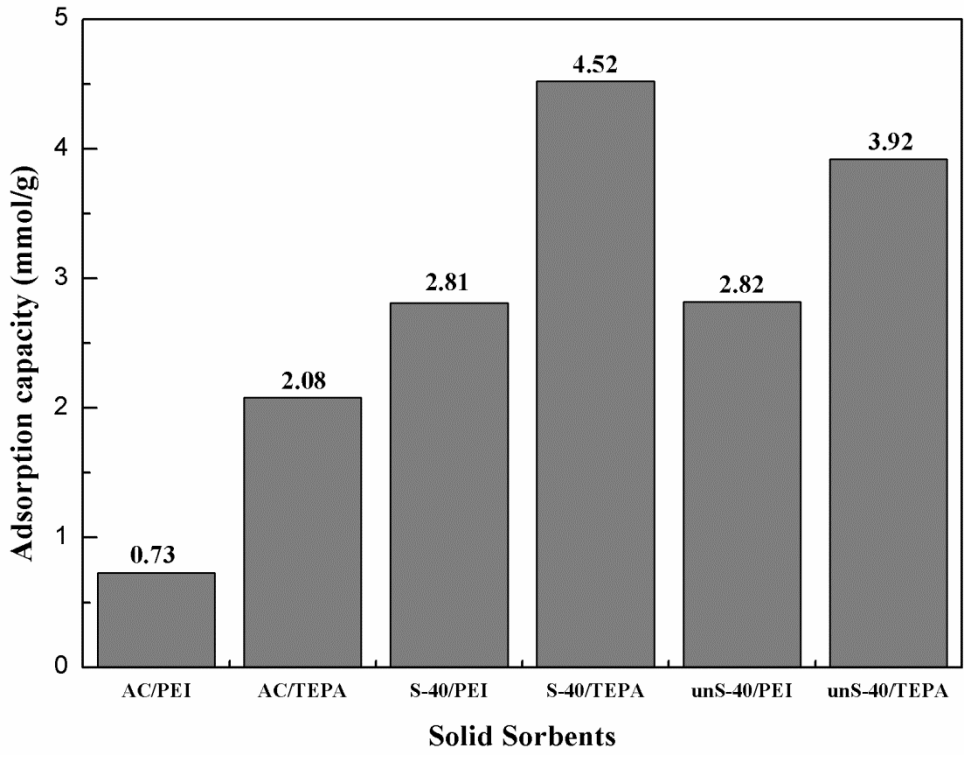

Figure 4-7. Comparison of CO_2 adsorption capacity on different solid supports impregnated with 60 wt% TEPA at 75 ℃ in pure CO_2 feed gas.

It should be further noted that TEPA modified sorbents outperform the counterparts loaded with the same amount of PEI. As shown in Table 2-3, single TEPA molecule is relatively small and linear oligomer which contains large amino groups fraction, whereas the bulk PEI (Average *MW*: ~800) contains long

chained skeleton with branches, which is far larger than that of TEPA (*MW*: 189). This inevitably leads to increased diffusion resistance via steric effect between CO_2 molecules and amino sites trapped in bulk PEI. Due to the favorable molecular structure of TEPA, CO_2 molecules can be more accessible to the affinity sites for capture than the case of PEI. Hence, TEPA was selected to functionalize SBA-15 support for this study.

Figure 4-8 displays a typical thermogravimetry-differential scanning calorimetry (TG-DSC) profile for CO_2 adsorption at 75 ℃. After 7 minutes the influent gas flow is switched to CO_2 instead of N_2 to initialize the adsorption study. It is observed that TEPA functionalized SBA-15 sorbent shows a very favorable adsorption kinetics. The composite demonstrates a sharp increase of adsorption during the initial adsorption stage. Approximately 90% of its equilibrium adsorption capacity is achieved within first 5 minutes at an adsorption rate of 23 wt%/min. The quick initial adsorption step indicates the CO_2 adsorbate is readily captured at affinity sites on the surface of TEPA in the mesopores. However, the affinity sites within the composite, especially in the micropores of sorbents, are not easily accessible because of diffusion limitations[7]. As a result, the rate of CO_2 adsorption decreases considerably to 0.22 wt%/min in the subsequent 3 minutes and becomes even slower afterwards. It takes more than 2 hours to attain the working adsorption capacity approaching to equilibrium status at extremely low adsorption rate (<0.001 wt%/min). Based on the observed results, it is likely that the adsorption of CO_2 on TEPA impregnated SBA-15 sorbent is a kinetically (diffusion)-controlled process[7-8], and the maximum or equilibrium adsorption

capacity is expected to be achieved provided that the CO_2 exposure time for adsorption is adequately sufficient.

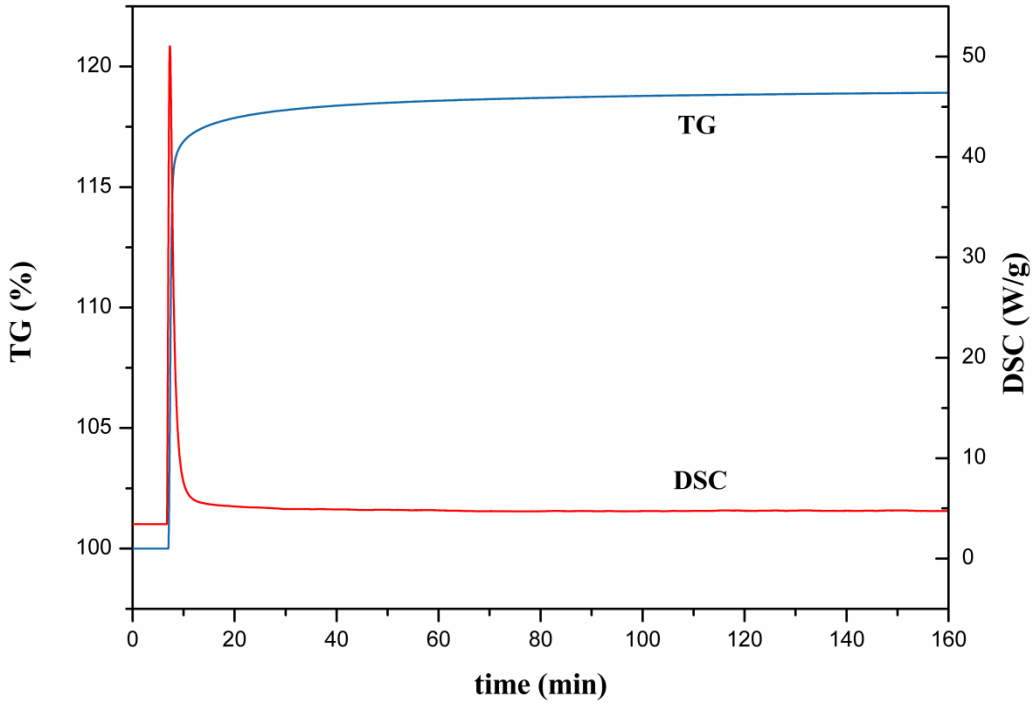

Figure 4-8. Typical TG and DSC curves of S-40/T60 sorbent for pure CO_2 adsorption at 75 ℃.

The determination of CO_2 sorption heat is also of great significance in evaluating the energy requirement in regeneration phase of an adsorbent. However, the measurement of fundamental thermodynamics definitions such as the heat of adsorption is rather more difficult than other equilibrium constants[9]. The heat of adsorption can be either approximated using multiple isotherms and Classius-Clapeyron type equation or measured directly via calorimetric methods. A heat of adsorption of – 60 to – 87 kJ/mol CO_2 was determined for TEPA impregnated SBA-15 sorbent by means of simultaneous TG-DSC apparatus throughout integration of heat flow profile in Figure 4-8. The heats of adsorption reported in the literature for covalently-tethered silica-supported amines are distributed in the

range of – 48 to ~ – 90 kJ/mol CO_2, depending on the adsorbents and analysis used[10-11]. It should be noted that since CO_2 adsorption in this study were measured over a relatively short time span, these CO_2 working adsorption capacities do not represent full equilibrium capacities, which makes the calculated sorption heat deviate somehow. Therefore, future detailed investigations adopting the proper measures will be targeted at quantitative assessment of the heat released during the adsorption.

4.3 Effect of Amine Loading on CO_2 Adsorption Capacity

To investigate the effect of amine loading on CO_2 adsorption capacity, a series of impregnated S-40 sorbent containing 50, 60 and 70 wt% TEPA were prepared. The adsorption capacity as a function of TEPA loading is shown in Figure 4-9. It was observed that the raw calcined SBA-15 substrate barely contributed to CO_2 adsorption (ca. 0.15 mmol g^{-1}), while pure bulk TEPA exhibited an adsorption capacity of approximately 3.69 mmol g^{-1} at 75 ℃ and in pure CO_2. As seen in Figure 4-8, as the amine loading increases from 50 to 70 wt%, an increasing trend of adsorption capacity is found in the following order: S-40/T70 (4.59 mmol g^{-1}) > S-40/T60 (4.52 mmol g^{-1}) > S-40/T50 (3.59 mmol g^{-1}). It is likely that the greater CO_2 adsorption capacity is because of the higher quantity of amines. All SBA-15 supported TEPA sorbents showed much higher adsorption capacities than the estimated composite capacity (2.63 mmol g^{-1} at maximum) by linear integration of parent substrate and pure TEPA. The result reveals that TEPA impregnated SBA-15 has a synergetic effect on CO_2 adsorption by favorable distribution of

affinity sites of TEPA to increase the chances of adsorbate–TEPA interaction, therefore to improve the mass transfer in the adsorption process.[8]

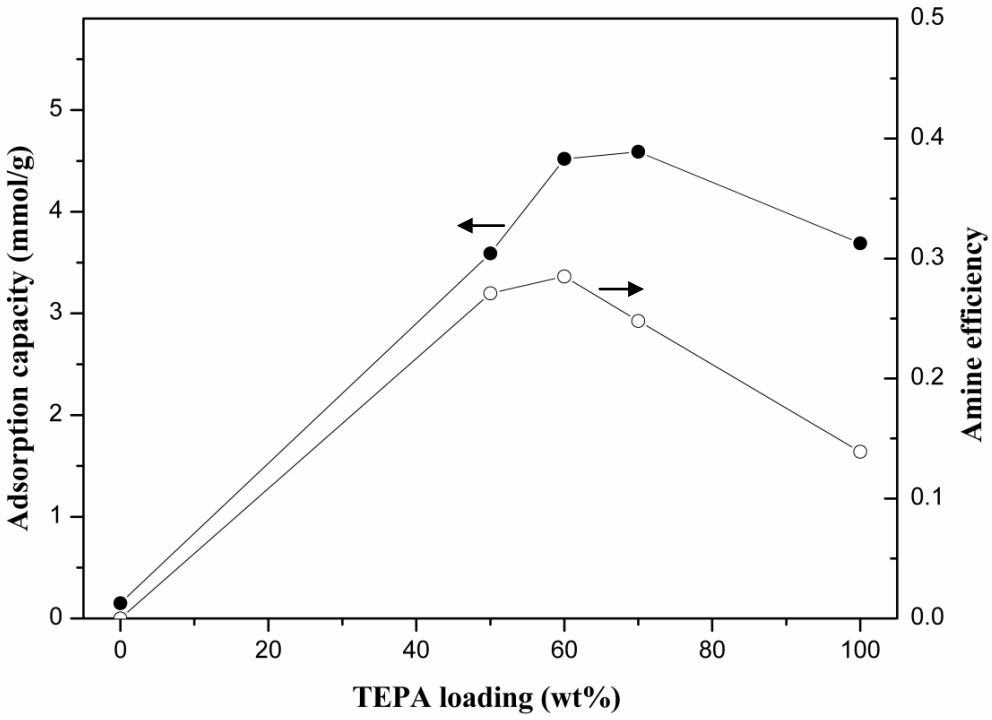

Figure 4-9. Pure CO_2 Adsorption capacity and amine efficiency of SBA-15 with different amine loadings

However, in contrast, the enhancement of adsorption capacity with respect to amine efficiency, defined as the ratio of moles of CO_2 captured to that of nitrogen element, does not follow similar trend: S-40/T60 exhibits the highest amine efficiency of 0.285, followed by 0.271 for S-40/T50 sorbent. While S-40/T70, which presents the highest adsorption capacity, has the lowest amine efficiency value of 0.248 (shown in Figure 4-9). This phenomenon may be attributed to the following. It is estimated that the maximum amine loading in the pores of SBA15-40 should be around 65 wt%, assuming that all the pore volume (~1.82 cm^3/g for S-40 in Table 4-1) ideally occupied by TEPA (density: 0.991 g/cm^3 at room temperature). After complete perfusion of inner pore, the excess amine exists in

the layer coated outside the surface of solid substrate. It is hypothesized that TEPA uniformly anchored on the inner pore channels of mesoporous SBA-15 works as a CO_2-capturing affinity sites and the external coated TEPA has low efficiency to capture CO_2 because of increased mass transfer resistance.[8,12] The results suggest an optimal amine loading plays an important role in adsorption performance of amine impregnated mesoporous materials. In this study, SBA-15 loaded with 60 wt% TEPA outperformed the other sorbents because of its satisfying adsorption capacity with the highest amine efficiency.

4.4 Effect of Adsorption Temperature and CO_2 Partial Pressure

To evaluate the optimum adsorption temperature, the influence of temperature on TEPA impregnated SBA-15 was investigated at different temperatures upon exposure to pure CO_2 and 10 % CO_2 in N_2 (shown in Figure 4-10). As indicated, the adsorption capacity increased with increasing the temperature, and reached the maximum CO_2 uptake at about 75 ℃. The low CO_2 uptake at low temperature could be a result of slow adsorption rate caused by kinetic limitations, because the overall process is diffusion controlled.[8] Therefore, higher temperature is beneficial to significantly accelerate the apparent adsorption rate by reducing diffusional resistance.[8,13] But both CO_2 uptakes under diluted or concentrated CO_2 decreased (approximately 89.1 % and 7.5 % of their maximum adsorption capacities at 75 ℃, respectively) when temperature was beyond 75 ℃. At higher temperature, the diffusional resistance is not a controlling factor. Instead, higher temperature inhibited the CO_2 adsorption on TEPA impregnated SBA-15 due to

its exothermal nature. Therefore, this might be due to the thermodynamic limitation that makes shifting in chemical equilibrium beyond 75 ℃.[13]

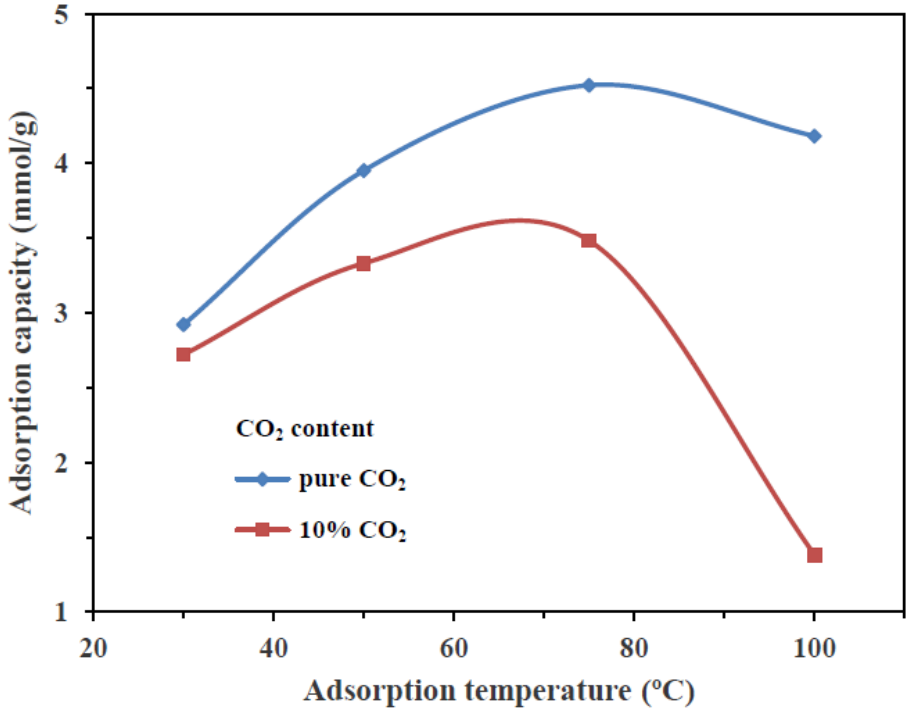

Figure 4-10. Adsorption capacity of S-40/T60 as a function of adsorption temperature in pure or 10 % CO_2 feed gas.

CO_2 adsorption measurements under different CO_2 partial pressures were also carried out. The result (in Figure 4-11) shows that the CO_2 adsorption capacity of TEPA impregnated SBA-15 was affected greatly by the partial pressure of CO_2 (P_{CO2}) from 1 to 0.10 atm at 75 ℃. As seen in Figure 4-11, the adsorption capacity increases as the CO_2 partial pressure increases. Moreover, as the partial pressure of CO_2 increases, it has been observed that the adsorption rate becomes faster (not shown in Figure 4-11). This is because the more CO_2 molecules are at present in abundance to be captured, the more tendency it has to reach higher adsorption, meanwhile the larger CO_2 concentration gradient it represents to accelerate the diffusion rate. The adsorption capacity of S-40/T60 sample at P_{CO2}

= 0.10 atm was found to be 3.48 mmol g^{-1}, approximately equaling to 77% of CO_2 uptake under pure CO_2 feed gas. Although reduced at dilute CO_2 environment, the adsorption capacity of TEPA loaded SBA-15 adsorbent is still economically promising and satisfying to be competitive with conventional aqueous amine scrubbers[14].

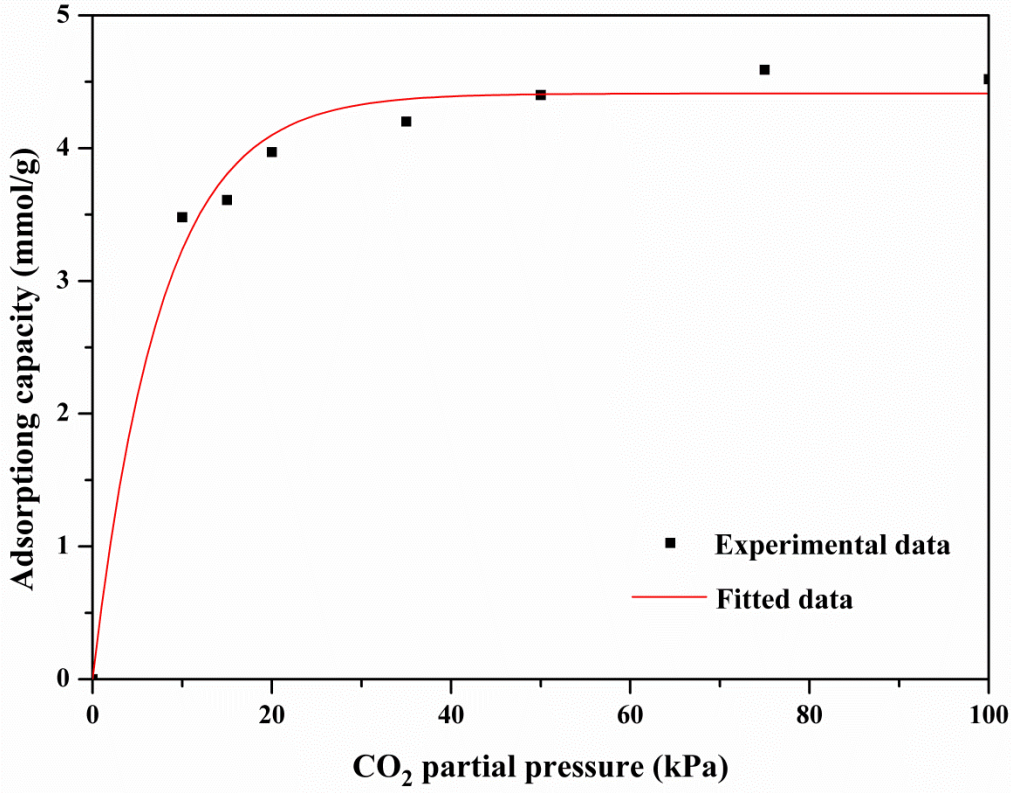

Figure 4-11. CO_2 adsorption isotherm of S-40/T60 after 1 h exposure to CO_2 feed gas at 75 ℃ using thermogravimetic (TG) apparatus.

4.5 Effect of Pore Structure on Performance of CO_2 Adsorption

SBA-15 substrates with different pore diameters were obtained via altering the synthesis conditions. In this work, preparation of SBA-15 was carried out at reaction temperatures between 40 to 60 ℃. The textural properties of S-40, S-50 and S-60 are summarized in Table 4-1. It is observed that the mean BJH pore size

of SBA-15 decreases considerably with increasing the synthesis temperature, reflecting the negative effect of higher temperature on the development of mesoporous morphology of SBA-15. The adsorption capacities of abovementioned sorbents loaded with 60 wt% TEPA at various adsorption temperatures in the presence of 10 % CO_2 are compared in Figure 4-12.

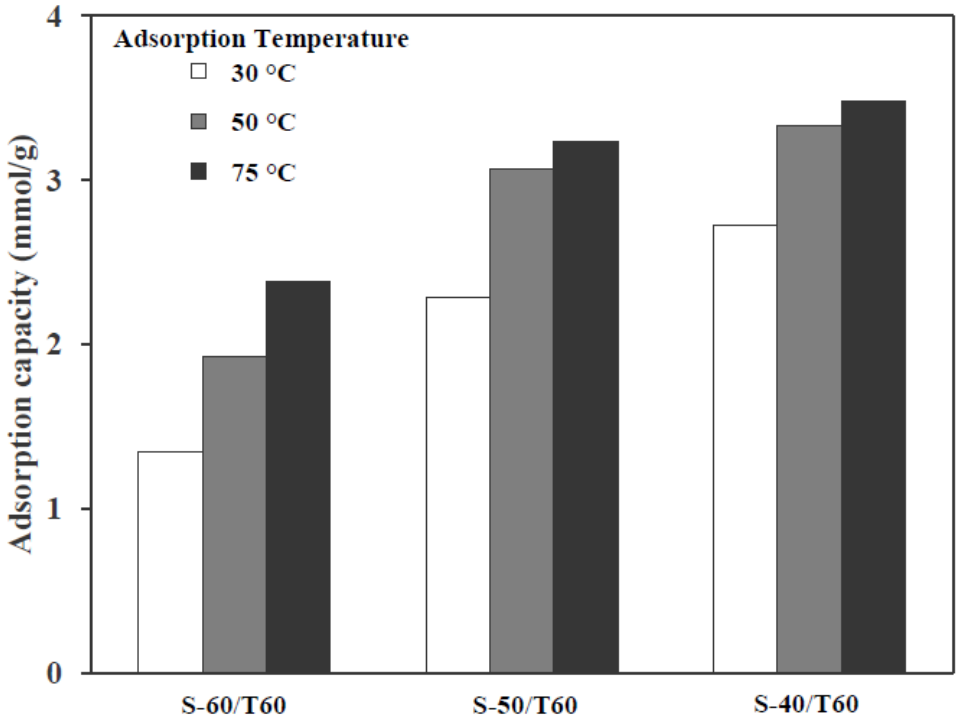

Figure 4-12. Comparison of adsorption capacities for different 60 wt% TEPA impregnated SBA-15 adsorbents at different adsorption temperatures in 10% CO_2.

It is observed that dispersed with the same loading of amine, every adsorbent composed of specific nanostructural SBA-15 differed greatly in adsorption capacity. For each type of SBA-15 sorbent tested in this work, the maximum adsorption uptake occurred at adsorption temperature of 75 ℃. On the other hand, the adsorption capacities of studied sorbents at the same adsorption temperature, for example at 75 ℃, was found to increase from S-60/T60 to S-40/T60. The

highest CO_2 uptake under 10 % CO_2/N_2 was observed 3.48 mmol g^{-1} for S-40/T60 at 75 ℃. The large variation in adsorption capacities could be attributed to the different nanostructures tuned by changing the synthesis temperature of substrate preparation. To correlate the effect of pore structure of SBA-15 substrate on CO_2 adsorption capacity, CO_2 uptake versus pore volume and pore size of SBA-15 substrate is plotted in Figure 4-13 and 4-14, since these properties greatly affect the CO_2 accessibility to the affinity sites on the amine. The adsorption tests in this study were conducted using a simulated gas mixture with 10 % CO_2/N_2 at a temperature range from 30 ℃ to 75 ℃.

Indicated in Figure 4-13, at each adsorption temperature, the sample S-40/T60 exhibited the highest CO_2 uptake with the highest pore volume of substrate. This is consistent with the observations found by Yan et al.[15] They also found a maximum adsorption capacity as the total pore volume reached the maximum. They also reported a linear trend relationship of adsorption capacity as a function of total pore volume. However, in this study, we did not conclude a clear correlation between total pore volume and adsorption capacity at all adsorption temperatures tested in this work (Figure 4-13). According to the implications of "molecule basket" concept, a lower pore volume cannot allow the accommodation with a large amount of bulky amine. Extra amines induce the coated layer around the external surface of substrate to prevent the contact of CO_2 with dispersed interior amine, which leads to some uncertainties in concluding the relationship between total pore volume and adsorption capacity. In addition, the contact

between CO_2 gas and bulky amine can be more efficient when a small space is still retained inside the pores of the mesoporous silica after amine loading.[1,15]

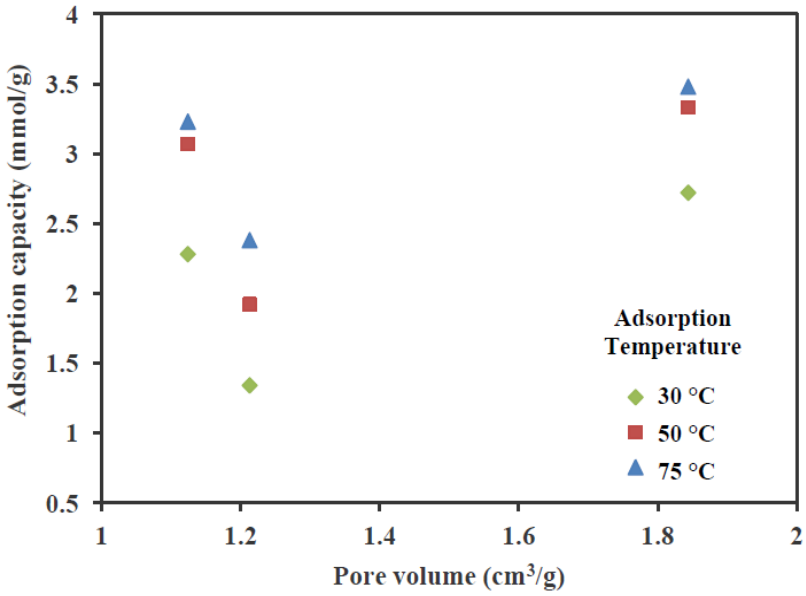

Figure 4-13. Relationship between total pore volume of SBA-15 substrates and CO_2 adsorption capacity.

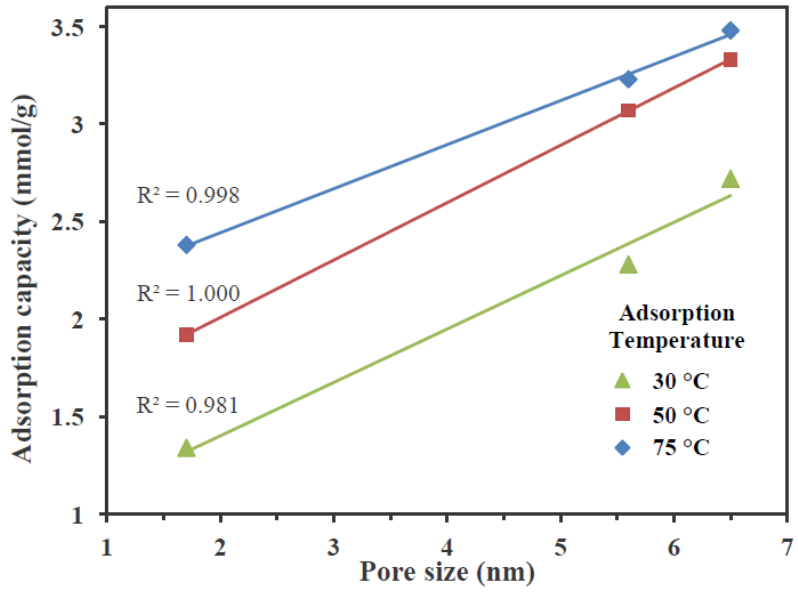

Figure 4-14. Correlation of pore size of SBA-15 substrates and adsorption capacity at different adsorption temperatures.

The adsorption capacity, on the contrary, coincided with the order of mean pore size of substrate, where a linear relationship was observed for each adsorbent composite at all temperatures. Linear regression analysis was conducted to draw a straight line that fitted best the data in Figure 4-14. The coefficients of determination (R^2) were 0.998 for adsorption at 75 ℃, while R^2 were 1.000 and 0.981 for adsorption at 50 ℃ and 30 ℃, respectively. The results showed a good agreement with the observations from Ahn et al.[1], who found the adsorption capacity increased as an increment of average pore diameter of the mesoporous silica samples: MCM-41 (2.8 nm) < MCM-48 (3.1 nm) < SBA-16 (4.1 nm) ≈ SBA-15 (5.5 nm) < KIT-6 (6.5 nm). This result indicates that the bulky amine can be distributed into the pore channels more easily as the pore size of the mesoporous substrate increases, and much better when the better uniformity of mesopore size is achieved.

4.6 Effect of Moisture on CO_2 Adsorption Capacity

It is important to investigate the effect of moisture during the CO_2-sorbent adsorption interaction, because a certain amount of moisture is also present in flue gas mixtures from thermal power plant. To study the effect of moisture on the CO_2 uptake water vapor was introduced into the simulated gas mixture (2 vol % moisture) through a water saturator prior to thermogravimetric (TG) apparatus. The influence of moisture on the adsorption removal of CO_2 from simulated flue gas was investigated at 75 ℃ and ambient pressure. The comparison of adsorption capacities of S-40/T60 in dry and moist CO_2 gases is summarized in Figure 4-15.

As indicated in Figure 4-15, the CO_2 uptakes were increased by 5.5 % and 15.5 % for dilute and concentrated CO_2 fractions, respectively. Contrary to the inhibition of moisture in CO_2 adsorption on physisorbents, the result reveals that the moisture has a positive effect on the adsorption of CO_2 by the TEPA impregnated SBA-15 which is in agreement with that reported in literature[16].

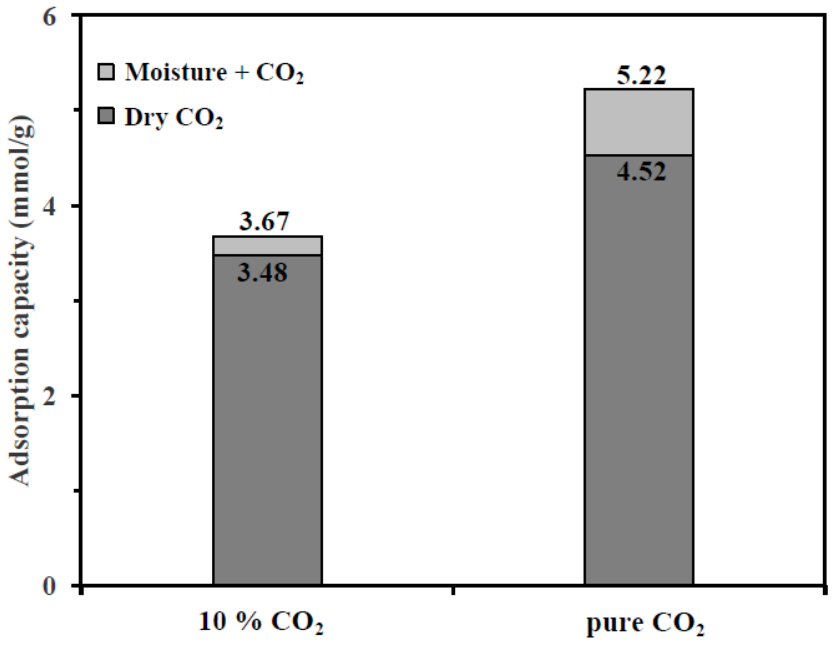

Figure 4-15. Comparison of CO_2 uptakes of S-40/T60 under dry and wet feed gas of pure or 10 % CO_2.

Table 4-2. Assignment of FTIR bands or peaks

wavenumber (cm^{-1})	assignment	correspond to	ref
3700–3200	OH stretching of hydrogen-bonded OH groups	adsorbed water	10,17
3358, 3285	asymmetric and symmetric N–H stretching	TEPA	10,18-19
2935, 2874	asymmetric and symmetric C–H stretching	TEPA	17-18
2820	C–H stretching	TEPA	20
1662	NH_3^+ deformation	protonated amino group with silica surface hydroxyls	19
~1643	bending N–H (no H bonding)	TEPA	18
~1625	NH_3^+ deformation	ionic carbamate	17-18
1576	bending N–H	TEPA	17,20
~1565	asymmetric COO^- stretching	ionic carbamate	17-18,21
1550	asymmetric C=O stretching	ionic carbamate	22
1473	symmetric deformation of NH_3^+	ionic carbamate	18,21
1457	deformation of CH_2	TEPA	10
~1410	symmetric COO^- stretching	ionic carbamate	17-18
1360	symmetric C–O band	bicarbonate	22
1298	C–H wagging	TEPA	20
1040 with broad shoulder at 1200	$(SiO)_n$ siloxane stretching	SBA-15 support	17
807	Si–O–Si vibration	SBA-15 support	20

The promoting effect of moisture content on amine functionalized adsorbent can be attributed to the alteration of chemical interactions between CO_2 and amines. A thorough infrared spectrum profile that traces the evolution of chemical bonds in each phase of TEPA impregnated SBA-15 sorbent is presented in Figure 4-6 assisted by the interpretation of infrared absorption results in Table 4-2.

The TEPA impregnated SBA-15 adsorbent was exposed to dry 10 % CO_2 balanced with N_2 feed at 75 ℃ for 1 hour. The resulting CO_2 saturated adsorbent displayed a significantly different infrared spectrum, where the new key peaks of

1565, 1473, and 1410 cm^{-1} appeared with the band loss at 3358, 3285 and 1576 cm^{-1}. This provided clear evidence for carbamate formation after dry CO_2 adsorption. In the presence of moisture added in the feed gas of dilute CO_2, a broad absorption band took place in the range of 3700–3000 cm^{-1} resulting from adsorbed water. Moreover, a peak at 1565 cm^{-1} slightly shifted to 1550 cm^{-1}, indicating the alteration of carboxyl to carbonyl. Meanwhile, a weak peak at 1360 cm^{-1} was also observed that may be assigned to symmetric C–O stretching band. Thence, the reaction pathway of CO_2 adsorption and amine loaded SBA-15 with and without moisture can be described in the case of primary amine as follows[23]:

under dry CO_2,

$$CO_2 + 2R_1R_2NH \leftrightarrow R_1R_2NH_2{}^+ + R_1R_2NCOO^- \text{ (carbamate)} \quad (1)$$

under moist CO_2,

$$CO_2 + R_1R_2NH + H_2O \leftrightarrow R_1R_2NH_2{}^+ + HCO_3{}^- \text{(bicarbonate)} \quad (2)$$

In dry conditions, the main reaction of CO_2 and amines is the carbamate formation that limits the stoichiometry of amine versus CO_2 to 2, whereas in the presence of moisture, 1 mol of amine group can adsorb 1 mol of CO_2 to form bicarbonate. Therefore, it is believed that the existence of moisture promotes the CO_2 adsorption performance on TEPA impregnated SBA-15 adsorbent by boosting the adsorption efficiency of amines.

4.7 Cyclic Regenerablity and Stability

A durable adsorption and desorption behavior of adsorbents is essential for long-term cyclic operation. In order to study the regenerablity and stability of TEPA impregnated SBA-15 adsorbent, 10 consecutive cycles of adsorption and

desorption via thermogravimetric method were carried out. Figure 4-16 depicts the CO_2 uptake of S-40/T60 during repetitive cycles of adsorption at 75 ℃ under flowing 10 v/v% CO_2 feed with and without moisture, and desorption at 105 ℃ under flowing stream of N_2. Each cycle encompassed the adsorption period of 30 minutes to ensure the CO_2 saturation, and desorption of 30 minutes to complete the regeneration of adsorbent. The results showed the adsorptive capacities of TEPA impregnated SBA-15 adsorbent as high as 3.32 mmol g^{-1} and 3.00 mmol g^{-1} in 10 % CO_2/N_2 with and without moisture, respectively, during prolonged cyclic operations. The CO_2 adsorption of S-40/T60 under both dry and moist CO_2 performed a slightly decreasing trend over 10 consecutive cycles of sorption-desorption to approximately 90% of CO_2 uptake of the first cycle. It is believed that the decrease in CO_2 uptake during cyclic operation may be caused by the amine leaching problem[24-25].

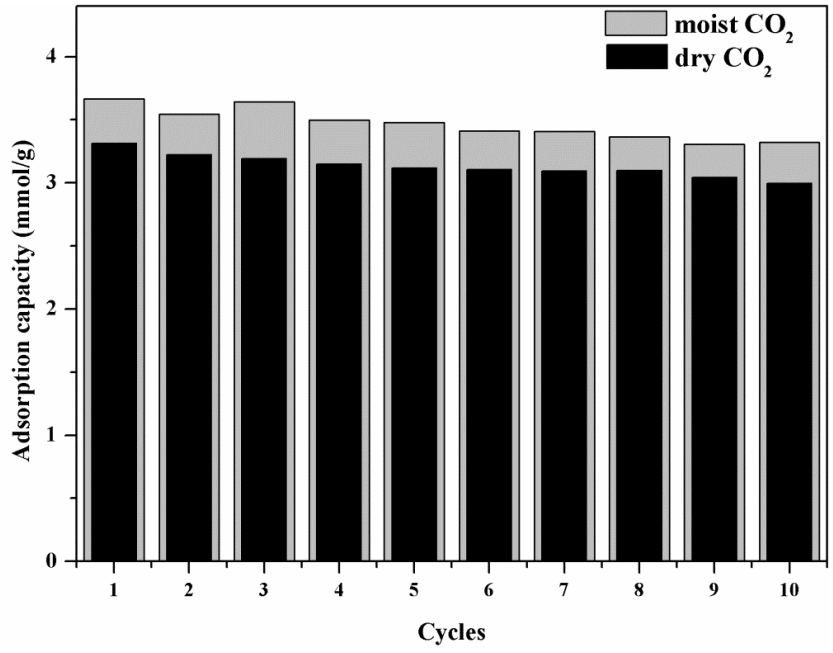

Figure 4-16. Cyclic adsorption of S-40/T60 under dry and wet CO_2 (adsorption at 75 ℃; desorption at 105 ℃)

4.8 CO_2 Adsorption/desorption in Fixed-Bed Reactor

The breakthrough profile of adsorption was obtained by recording the CO_2 concentration of effluent stream as a function of adsorption time as shown in Figure 4-17. At initial stages of breakthrough adsorption, most of mass transfer occurred near the bed inlet once the adsorbate fluid contacted with the adsorbent bed. As mass transfer proceeded until the adsorbent near the bed inlet became saturated, the mass-transfer front moved further along with the direction of gaseous fluid. Most of the mass transfer took place in the mass-transfer front which exhibited an S-shaped effluent concentration profile (seen in Figure 4-17). At break point, which is the time corresponding to the concentration of CO_2 that can be detected in the effluent stream, the adsorbents between the bed inlet and the start of the mass-transfer zone were nearly saturated with CO_2. Ideally, the length of mass transfer front would be infinitesimal provided that there were no mass-transfer resistance and no axial dispersion. In the ideal case, the breakthrough profile would be a straight line vertically from 0 to 1 when all the sorbents were saturated[26]. Therefore, the steep nature of breakthrough shape is indicative of excellent gas-solid contact and mixing in dynamic processes. A steep and narrow breakthrough curve is thus desirable to make efficient use of adsorbents and to reduce the energy requirement of regeneration[26-27].

On the basis of previous results of adsorbent screening, S-40/T60 was selected for breakthrough adsorption in lab-scale fixed-bed reactor. The breakthrough experiments were conducted at different adsorption temperatures with a feed rate of 400 mL/min containing 10 % CO_2 at ambient pressure. Figure 4-17 illustrates

the influence of adsorption temperature on breakthrough adsorption. The results show that the steepness of breakthrough curve at 75 ℃ was much narrower than those at 30 and 50 ℃, where no large difference in the shape of breakthrough curves were observed. It is probably due to the increased diffusion rate at higher temperature so as to accelerate the mass transfer and reduce the length of mass-transfer zone.

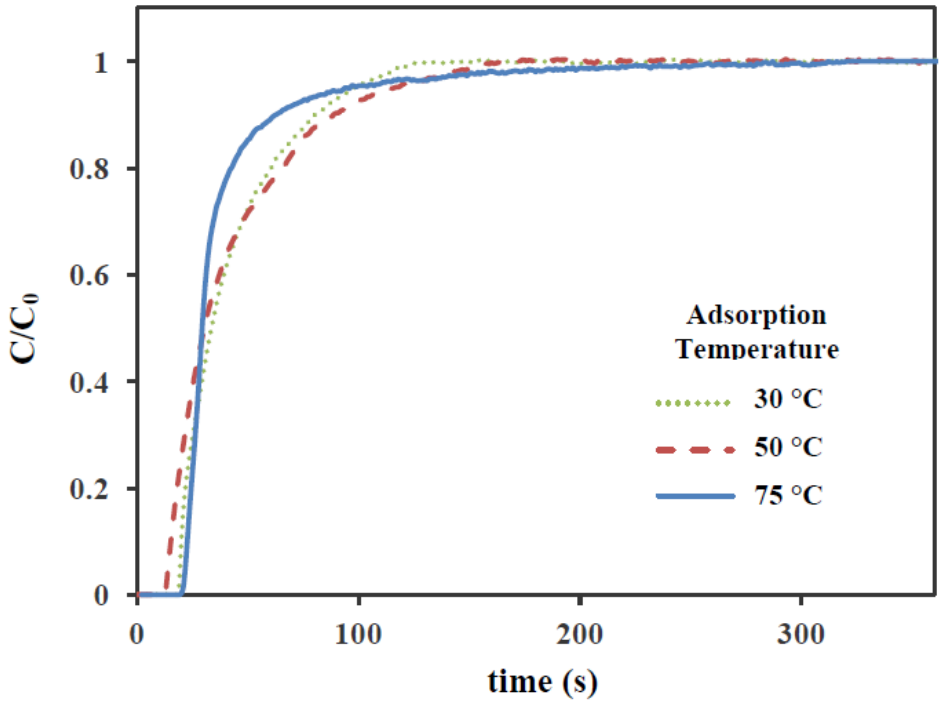

Figure 4-17. Breakthrough curves of S-40/T60 in fixed bed reactor at different adsorption temperatures.

Consecutive sorption-desorption cycles were also carried out using fixed-bed reactor. As soon as the adsorption breakthrough reached the unity, CO_2 feed was switched off to conduct N_2 flushing to remove most of CO_2 retained in dead volume in whole system. As shown in Figure 4-18, the significant CO_2 desorption occurred during the temperature swing process because of the reversible nature of Eq.(1). After 10 minutes for desorption, the effluent CO_2 concentration was hardly detected, which could be considered as the completion of desorption. The result also revealed a quick and efficient desorption process via temperature swing operation.

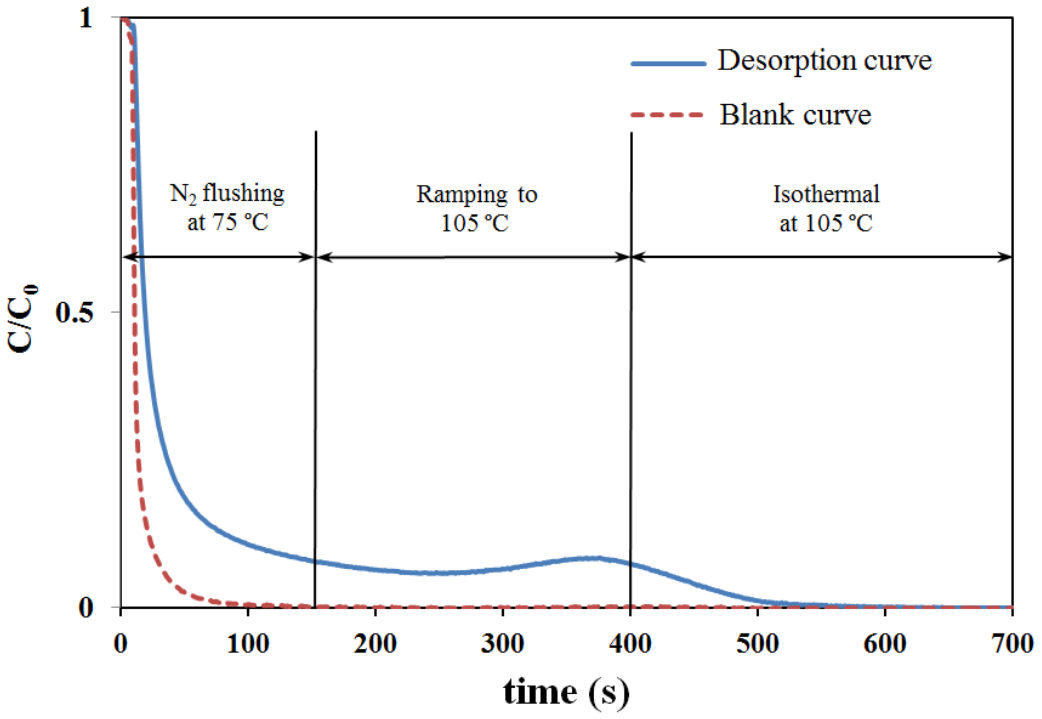

Figure 4-18. Typical CO_2 desorption profile of S-40/T60 at 105 ℃ in fixed-bed reactor. (Blank curve was mearsured using inert partical substitute at the same experimental conditions)

Two key parameters were calculated to evaluate the CO_2 column adsorption: the dynamic adsorption capacity estimated via Eq. (1) and (2), and the break point, which is defined arbitrarily in this work as the time corresponding to $C/C_0 = 10\%$, although this value normally varies according to specific applications. As indicated in Figure 4-18, the adsorption capacity calculated on the basis of each breakthrough profile fluctuated from cycle to cycle in an oscillated manner around the center-weighted value of 2.17 mmol g^{-1} (red dashed line in Figure 4-19), which is lower than 3.48 mmol g^{-1} acquired in thermogravimetric analysis at a smaller scale. Since a relative high flow rate of feed (400 ml/min) and a large adsorption column in size were used in this study than ever reported literature[15,26-28], the oscillation in dynamic adsorption capacity may be probably due to the uneven distribution of gaseous adsorbate. It should be also noted that since zero breakthrough at break point typically means a complete removal of CO_2 in the feed, the adsorption capacity at break point is more realistic and closer to the actual application for practical use. On the contrary to dynamic adsorption capacity of each cycle, the adsorption capacity at each break point displayed an increasing trend until reaching the stable value from 6^{th} cycle (Figure 4-19). The results, especially in line with high flow rate of CO_2 feed possessed in this work during prolonged cyclic operation, suggest a great promise of TEPA impregnated SBA-15 adsorbents in CO_2 removal in large volumetric flue gases.

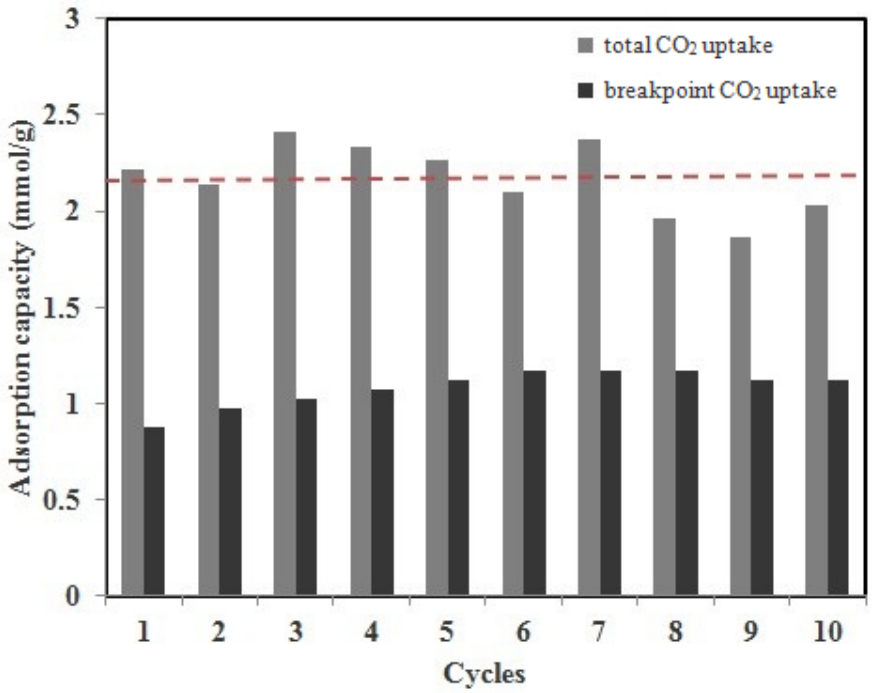

Figure 4-19. Cyclic adsorption-desorption of S-40/T60 in fixed bed column at 75 ℃. Red dashed line represents the averaged value of adsorption capacity.

References

1. Son, W.-J.; Choi, J.-S.; Ahn, W.-S., Adsorptive removal of carbon dioxide using polyethyleneimine-loaded mesoporous silica materials. *Microporous and Mesoporous Materials* **2008,** *113* (1–3), 31-40.

2. Zhao, D.; Huo, Q.; Feng, J.; Chmelka, B. F.; Stucky, G. D., Nonionic Triblock and Star Diblock Copolymer and Oligomeric Surfactant Syntheses of Highly Ordered, Hydrothermally Stable, Mesoporous Silica Structures. *Journal of the American Chemical Society* **1998,** *120* (24), 6024-6036.

3. Xu, X.; Song, C.; Andrésen, J. M.; Miller, B. G.; Scaroni, A. W., Preparation and characterization of novel CO_2 "molecular basket" adsorbents based on polymer-modified mesoporous molecular sieve MCM-41. *Microporous and Mesoporous Materials* **2003,** *62* (1–2), 29-45.

4. Kruk, M.; Jaroniec, M.; Sakamoto, Y.; Terasaki, O.; Ryoo, R.; Ko, C. H., Determination of Pore Size and Pore Wall Structure of MCM-41 by Using Nitrogen Adsorption, Transmission Electron Microscopy, and X-ray Diffraction. *The Journal of Physical Chemistry B* **1999,** *104* (2), 292-301.

5. Zhang, F.; Yan; Yang, H.; YanMeng, Y.; Yu, C.; Tu, B.; Zhao, D., Understanding Effect of Wall Structure on the Hydrothermal Stability of Mesostructured Silica SBA-15. *The Journal of Physical Chemistry B* **2005,** *109* (18), 8723-8732.

6. Fulvio, P. F.; Pikus, S.; Jaroniec, M., Tailoring properties of SBA-15 materials by controlling conditions of hydrothermal synthesis. *Journal of Materials Chemistry* **2005,** *15* (47), 5049-5053.

7. Yue, M. B.; Chun, Y.; Cao, Y.; Dong, X.; Zhu, J. H., CO_2 Capture by As-Prepared SBA-15 with an Occluded Organic Template. *Advanced Functional Materials* **2006,** *16* (13), 1717-1722.

8. Xu, X.; Song, C.; Andresen, J. M.; Miller, B. G.; Scaroni, A. W., Novel Polyethylenimine-Modified Mesoporous Molecular Sieve of MCM-41 Type as High-Capacity Adsorbent for CO_2 Capture. *Energy & Fuels* **2002,** *16* (6), 1463-1469.

9. Birkett, G. R.; Do, D. D., Correct Procedures for the Calculation of Heats of Adsorption for Heterogeneous Adsorbents from Molecular Simulation. *Langmuir* **2006,** *22* (24), 9976-9981.

10. Khatri, R. A.; Chuang, S. S. C.; Soong, Y.; Gray, M., Carbon Dioxide Capture by Diamine-Grafted SBA-15: A Combined Fourier Transform Infrared and Mass Spectrometry Study. *Industrial & Engineering Chemistry Research* **2005,** *44* (10), 3702-3708.

11. Knöfel, C.; Descarpentries, J.; Benzaouia, A.; Zeleňák, V.; Mornet, S.; Llewellyn, P. L.; Hornebecq, V., Functionalised micro-/mesoporous silica for the adsorption of carbon dioxide. *Microporous and Mesoporous Materials* **2007,** *99* (1–2), 79-85.

12. Xu, X.; Song, C.; Miller, B. G.; Scaroni, A. W., Adsorption separation of carbon dioxide from flue gas of natural gas-fired boiler by a novel nanoporous "molecular basket" adsorbent. *Fuel Processing Technology* **2005,** *86* (14–15), 1457-1472.

13. Heydari-Gorji, A.; Yang, Y.; Sayari, A., Effect of the Pore Length on CO_2 Adsorption over Amine-Modified Mesoporous Silicas. *Energy & Fuels* **2011,** *25* (9), 4206-4210.

14. Gray, M. L.; Champagne, K. J.; Fauth, D.; Baltrus, J. P.; Pennline, H., Performance of immobilized tertiary amine solid sorbents for the capture of carbon dioxide. *International Journal of Greenhouse Gas Control* **2008,** *2* (1), 3-8.

15. Yan, X.; Zhang, L.; Zhang, Y.; Yang, G.; Yan, Z., Amine-Modified SBA-15: Effect of Pore Structure on the Performance for CO_2 Capture. *Industrial & Engineering Chemistry Research* **2011,** *50* (6), 3220-3226.

16. Huang, H. Y.; Yang, R. T.; Chinn, D.; Munson, C. L., Amine-Grafted MCM-48 and Silica Xerogel as Superior Sorbents for Acidic Gas Removal from Natural Gas. *Industrial & Engineering Chemistry Research* **2002,** *42* (12), 2427-2433.

17. Knöfel, C.; Martin, C. l.; Hornebecq, V.; Llewellyn, P. L., Study of Carbon Dioxide Adsorption on Mesoporous Aminopropylsilane-Functionalized Silica and Titania Combining Microcalorimetry and in Situ Infrared Spectroscopy. *The Journal of Physical Chemistry C* **2009,** *113* (52), 21726-21734.

18. Danon, A.; Stair, P. C.; Weitz, E., FTIR Study of CO_2 Adsorption on Amine-Grafted SBA-15: Elucidation of Adsorbed Species. *The Journal of Physical Chemistry C* **2011,** *115* (23), 11540-11549.

19. Heydari-Gorji, A.; Sayari, A., Thermal, Oxidative, and CO_2-Induced Degradation of Supported Polyethylenimine Adsorbents. *Industrial & Engineering Chemistry Research* **2012,** *51* (19), 6887-6894.

20. Yang, Y.; Li, F.; Yang, C.; Zhang, W.; Wu, J., Grafting Morphologies of TEPA on SBA-15(P) and Its Effect on CO_2 Adsorption Performance. *Acta Phys. Chim. Sin.* **2012,** *28* (1), 195-201.

21. Bossa, J.-B.; Borget, F.; Duvernay, F.; Theulé, P.; Chiavassa, T., Formation of Neutral Methylcarbamic Acid ($CH_3NHCOOH$) and Methylammonium Methylcarbamate [CH_3NH^{3+}][CH_3NHCO^{2-}] at Low Temperature. *The Journal of Physical Chemistry A* **2008,** *112* (23), 5113-5120.

22. Park, H.; Jung, Y. M.; You, J. K.; Hong, W. H.; Kim, J.-N., Analysis of the CO_2 and NH_3 Reaction in an Aqueous Solution by 2D IR COS: Formation of Bicarbonate and Carbamate. *The Journal of Physical Chemistry A* **2008,** *112* (29), 6558-6562.

23. Xu, X.; Song, C.; Miller, B. G.; Scaroni, A. W., Influence of Moisture on CO_2 Separation from Gas Mixture by a Nanoporous Adsorbent Based on Polyethylenimine-Modified Molecular Sieve MCM-41. *Industrial & Engineering Chemistry Research* **2005,** *44* (21), 8113-8119.

24. Chen, C.; Yang, S.-T.; Ahn, W.-S.; Ryoo, R., Amine-impregnated silica monolith with a hierarchical pore structure: enhancement of CO_2 capture capacity. *Chemical Communications* **2009,** (24), 3627-3629.

25. Hicks, J. C.; Drese, J. H.; Fauth, D. J.; Gray, M. L.; Qi, G.; Jones, C. W., Designing Adsorbents for CO_2 Capture from Flue Gas-Hyperbranched Aminosilicas Capable of Capturing CO_2 Reversibly. *Journal of the American Chemical Society* **2008,** *130* (10), 2902-2903.

26. Garc á, S.; Gil, M. V.; Mart ń, C. F.; Pis, J. J.; Rubiera, F.; Pevida, C., Breakthrough adsorption study of a commercial activated carbon for pre-combustion CO_2 capture. *Chemical Engineering Journal* **2011,** *171* (2), 549-556.

27. Serna-Guerrero, R.; Sayari, A., Modeling adsorption of CO_2 on amine-functionalized mesoporous silica. 2. Kinetics and breakthrough curves. *Chemical Engineering Journal* **2010**.

28. Wang, X.; Ma, X.; Schwartz, V.; Clark, J. C.; Overbury, S. H.; Zhao, S.; Xu, X.; Song, C., A solid molecular basket sorbent for CO_2 capture from gas streams with low CO_2 concentration under ambient conditions. *Physical Chemistry Chemical Physics* **2012,** *14* (4), 1485-1492.

CHAPTER 5

Kinetic Modeling

5.1 Adsorption Kinetic Models

Kinetics of adsorption is an important characteristic to evaluate the adsorption performance of an adsorbent. A good solid sorbent is the one that provides good adsorptive capacity as well as good kinetics. For the rational design and simulation of gas-treating units involving adsorption processes, it is essential to develop gas-solid adsorption kinetics, besides the adsorption equilibria. It is

important as it provides valuable insights into the overall mass transfer in adsorption. Therefore, it is essential to know how adsorption kinetics would vary with parameters such as temperature, pressure, bulk concentration, particle size, pore size and adsorption affinity.

The subject in predicting intrinsic adsorption parameters such as diffusivity (k_c) is still found to be challenging and complex currently. An alternative but more straightforward approach is to propose a semi-empirical kinetic equation that better fits the experimental data. In addition to investigating the adsorptive properties of amine grafted mesoporous silica sorbents, Sayari et al.[1] demonstrated a general kinetic model developed based on Avrami's kinetic model[2] aiming at simulating the particle nucleation phenomena at earliest. However, there is still little work that has been done in the realm of CO_2 adsorption on amine impregnated sorbents. Therefore, the study on CO_2 adsorption kinetics of amine impregnated mesoporous silica sorbent is interesting and desirable to understand and describe its CO_2 adsorptive kinetic behavior.

Three different kinetic models were considered in this work. These include Lagergren's pseudo-first order represented by Eq. (1) and pseudo-second order represented by Eq. (2) and modified fractional-order kinetic model represented by Eq. (3):

$$\frac{\partial q_t}{\partial t} = k_1(q_e - q_t) \tag{1}$$

$$\frac{\partial q_t}{\partial t} = k_2(q_e - q_t)^2 \tag{2}$$

$$\frac{\partial q_t}{\partial t} = k_n(q_e - q_t)^m t^{n-1} \quad (3)$$

where q_e and q_t are the adsorption capacity at equilibrium and at time *t*, respectively. k_1 and k_2 are the rate constant for pseudo-first order and pseudo-second order model, respectively. k_n, *m* and *n* are the model constants for fractional-order model. In fractional-order kinetic model (Eq. (3)), the adsorption rate is assumed to be affected by the mth power of the driving force and nth power of the adsorption time.

After integration and applying the boundary conditions $q_t = 0$ at $t = 0$ and $q_t = q_e$ at $t = \infty$, the integrated forms of the Eqs. (1) to (3) become:

$$q_t = q_e(1 - e^{-k_1 t}) \quad (4)$$

$$q_t = \frac{q_e t}{\frac{1}{k_2 q_e} + t} \quad (5)$$

$$q_t = q_e - \frac{1}{[((m-1)k_n/n)t^n + (1/q_e^{m-1})]^{1/m-1}} \quad (6)$$

The least squares criterion was applied in deducing the characteristic parameters of each model for modeling and optimization in MATLAB. The average absolute deviations (AAD) according to Eq (7) were also used to examine the adequacy of each model in fitness between the experimental and predicted adsorption profiles[1].

$$\text{AAD\%} = \frac{\sum_{i=1}^{N}[(q_{exp} - q_{cal})/q_{exp}]}{N} \times 100\% \quad (7)$$

Where q_{exp} and q_{cal} are the experimental and calculated adsorption capacity, respectively and N is the total number of experimental points.

5.2 Results and Discussions

Figure 5-1 dipicts the CO_2 uptake curves as a function of adsorption time at different temperatures in dilute (10 v/v%) CO_2 situation and the corresponding adsorpton behaviors predicted by different kinetic models. Typically, most of adsorption (>90% of equilibrium capacity) took place during the first 4-5 minutes of CO_2 exposure, afterwards the rate of adsorption became much slower until complete CO_2 saturation. The fast kinetics of CO_2 adsorption on prepared TEPA impregnated SBA-15 adsorbent can be attributed to the favorable nature of affinity sites and the improved diffusion due to the excellent textual properties of substrate permitting a better adsorbate-adsorbent interation. The simulated parameters of each kinetic model as well as the associated errors are summerized in Table 5-1.

Table 5-1. Parameter values of different kinetic models

		30 ℃	50 ℃	75 ℃
Pseudo-first	k_1 (s^{-1})	0.228	0.059	0.007
	q_e (mmol g^{-1})	2.81	3.75	3.38
	AAD%	14.21	22.24	7.019
Pseudo-second	k_2 (g $mmol^{-1}$ s^{-1})	0.387	0.164	0.012
	q_e (mmol g^{-1})	2.65	3.34	3.28
	AAD%	21.47	43.01	10.32
Fractional-order	k_n ($mmol^{1-m}$ g^{m-1} s^{-n})	0.177	0.039	0.001
	q_e (mmol g^{-1})	2.66	3.31	3.27
	m	2.00	1.546	1.265
	n	2.326	0.039	1.636
	AAD%	2.18	2.424	0.955

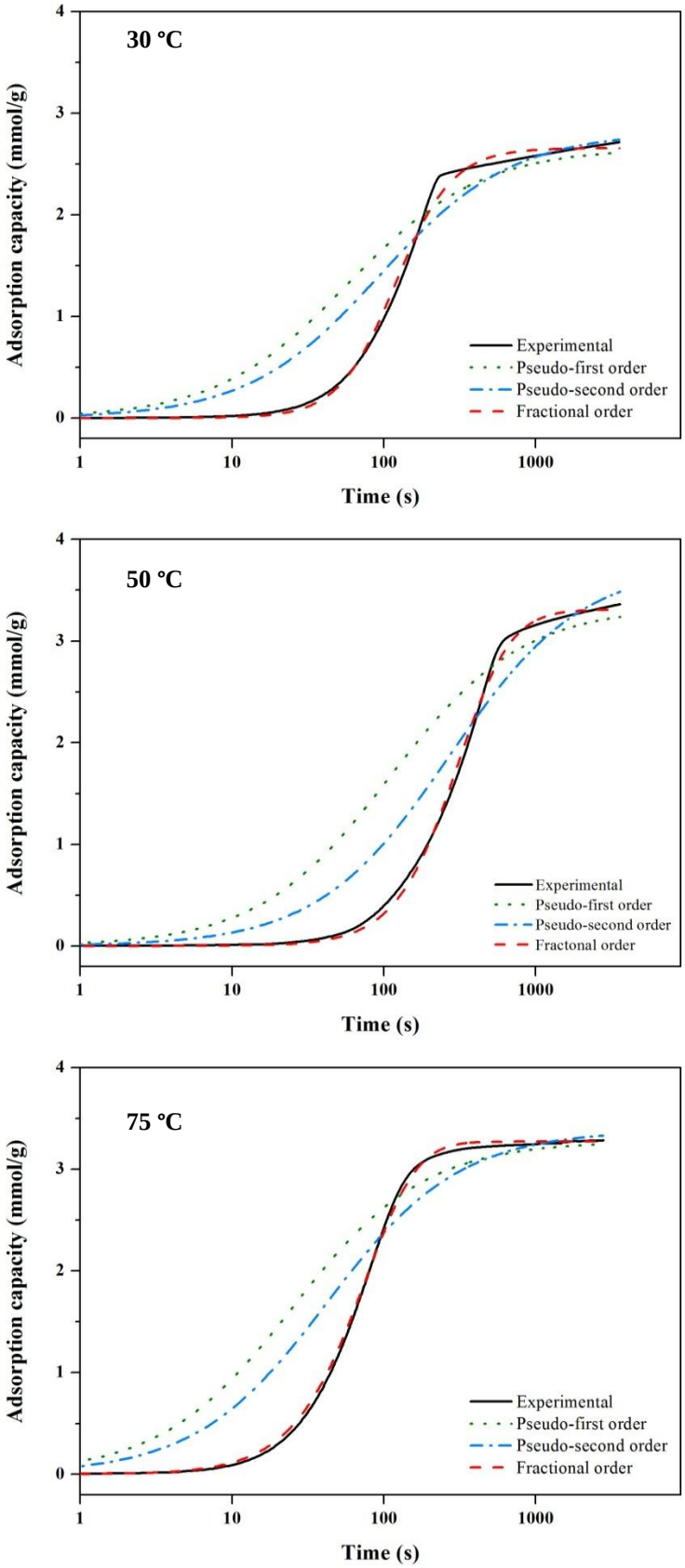

Figure 5-1. Comparison of kinetic models on experimental CO_2 uptake of S-40/T60 at different adsorption temperatures.

As observed in Figure 5-1, the fractional-order kinetic model (eq. (3)) represents experimental adsorption data comparatively better than the pseudo-first order (eq. (4)) and pseudo-second order (eq. (6)) models. The inadequacy of pseudo-first order and pseudo-second order kinetic models leads to large deviations between model predictions and experimental data. Both the models overestimate the CO_2 uptake at the initial phase of adsorption within 5 min, when the significant fast adsorption occurs. On the contrary, the fractional-order model well represents the progress of adsorption curve in the fast adsorption region as well as in the deferred adsorption region close to equilibrium. The significantly lower value of AAD% suggests the applicability of fractional-order kinetic model for TEPA impregnated SBA-15 adsorbents.

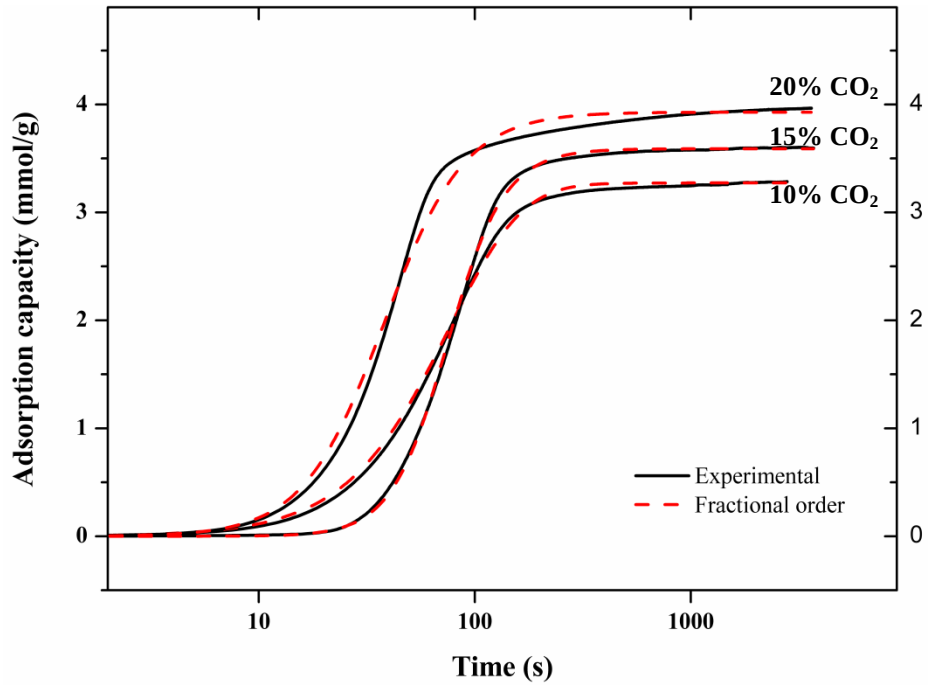

Figure 5-2. CO_2 uptake vs. time for S-40/T60 at low CO_2 concentration at 75 °C

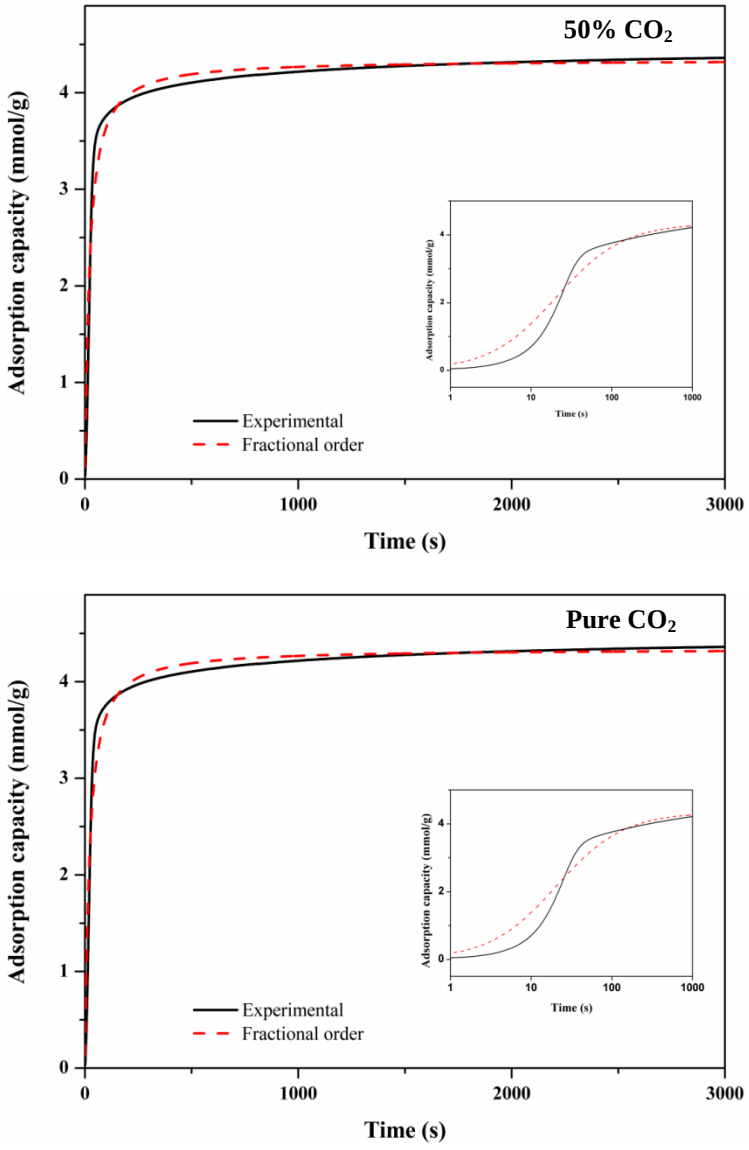

Figure 5-3. CO_2 uptake vs. time for S-40/T60 under pure and 50 % CO_2 feed at 75 ℃

The experimental and model predicted (via fractional-order model) CO_2 uptake results as a function of CO_2 partial pressures are shown in Figures 5-2 and 5-3. For CO_2 concentration below 20%, it has been observed that fractional-order model is comparatively better to demonstrate the CO_2 adsorption behaviors with an acceptable degree of accuracy (Figure 5-2). However, when CO_2 concentration is increased beyond 50%, there is a discrepancy between predicted and

experimental data (in Figure 5-3). The CO_2 uptake values using fractional-order model deviate from the experimental values particularly in the fast adsorption region below 5 minutes. As observed in the inset graghes of Figure 5-3, the experimental adsorption shows faster CO_2 uptake than the prediction of fractional-order model, which represents an extended and slower adsorption profile in this region. A possible reason may be the exothermal nature of chemisorption of CO_2 on TEPA impregnated SBA-15. Since the kinetic models are considered to be applicable under specific isothermal conditions, apparent thermal effect may possibly affect the adsorption from undergoing isothermally, which consequently leads to a discrepancy between predicted and experimental CO_2 uptake results. Especially in the presence of concentrated CO_2, the elevation of temperature caused by significant thermal effect inevitably favors in turn the chemisorption process. Therefore, experimantal CO_2 uptake under concentrated CO_2 exhibits a faster adsorption rate than the prediction isothermally using fractional-order model.

Since the fractional-order kinetic model represents the complexity of the reaction mechanism that may involves more than one reaction pathway[2-3], the value of k obtained from the fractional-order is not the kinetic constant for adsorption in a strict sense, but rather an overall function that may represent various adsorption related factors. Other characteristic parameters such as *m* and *n* stand for the effect of the driving force and diffusion resistance. Besides, *m* also represents the pseudo-order of reaction of CO_2 with amine affinity sites.[1] However, the value of *m* increases as the temperature increases as shown in Table 5-1, exhibiting an

opposite trend with that of PEI loaded pore-expanded MCM-41.[1] This might be due to a change in adsorption mechanisms with the hypothesis that a different physical state of PEI and TEPA may occur on various mesostructural substrates[4].

References

1. Heydari-Gorji, A.; Sayari, A., CO_2 capture on polyethylenimine-impregnated hydrophobic mesoporous silica: Experimental and kinetic modeling. *Chemical Engineering Journal* **2011,** *173* (1), 72-79.

2. Lopes, E. C. N.; dos Anjos, F. S. C.; Vieira, E. F. S.; Cestari, A. R., An alternative Avrami equation to evaluate kinetic parameters of the interaction of Hg(II) with thin chitosan membranes. *Journal of Colloid and Interface Science* **2003,** *263* (2), 542-547.

3. Cestari, A. R.; Vieira, E. F. S.; Vieira, G. S.; Almeida, L. E., The removal of anionic dyes from aqueous solutions in the presence of anionic surfactant using aminopropylsilica—A kinetic study. *Journal of Hazardous Materials* **2006,** *138* (1), 133-141.

4. Serna-Guerrero, R.; Sayari, A., Modeling adsorption of CO_2 on amine-functionalized mesoporous silica. 2. Kinetics and breakthrough curves. *Chemical Engineering Journal* **2010**.

CHAPTER 6

Conclusions & Recommendations

6.1 Conclusions

In present work, amine functionalized SBA-15 adsorbents were successfully developed by the impregnation of TEPA onto nanocomposite SBA-15 substrate. The characterization of SBA-15 material showed its excellent mesoporous textual properties such as high pore volume, high surface area, large pore size and thicker silica wall. The unique and uniform mesoporous nature of SBA-15 substrate

permitted a better dispersion of amines and exerted a synergetic effect on the interaction of CO_2 adsorbate with affinity sites on the surface of amines. Investigations on the synthetic conditions of SBA-15 substrate preparation revealed that the calcination procedure was essential in order to optimize the nanoporous texture by removing the organic template to accommodate more amine substrates.

The composite of TEPA and SBA-15 exhibited a great potential in CO_2 removal from flue gases in coal fired power plants. It was observed that CO_2 uptake was not in a linear relationship as the amine loading increased, suggesting an optimal amine loading was essential in consistence with "molecular basket" concept. Besides, the CO_2 adsorption study at various adsorption temperatures revealed that the adsorption of CO_2 on TEPA impregnated SBA-15 adsorbent was a diffusion controlled process and the optimal adsorption temperature was found to be 75 ℃. It was observed that the adsorption capacity of CO_2 was correlated with the order of mean pore size of substrate. The result indicated the bulky amine can be distributed into the pore channels more easily as the pore size of the mesoporous substrate increases, and much better when the better uniformity of mesopore size is achieved.

CO_2 separation in a simulated flue gas showed that TEPA impregnated SBA-15 adsorbents was competent to separate CO_2 from dilute CO_2 environment at ambient pressure, where the CO_2 uptake reached ca. 3.48 mmol/g. Moreover, in the presence of moisture in the simulated flue gas, the CO_2 uptake was found to be improved rather than deteriorated, because of the shift of reaction mechanism

towards more capturing efficiency of amine. For practical applications, cyclic sorption-desorption experiments were carried out in thermogravimetric (TG) apparatus and fixed-bed reactor. The TEPA impregnated SBA-15 adsorbent exhibit good, albeit slightly decreasing, adsorptive capacities during prolonged cyclic measurements with and without moisture. The breakthrough in fixed-bed reactor showed a steep S-shaped profile, suggesting a fast and effective adsorption process. The stable CO_2 uptakes at break point also suggested a great promise of TEPA impregnated SBA-15 adsorbents in CO_2 removal in large volumetric feed.

The CO_2 adsorption over TEPA impregnated SBA-15 adsorbents preceded very quickly with fast adsorption kinetics. The fraction order kinetic model showed the best fitness in comparison with pseudo-first and pseudo-second order models. The adequacy of fractional-order model was sufficient especially in the low partial pressure of CO_2, while more complex factors might be considered at concentrated CO_2.

6.2 Recommendations for Future Work

The findings of this work provide a fundamental guidance for future endeavor to describe a complete picture of post-combustion CO_2 capture from flue gases using amine functionalized adsorbents. Within the scope of study, a few recommendations on the basis of current contribution in this study are:

- Study the improvement of cyclic adsorption and desorption stability to avoid excess deterioration of adsorption capacity.
- Investigate further the CO_2 adsorption performance in fixed-bed reactor to study the applicability of amine functionalized adsorbents under various

operational conditions, including different influent gas flow rates, moisture content in the simulated flue gas, etc.

- Understand and describe theoretically the CO_2 adsorption using amine functionalized in fixed-bed reactor to predict the CO_2 adsorption performance and guide the future scale-up reactor design.

Appendix A. CO_2 Adsorption Study in Thermogravimetric Apparatus

Calculations for CO_2 adsorption capacity based on data acquired from TGA:

$$q = \frac{\Delta M}{44 M_{dry}} \times 1000$$

Where, q — CO_2 adsorption capacity (mmol g^{-1});

M_{dry} — Mass of dry sorbent before CO_2 exposure (mg);

ΔM — Weight gain of sorbent after CO_2 adsorption (mg).

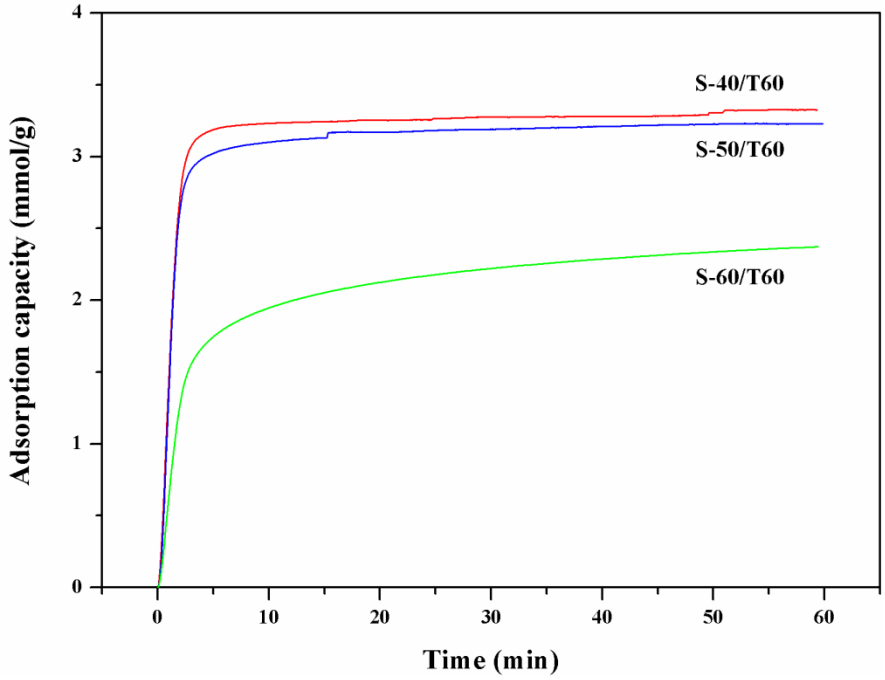

Figure 1A. CO_2 uptakes of S-40, S-50 and S-60 with 60 wt% TEPA loading at 75 ℃ in 10% CO_2 feed gas

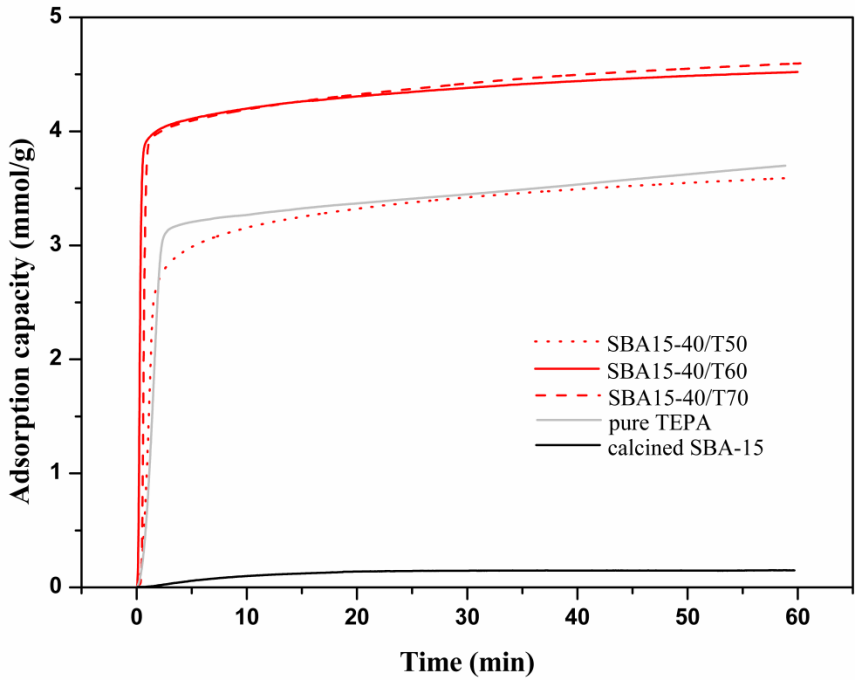

Figure 2A. Comparison of CO_2 adsorption profiles for pure TEPA, raw SBA-15 substrate and TEPA impregnated sorbents with different amine loadings. All the adsorption tests were conducted at 75 ℃ under 100 ml/min flow rate of pure CO_2 in TGA.

Appendix B. Adsorptive Removal of CO_2 in Fixed-bed Reactor

To eliminate the influence of response time of detector on the measurement of CO_2 adsorption, a blank test was carried out under specific conditions.

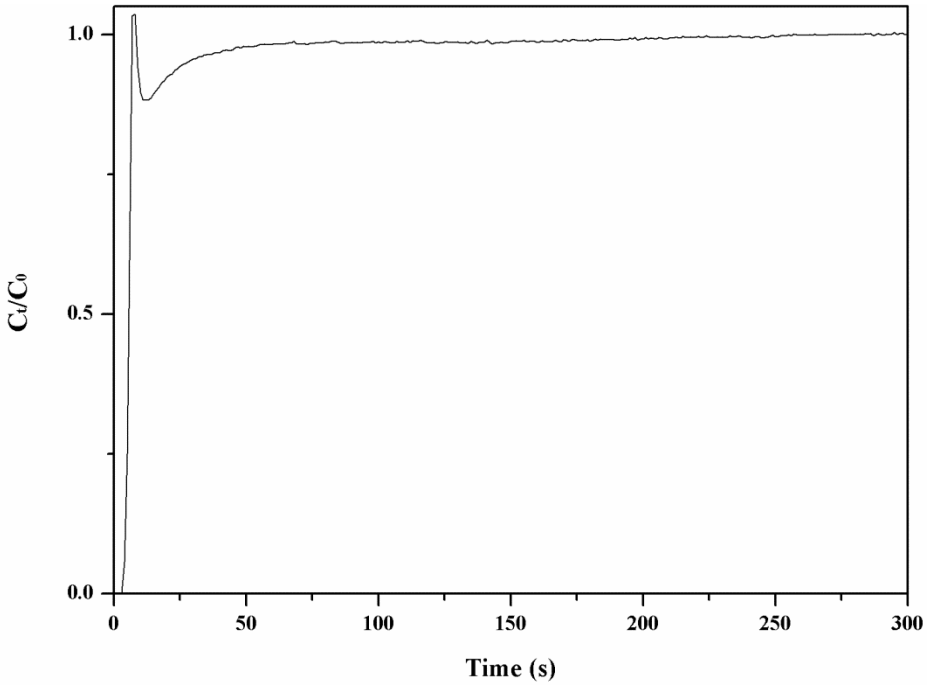

Figure 1B. Blank breakthrough of CO_2 flowing through fixed-bed reactor (10% CO_2; 400 ml/min flow rate)

A quick and steep step change is observed from Figure 1B, indicating the fast response time of mass spectometry in determining effluent CO_2 concentration signal. The intial vibration in the step change is probably due to the CO_2 injection pulse which is not seen in the experimental breakthrough curves in the presence of loaded adsorbents.

Appendix C. MATLAB Code for Kinetic Modeling

Fractional-order model target function defined in .m file.

```
function y=fractional_fn(a)
global t q
sum=0;
n=a(1); kn=a(2); m=a(3); qe=a(4);
nn=length(t);
for i=1:nn
   x=(n-1)*kn*(t(i)^m)/m;
   y=1/(qe^(n-1));
   qcal(i)=qe-1/((x+y)^(1/(n-1)));
   err(i)=(q(i)-qcal(i))^2; % least square
   sum=sum+err(i);
end
y=sum;
```

Scripts for optimization to obtain model parameters:

```
clc
clear all
global t q
% No of unknown=4:
% n=a(1); kn=a(2); m=a(3); qe=a(4);

load TP6015CO2_75C.txt

t=TP6015CO2_75C(:,1);
q=TP6015CO2_75C(:,2);

options=optimset('Display','iter','MaxFunEvals',20000,'MaxIter',20
000,'TolFun',1e-12, 'TolX',1e-12);

x0=[  2.0000  0.1770  2.3264  2.6562];
LB = [0.01 0.001 0.01 0.01];
UB = [ 3 15 5 6];
```

```
% [a,FAL,EXITFLAG] = fminsearch('AvRM_fn',x0, options);
[a,FVAL,EXITFLAG]=fminsearchbnd('fractional_fn',x0,LB,UB,options);
   fprintf('Exitflag:%2d\n',EXITFLAG);
   fprintf('FVAl(Value of the objective function):%12.4f\n',FVAL);
disp('**************Coeffs for Fractional Model*****************')
 %n=a(1); kn=a(2); m=a(3); qe=a(4);
 disp('   n         kn         m         qe')
 for i=1:length(a)
 fprintf('%8.4f',a(i))
 end
 fprintf('\n')
 %.....................................................................%
qe=a(4);
nn=length(q);
SStot=0;
SSerr=0;
for i=1:nn
   u=a(1)-1;
   x=(u*a(2)/a(3))*(t(i)^a(3));
   y=1/(qe^u);
   qcal(i)=(qe-(1/(x+y)^(1/u)));
   rerr(i)=abs((q(i)-qcal(i))/q(i));
   %coefficient of determination
   sst(i)=(q(i)-sum(q)/nn)^2;
   SStot=SStot+sst(i);
   sse(i)=(q(i)-qcal(i))^2;
   SSerr=SSerr+sse(i);
end
 Rsqr=1-SSerr/SStot;
 sumrdev=0;
 fid = fopen('TP6015CO2_75C_cal.txt','w');
for i=1:nn
 sumrdev=sumrdev+rerr(i);
 fprintf(fid,'%12.4f\t  %12.8f\t %12.8f\t %12.8f\n',t(i), q(i),
qcal(i),rerr(i));
 A(i,:)=[t(i) q(i) qcal(i) rerr(i)];
end
```

```
 aad=(sumrdev/nn*100);
 fclose(fid);

fprintf('.....................................................\n')
 fprintf('Percent ABPD of this study =%12.8f\n',aad)
 fprintf('Coefficient of Determination R^2 =%12.8f\n',Rsqr)

disp('.....................................................')
 qc=qcal';
 % disp([t(:), q(:),qc(:)])
 plot(t,q,t,qcal,'r')
 xlswrite('TP6015CO2_75C_cal', A, 4);
```